In presenting the dissertation as a partial fulfillment of the requirements for an advanced degree from the Georgia Institute of Technology, I agree that the Library of the Institute shall make it available for inspection and circulation in accordance with its regulations governing materials of this type. I agree that permission to copy from, or to publish from, this dissertation may be granted by the professor under whose direction it was written, or, in his absence, by the Dean of the Graduate Division when such copying or publication is solely for scholarly purposes and does not involve potential financial gain. It is understood that any copying from, or publication of, this dissertation which involves potential financial gain will not be allowed without written permission.

7/25/68

AUGER ELECTRON SPECTROSCOPY AND SECONDARY EMISSION IN SEMICONDUCTORS

A THESIS

Presented to

The Faculty of the Graduate Division

by

Gilbert Frank Amelio

In Partial Fulfillment

of the Requirements for the Degree

Doctor of Philosophy in the School of Physics

Georgia Institute of Technology

September 1968

AUGER ELECTRON SPECTROSCOPY AND SECONDARY

EMISSION IN SEMICONDUCTORS

Approved:

Chairman

Date approved by Chairman: 9/25/68

ACKNOWLEDGMENTS

I would like to express gratitude to my advisor Dr. Edwin J. Scheibner for his patient and able guidance throughout my graduate career. In addition I wish to thank Dr. Marvin B. Sledd and Dr. Harold A. Gersch not only for their effective efforts as members of my reading committee but also for their inspirational guidance during my years at the Georgia Institute of Technology. I would also like to acknowledge the contributions of the School of Physics for their instruction and of my colleagues, Dr. Gary W. Simmons and Leland K. Jordan, for their stirring discussions and much appreciated encouragement.

I wish to acknowledge the Atomic Energy Commission through the program "Surface Properties of Magnetic Materials" from which this dissertation derived its support. I would especially like to thank Mrs. Sandy Tilley for the typing of the manuscript.

And lastly, I would like to recognize the author's family without whose patient and everpresent moral support this thesis could not have been accomplished.

TABLE OF CONTENTS

TABLE OF CONTENTS (Continued)

LIST OF ILLUSTRATIONS

LIST OF ILLUSTRATIONS (Continued)

LIST OF ILLUSTRATIONS (Concluded)

SUMMARY

The Auger Effect is the emission of discretely energetic electrons, rather than photons, in an atomic transition. In a solid state system, however, the Auger electrons produced by the analogous process are observed to have a continuous, rather than discrete, energy spectrum resulting from the replacement of atomic energy levels by continuous bands. By use of first-order time-dependent perturbation theory the detailed structure of this Auger spectrum can be related to an appropriately defined function of the participating band by means of a convolution integral. Practical methods for solving the convolution problem for the band function are investigated and applied to the experimentally observed Auger spectra in selected semiconductors (silicon, germanium, and graphite). In order to apply the theory consistently it is necessary to subtract out the background present in the data. The background is a consequence of secondary electrons excited by single electron transitions and subsequently scattered into the Auger energy region by multiple inelastic collisions. Further, the Auger electrons are also subject to such inelastic collisions resulting in a distortion of the true Auger distribution. Consequently, to take care of the background problem adequately, one is forced to consider the problem of the diffusion of electrons through the solid semiconductors. This is successfully approached by use of the Boltzmann transport equation, including the collision integral, and solutions are obtained by a Green's function technique.

Such a formal approach to the treatment of electron diffusion through a solid is sufficiently general that it is applicable not only in the Auger energy region but also throughout the entire secondary spectrum. Hence, by combining theoretical calculations with empirical observations derived from the data and the literature, all essential secondary electron source functions and loss mechanisms are judiciously woven into the formalism and the predicted secondary spectrum is compared with the experimental results.

A knowledge of the previously mentioned band function (called the transition density) and of the electron diffusion mechanism leads to the following.

1. Test of theoretical calculations - The transition density is relatable to the density of occupied states and the band structure. Comparison with other results and predictions are then possible.

2. Surface influence on electronic structure - Since the observed Auger electrons are created within the surface vicinity, surface modifications (such as due to contaminants), which are expected to influence the electronic structure at the surface, can be investigated. Similar measurements could allow for a better understanding of the Auger neutralization phenomena because a transition density analysis, with minor modifications in concept, is also applicable to Auger neutralization electrons (electrons resulting from the two electron process between a gas residing on the surface and the bulk).

3. Predictions of true secondary spectra - The electron diffusion formalism indicates the fundamental importance of plasmon excitation as an energy loss mechanism and it can be used to predict true

secondary spectra as a function of such parameters as the band gap, work function and primary energy. The formalism can be used to correct for the effects of background and inelastic scattering distortion in true secondary phenomenon as in the case of the Auger effect.

CHAPTER I

INTRODUCTION

Scope and Objective

The question of the behavior and the interactions of crystal electrons has been and is one of singular importance to the study of solid state materials. This question, with particular reference to surface influences, is explored theoretically and experimentally in this dissertation by consideration of electrons ejected from single crystal semiconductors as a result of the low energy electron bombardment of the surface. These ejected electrons form a continuous energy spectrum most notably characterized by an elastic peak due to elastically reflected primaries, a characteristic loss region due to inelastically rediffused primaries and a true secondary region comprising all electrons with energy less than half the primary energy. The current investigation is restricted to the true secondary electron energy distributions including characteristic Auger spectra which appear as subsidiary maxima in this region. Based on these Auger spectra, a spectroscopy similar to photoelectron and soft x-ray spectroscopy is developed. In close relation to this development a model to explain true secondary electron energy distributions is proposed and the resulting theoretical distributions are compared with experimental observations from selected semiconductors.

Strictly, the Auger Effect is the emission of discretely energetic electrons, rather than photons, in an atomic transition. In a

solid state system, however, the Auger electrons produced by the analogous process are observed to have a continuous, rather than discrete, energy spectrum resulting from the replacement of atomic energy levels by continuous bands. The characteristic two-electron Auger process typically follows the creation of a vacancy in an inner band, usually narrow enough to be considered uniquely energetic, in which one electron of an electron pair originating in a broad, higher lying band fills the inner vacancy, the other electron becoming the Auger electron. It is not surprising, then, that the detailed shape of the resultant Auger spectrum is dependent on the electronic properties of the participating broad band. With the aid of an appropriately defined function of the band (the transition density) it is possible to write a mathematical expression for this dependence. Solutions for the transition density naturally rely on the availability of accurate Auger data. Obtaining such data is both an experimental and theoretical task. The number of Auger electrons ejected by the sample is somewhat less than one per cent of the total number of secondary electrons. The experimental problem, then, is to detect a very weak signal buried in a much larger signal and obtain highly accurate, detailed distributions. Theoretically, the background in the data must be accounted for in some reasonable manner and any distortion in the true distribution resulting from the multiple inelastic scattering of Auger electrons before ejection must be considered. Consequently, one is forced to regard the problem of the diffusion of electrons through the solid semiconductors. The solution of such a problem leads in a natural way to a complete theory of true secondary emission -- the ejection of excited crystal electrons as a result of primary bombardment.

The objective of the present work is therefore twofold. The characteristic Auger Effect observed in specific solid semiconductor single crystals (silicon, germanium, and graphite) is considered. The associated Auger distributions are used to establish a spectroscopy based on the previously mentioned band function, the transition density. Indications are made as to how the transition density can be used to obtain further insight into the electronic structure in the surface vicinity of the specified semiconductors and into the dependence of this structure on surface conditions. Secondly, a theory describing the diffusion of electrons through a solid is given in which the crucial dependences are explicitly exhibited. This theory permits predictions of true secondary electron spectra, and comparisons are made with the results in the semiconductor single crystals studied to test the theory and the dependences assumed.

Historical Survey

Since the induced emission of secondary electrons by primary electron impact was first observed by Austin and Starke[1] in 1902, physicists have continuously sought to understand the mechanisms of this phenomenon. The initial studies were primarily experimental in nature with emphasis on yield measurements, i.e., the number of secondaries emitted (without reference to energy) per primary electron. Of notable exception was the work of Rudberg[2-4] who, beginning in the late twenties, studied the energy distribution of electrons emitted by various metals upon primary electron bombardment. The early theoretical attempts[5-8] were generally characterized by strongly simplifying assumptions concerning the escape mechanism and by the ignoring of electron multiplication.

Correspondingly, the results were not entirely satisfactory. This work was later refined by Baroody[9] in 1950 who, using a classical free electron approach, drew upon the semiempirical work of Salow[10] to obtain good qualitative agreement with observed energy distributions. In the few years following Baroody's work theorists were rather active in pursuing the problem of the production of secondaries in metals from a quantum mechanical point of view.[11-15] However, it was not until the work of Streitwolf[16] in 1959 that a truly satisfactory quantum mechanical treatment of secondary electron excitation was available. During this decade the treatment of the escape mechanism also made substantial progress as a result of the investigations of Wolff.[17] Wolff recognized that the exponential decay law used heretofore was not sufficient and, calling upon the neutron absorption work of Marshak,[18] proposed use of the Boltzmann transport equation to describe the electron cascade. However, in an attempt to treat the secondary emission problem, Wolff inadequately treated the sources of secondaries and their escape across the surface boundary. This was partially rectified by Stolz[19] who, taking advantage of Streitwolf's efforts, treated the special case of low energy secondaries generated by primary electrons incident on metal surfaces. Guba[20] and Grinchak[21] suggested how to generalize the approach somewhat by inclusion of higher energy secondaries, but their work suffered from serious errors in analysis.

During the years following Baroody's effort the experimental work continued as well. In 1953, J. J. Lander[22] observed the presence of subsidiary maxima in the energy distribution curves which he ascribed to characteristic Auger processes. About this same time, Hagstrum began his

work on the Auger spectra resulting from the neutralization of an inert gas ion incident on a crystal surface.[23-26] Hagstrum observed that these spectra were sensitive to surface conditions and crystallographic face. However, because of mathematical and experimental complexities, it was not until late 1966[27] that he was able to interpret the results in terms of the electronic structure of the surface. Meanwhile, primarily because of the contribution of Scheibner[28] in making possible a sufficiently flexible low energy electron diffraction (LEED) system, secondary emission studies became more detailed. Initially, investigators focused their attention on the characteristic loss portion of the energy distribution. However, with the refinement of electronic techniques, the more difficult studies of the true secondary region became possible with much of the first work being done at the Georgia Institute of Technology[29,30] from which this investigation was inspired.

In Chapter II of this dissertation the theory of the Auger Effect is discussed. The Auger spectrum is shown to be related to the transition density through a convolution integral derived from arguments based on time-dependent perturbation theory. Various approaches to obtain practical solutions for the transition density are discussed. In Chapter III the theory of electron diffusion is developed culminating in a general expression for true secondary electron energy distributions. The Auger process is explicitly included in the treatment, and methods of correcting the observed Auger spectrum for the effects of background and inelastic scattering are presented. In the following chapter the experimental instrumentation and procedures required to obtain accurate Auger and secondary emission data are presented. The results in the cases of

silicon, germanium and graphite with accompanying discussions are given next. A detailed description of the analysis of Auger data is included. In Chapter VI the results are compared with available band structure calculations and interpreted in terms of the electronic properties near the surface. In the final chapter the work is summarized with recommendations as to the course of future work along these lines.

CHAPTER II

THEORY OF THE AUGER EFFECT

The Auger Effect in a Single Atom

Before treating the solid state case, it is helpful to consider the simpler situation of the Auger Effect in a single atom. The Auger Effect is the radiationless reorganization of an ion as it proceeds from a highly excited state to a less energetic doubly ionized state. The additional electron lost is the Auger electron which leaves the ion with a kinetic energy depending on the initial and final states of the ion. As an example of the process, imagine an atom of atomic number Z which is ionized in the K shell by high energy electron bombardment. This highly excited ion may then have the K shell refilled by, say, a valence electron giving the excess energy by direct Coulomb interaction to a neighboring electron, often of the same shell. The result is an ion with Z-2 electrons and an Auger electron of kinetic energy (ignoring recoil)

$$E = E_i - E_i' - E_s \qquad (1)$$

where $E_i - E_i'$ is the energy difference of the ion before and after the K shell is filled, and E_s is the ionization energy of the Auger electron from the final state ion. Unlike the solid state case, the energy of the ejected Auger electron is seen to be discrete.

The standard method for calculating the transition probability, first investigated by Wentzel,[31] is to treat the electron-electron interaction as a perturbation; (more recent detailed calculations have included a phenomenological spin-orbit term[32,33,34] with reasonable success; however, since this does not carry over to the solid state case in an unambiguous manner, the spin-orbit term is not considered here). Thus, in first-order time-dependent perturbation theory, the transition probability per unit time is given as

$$w_a = \frac{2\pi}{\hbar} |\langle f|e^2/r_{12}|i\rangle|^2 \rho \,. \tag{2}$$

Note that, as one might expect, the means by which the original ion was formed has no influence on the probability of the Auger Effect. Since the electron-electron interaction is treated as a perturbation, the initial and final states are described by product wavefunctions. Consequently, if $u_a(r_1)$ and $v_a(r_2)$ are the initial-state single-particle wavefunctions and if $u_b(r_1)$ is the final bound-state wavefunction and $v_b(r_2)$ is the free electron wavefunction of positive energy then

$$w_a = \frac{2\pi}{\hbar} \frac{1}{4} |\langle u_b(r_1)v_b(r_2) - u_b(r_2)v_b(r_1)|e^2/|r_1-r_2||$$

$$u_a(r_1)v_a(r_2) - u_a(r_2)v_a(r_1)\rangle|^2 \delta(E_i - E_i' - E_s - T_a) \tag{3}$$

where exchange and energy conservation as a result of (1) have been

included. The right of equation (3) can be evaluated if assumptions are made about the form of the various eigenfunctions. The functions u_a, u_b and v_a are generally taken as hydrogenic in form. The Auger electron eigenfunction v_b is found by solving the Schrodinger equation for the bounded positive-energy solutions. With the potential taken as $\frac{ZZ'e^2}{r} = \frac{2e^2}{r}$ the solutions are well known to be[32]

$$v_b(r) = Y_{\ell m}(\theta,\varphi)e^{-\frac{\pi\alpha}{2}} \frac{|\Gamma(\ell+1+i\alpha)|}{(2\ell+1)!} (2kr)^{\ell} e^{ikr} F(i\alpha+1, 2\ell+2; -2ikr) \qquad (4)$$

where $Y_{\ell m}(\theta,\varphi)$ are the spherical harmonics, $\alpha = \frac{2e^2m}{\hbar^2 k}$ and F is the confluent hypergeometric function. Since the Auger electron is observed at distances far from the origin, expression (4) is simplified by investigating its asymptotic behavior. One finds

$$v_b(r) \approx Y_{\ell m}(\theta,\varphi) \frac{e^{i(kr - \frac{1}{2}\ell\pi + \eta_1 - \alpha \log 2kr)}}{\sqrt{\pi E}\ 2ir} \qquad (5)$$

r large

where Auger energy = $E \cong \frac{\hbar^2 k^2}{2m}$ and

$$\eta_1 = \arg \Gamma(1 + i + i\alpha)$$

By use of (5) and the hydrogenic wavefunction, eq. (3) can be

integrated, usually numerically, to obtain an expression for the transition probability per unit time. Comparison with experiment indicates correspondence to the theory within about 30 per cent.[33] For elements above atomic number 80 it is often necessary to take into account relativistic effects to get reasonable results.[34]

Strictly, eq. (2) can be carried over to the solid state system in which there is not one but many atoms present. One is no longer sure, however, about what to assume for the wavefunctions. Indeed, the choice in the relatively simple cases of the single atom did not give impressive results. The situation is further complicated by virtue of the fact that atomic energy levels are replaced by allowed bands resulting in a continuous Auger spectrum for each permissible process. Nevertheless, it is possible to infer considerable information about a material by studying its Auger spectra. In the next section, eq. (2) is investigated in the solid state case and the detailed structure appearing in the Auger distributions is related to physical properties of the material.

The Auger Effect in the Solid State

As mentioned earlier, the Auger process in the solid state case is characterized by a continuous spectrum resulting from the energy band nature of solid matter. In the work to be presented, attention is restricted to those Auger processes which involve the highest valence band (limited by the band gap in semiconductors and the Fermi level in metals) and a low lying, very narrow level. Experimentally, such processes appear to be the most likely and thereby offer the greatest possibility for investigation.

Such a solid state Auger event is schematically illustrated in Figure 1. Following the removal of an electron from an inner level by primary bombardment a valence band electron (the "down" electron) makes a transition to fill the unoccupied state while, in order to conserve energy, another valence band electron (the "up" electron) is ejected into the continuum. In this energy level diagram the zero of energy is taken at the vacuum level and the energy difference between the two initial electron states is 2Δ. The midpoint between the two initial electron states is designated ζ. It is convenient for the later calculations to use ζ as a new energy variable which is zero at the Fermi level and increases for more negative energies. In terms of this variable the initial states are defined by energies $\zeta - \Delta$ and $\zeta + \Delta$ as indicated. Note that there is a one-to-one correspondence between ζ and E, the Auger kinetic energy. By use of conservation of energy an expression relating ζ and E can be written. Thus where $-E_2$ is the energy of the inner "band" and φ is the work function

$$E = E_2 - 2(\zeta + \varphi) \quad . \tag{6}$$

Since E_2 and φ are considered constant, E and ζ are equivalent and either can be used in the mathematical development; however, ζ is the more convenient.

Note that in equation (6) the variable Δ does not appear. Thus it must be that for a particular E (or ζ), Δ is arbitrary so long as $\zeta + \Delta$ and $\zeta - \Delta$ stay within the allowed band limits. These limitations can be formally invoked by the following set of inequalities.

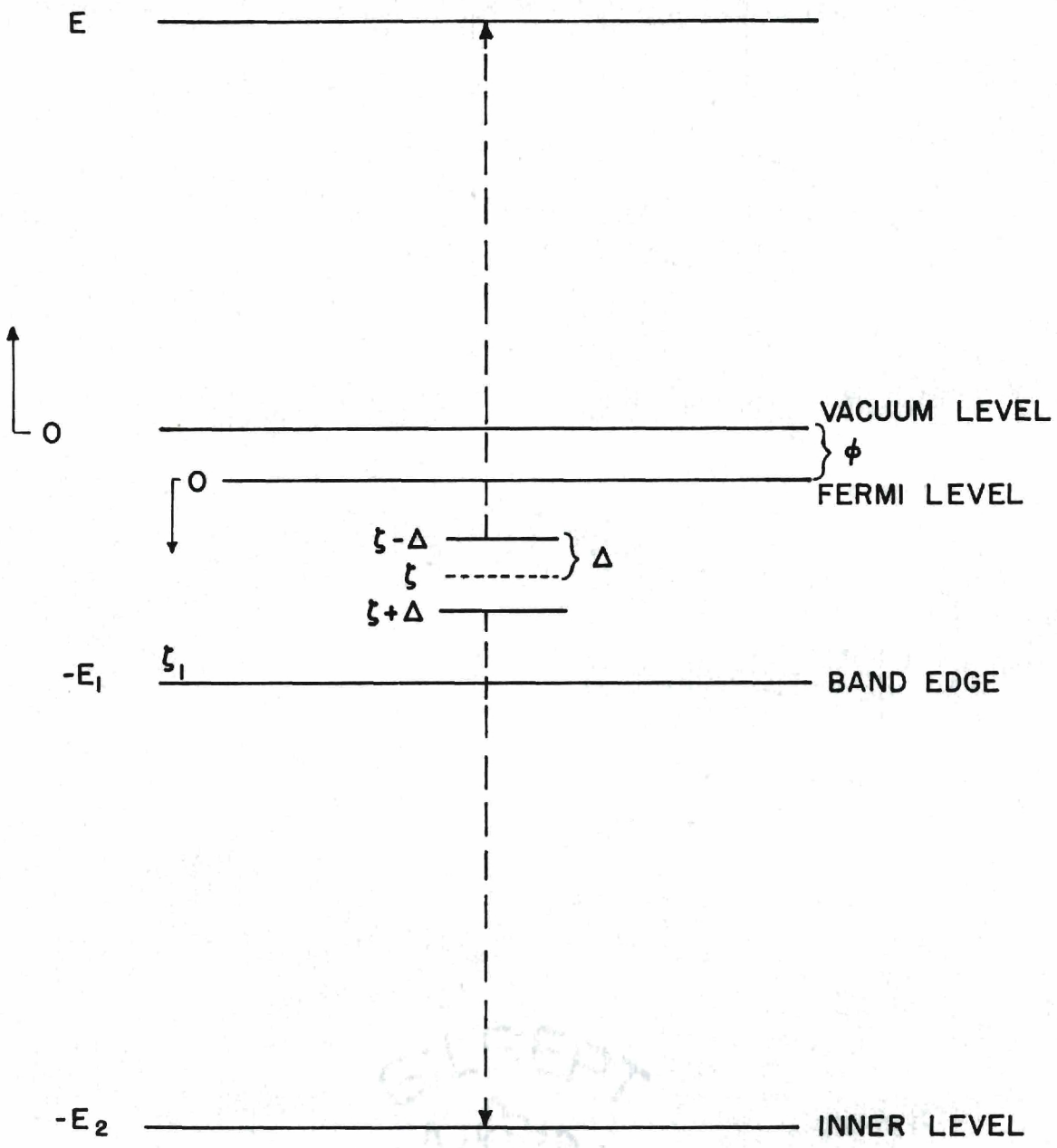

Figure 1. Energy Level Diagram of a Typical Auger Process.

$$-\zeta \leqq \Delta \leqq \zeta \quad \text{when} \quad 0 \leqq \zeta = \frac{E_1 - \varphi}{2} = \frac{\zeta_1}{2} \tag{7}$$

$$-(\zeta_1-\zeta) \leqq \Delta \leqq \zeta_1-\zeta \quad \text{when} \quad \frac{\zeta_1}{2} \leqq \zeta \leqq \zeta_1$$

The relations follow in a straightforward manner from Fig. 1. It follows that this arbitrariness of Δ (within the limits dictated by eqs. (7)) implies that to obtain the total number of electrons with energy E integration of the transition probability over the variable Δ is necessary. Thus

$$F(E) \propto \int TP_A \, d\Delta$$

where the integration is carried over the limits indicated by eqs. (7). TP_A is the transition probability of the Auger Effect with initial electstates at energies $\zeta+\Delta$ and $\zeta-\Delta$ and final electron states at E and $-E_2$. Since it turns out that it is more convenient to work with ζ as the independent variable, define $f(\zeta) = F(E)$. Hence

$$f(\zeta) \propto \int TP_A(\zeta, \Delta) \, d\Delta \, . \tag{8}$$

In order to obtain an expression for the transition probability for the Auger Effect, the Coulombic interaction between the two electrons involved is considered a perturbation of their normal states. The respective solutions of the unperturbed problem are uncoupled and

the system is described consistently by product wavefunctions. Thus the process can be visualized as follows: The initial state is characterized by two electrons in the allowed band residing in some state with wavefunction $|\psi_i\rangle = U(1, \zeta \pm \Delta)\ U(2, \zeta \mp \Delta)$ where the one and two label the electrons and the $\pm$, $\mp$ indicate the possible pairwise energy states for one and two -- this is because of the indistinguishability of which electron is the "up" electron and which is the "down." The electrons are then affected by a perturbation Hamiltonian of the form $\frac{e^2}{r_{12}}$ and are found in the final state $|\psi_f\rangle = V_a(1)\ V_b(2)$ where $V_a(1)$ is the wavefunction describing the Auger electron and $V_b(2)$ is the wavefunction of the other electron with energy $- E_2$. Notice that the final state of the process is well characterized with respect to energy if E_2 is assumed to be a well defined energy. For such a process the Golden Rule of first order time dependent perturbation theory takes the form

$$TP_A = \frac{2\pi}{\hbar} \left| \langle V_a(1)\ V_b(2) \left| \frac{e^2}{r_{12}} \right| U(1,\zeta\pm\Delta)\ U(2,\zeta\mp\Delta) \rangle \right|^2 \rho \qquad (9)$$

where now ρ is the density of initial (not final) states.[37] This follows from the assumption that the final states are well characterized. On the other hand, the initial states can vary in the allowed band in a way subject to the limitations expressed in eqs. (7). Hence if $N(\zeta)$ is the density of occupied states in the allowed band then

$$\rho \propto N(\zeta + \Delta)\ N(\zeta - \Delta) \qquad (10)$$

Consequently, combining eqs. (8), (9) and (10), the electron energy distribution takes the form

$$f(\zeta) \propto \int |\langle f| \frac{e^2}{r_{12}} |i\rangle|^2 N(\zeta + \Delta)\, N(\zeta - \Delta)\, d\Delta \qquad (11)$$

The Matrix Element

Attention is now directed toward the matrix element appearing in the expression for the transition probability of the Auger process. Thus far neither spin nor the Pauli principle have been included explicitly except to mention that the Auger electron can arise from either the $\zeta + \Delta$ or the $\zeta - \Delta$ level. To do this, symmetric and antisymmetric orthonormal space functions are constructed in the usual way for the initial and final states.

$$U^{\pm} = \frac{1}{\sqrt{2}} [U(1,\zeta+\Delta)\, U(2,\zeta-\Delta) \pm U(1,\zeta-\Delta)\, U(2,\zeta+\Delta)] \qquad (12)$$

$$V^{\pm} = \frac{1}{\sqrt{2}} [V_a(1)\, V_b(2) \pm V_a(2)\, V_b(1)]$$

Still proceeding in a standard manner, orthonormal spin wavefunctions are selected as follows

$$S_1 = \alpha(1)\, \alpha(2)\,, \qquad (13)$$

$$S_2 = \frac{1}{\sqrt{2}} [\alpha(1)\ \beta(2) + \beta(1)\ \alpha(2)] ,$$

$$S_3 = \beta(1)\ \beta(2) ,$$

$$S_4 = \frac{1}{\sqrt{2}} [\alpha(1)\ \beta(2) - \beta(1)\ \alpha(2)] ,$$

where the first three are symmetric and the last antisymmetric under particle exchange.

Combining the space and spin functions to form a complete wavefunction, it is seen that only four initial state and four final state antisymmetric wavefunctions are possible. These are $V^- s_1$, $V^- s_2$, $V^- s_3$, $V^+ s_4$; $U^- s_1$, $U^- s_2$, $U^- s_3$, $U^+ s_4$. Sixteen matrix elements are therefore possible but because of orthogonality of the spin portions only four remain. Three of these are of the form

$$H_a = \langle V^- | \frac{e^2}{r_{12}} | U^- \rangle$$

and one is of the form

$$H_b = \langle V^+ | \frac{e^2}{r_{12}} | U^+ \rangle \ .$$

For purposes which will soon be obvious, two "elemental" matrix elements

are now defined.

$$H_{A1} = \langle V_a(1)\ V_b(2)\ \left|\frac{e^2}{r_{12}}\right|\ U(1,\zeta+\Delta)\ U(2,\zeta-\Delta)\rangle \tag{14}$$

$$H_{A2} = \langle V_a(1)\ V_b(2)\ \left|\frac{e^2}{r_{12}}\right|\ U(1,\zeta-\Delta)\ U(2,\zeta+\Delta)\rangle$$

Expressed in terms of these quantities the basic matrix elements H_a and H_b become

$$H_a = H_{A1} - H_{A2},$$

$$H_b = H_{A1} + H_{A2}.$$

Consequently, the square of the matrix element appearing in the transition probability is

$$\left|\langle f|\frac{e^2}{r_{12}}|i\rangle\right|^2 = \tfrac{1}{4}\,(3H_a^{\,2} + H_b^{\,2}) \tag{15}$$

$$= H_{A1}^{\,2} + H_{A2} - H_{A1}\,H_{A2}$$

Now H_{A1} and H_{A2} are integrals over spatial coordinates and, consequently

they will either be equal or one will be greater than the other. Suppose then that

$$H_{A2} = mH_{A1} \quad (0 \leqq m \leqq 1)$$

where m is a function of Δ only. Then eq. (15) becomes

$$|\langle f|\frac{e^2}{r_{12}}|i\rangle|^2 = (1 - m + m^2)H_{A1}{}^2; \quad 3/4 \leqq 1 - m + m^2 \leqq 1 \tag{16}$$

and only one of eqs. (14) has to be considered.

Introduction of the Transition Density

The matrix element H_{A1} is nothing more than an integration over spatial dimensions. Imagining the spatial integration to have been performed the expression for the Auger distribution $f(\zeta)$ becomes

$$f(\zeta) \alpha \int (1 - m + m^2)\, g'^2(\zeta,\Delta)\, N(\zeta + \Delta)\, N(\zeta - \Delta)\, d\Delta \tag{17}$$

where $g'^2(\zeta,\Delta)$ is the squared matrix element after integration.

The proper limits for this integral follow from relations (7). Further, if a band function $g(\zeta)$ is introduced such that

$$g(\zeta + \Delta) = K\sqrt{1 - m + m^2}\; g'(\zeta,\Delta)\, N(\zeta + \Delta) \tag{18}$$

$$g(\zeta - \Delta) = K\sqrt{1 - m + m^2}\; g'(\zeta,\Delta)\, N(\zeta - \Delta)$$

with K as a constant of proportionality, (17) becomes

$$f(\zeta) = \begin{cases} \int_0^{\zeta} g(\zeta + \Delta)\, g(\zeta - \Delta)\, d\Delta; & 0 \leqq \zeta \leqq \frac{\zeta_1}{2} \\ \int_0^{\zeta_1 - \zeta} g(\zeta + \Delta)\, g(\zeta - \Delta)\, d\Delta; & \frac{\zeta_1}{2} \leqq \zeta \leqq \zeta_1 \end{cases} \tag{19}$$

The <u>function $g(\zeta)$</u> thus introduced is termed the <u>transition density</u> and is defined on the interval $(0,\zeta_1)$. Equations (19) can be written in a more convenient form if the region of definition is extended to $(0,\infty)$ where the extended function is identically zero for values of ζ greater than ζ_1. To avoid confusion, this <u>extended transition density</u> function shall be denoted $\bar{g}$. With this definition eqs. (19) can be written simply

$$f(\zeta) = \int_0^{\zeta} \bar{g}(\zeta + \Delta)\, \bar{g}(\zeta - \Delta)\, d\Delta \tag{20}$$

This equation is called the Auger transform in this work. Subsequent efforts will consider the problem of solving this equation for the transition density function $g(\zeta)$. The transition density contains the fundamental physical parameters of interest as is clearly evident from eq. (18). Thus, if the Auger transform can be inverted, an inherently experimental approach is available to determine these important physical

quantities. Furthermore, by relating available theoretical band calculations to the results of this Auger electron spectroscopy, similarities can be recognized and new insight into basic solid state interactions is possible. Moreover, with adsorption of gases on the surface, the Auger spectrum is empirically observed to change for most materials. This is associated with the modification of the potentials in the surface vicinity as well as the interaction of the crystal electrons with the adsorbed species. Greater understanding of such important mechanisms could be attained through use of Auger electron spectroscopy. In this same spirit Auger neutralization by band electrons of adsorbed ions by an Auger event is possible. Resultant distributions can be analyzed by the same techniques to be described with only some minor modifications in concept. Motivated by such considerations, the next section is devoted to methods of solving the Auger transform.

Solutions of the Auger Transform

The transition density, the physical quantity of interest, is related to the Auger spectrum through the Auger transform. Expressed as it is in this equation, however, the form of the transition density is not transparent. Therefore inversion of the Auger transform is now investigated. The Auger transform, equation (20) of the previous section, is a non-linear integral equation with variable limits (Volterra type). Such equations are generally difficult to handle; however, as shall be shown, it is possible to invert the Auger transform exactly. As is sometimes the case, though, this is not always the most practical way to proceed in the applications. Consequently, three methods for evaluating the transition density are offered in this section. The first method --

the Unfold technique -- was conceived by H. D. Hagstrum[36] and, since it is treated extensively in the literature, is considered only briefly. The second method solves the equation exactly in terms of Laplace transforms. In the discussion of this approach, the opportunity is taken to discuss two possible mathematical representations of the data. For these particular choices of representation the formalism transforms the problem to a linear system which can be attacked with standard methods. Finally, a self-consistent iterative approach similar to the Feynman perturbation scheme popular in field theory is offered. With only minimal restrictions in applicability, this analysis allows one to obtain approximate solutions with a precision dependent on the number of terms included. As will become clear, each of the methods has certain advantages as well as disadvantages. The approach selected to obtain an expression for the transition density therefore depends on the particular case at hand and the accuracy desired in the resultant solution.

Unfold Analysis

This method is based on approximating the Auger transform with a sum rather than integral. The energy axis ζ is partitioned into increments of length ϵ and the value of g on this interval is taken as constant. Thus the transition density is given by a histogram which, expressed mathematically, is

$$\bar{g}(t) = \sum_{i=1}^{\infty} g_i \delta_i(t) \tag{21}$$

where

$$\delta_i(t) = \begin{cases} 1 & \text{for } (i-1)\,\epsilon < t < i\epsilon \\ 0 & \text{otherwise .} \end{cases} \tag{22}$$

It is desired to determine the g_i steps. The Auger distribution $f(\zeta)$ is evaluated at points separated by $\frac{\epsilon}{2}$ starting with $\zeta = \frac{\epsilon}{2}$ and a successive index is given to each subsequent value. Thus

$$f(\tfrac{\epsilon}{2}) = f_1 = \tfrac{\epsilon}{2}\, g_1 g_1 ; \tag{23}$$

$$f(2\,\tfrac{\epsilon}{2}) = f_2 = \tfrac{\epsilon}{2}\,(g_1 g_2 + g_2 g_1) ;$$

$$\vdots$$

$$f(k\,\tfrac{\epsilon}{2}) = f_k = \tfrac{\epsilon}{2} \sum_{i=1}^{k} g_i g_{k+1-i} .$$

The f_k's are obtained from the empirical evaluation of the Auger data and solutions for the transition density steps are obtained by sequentially solving each equation. Thus

$$g_1 = \sqrt{\frac{2f_1}{\epsilon}} \tag{24}$$

$$g_2 = \frac{1}{g_1} \frac{f_2}{\epsilon} = \frac{f_2}{\sqrt{2f_1\epsilon}}$$

$$\vdots$$

$$g_s = \sqrt{\frac{\epsilon}{2f_1}} \times \left[\frac{1}{\epsilon} f_s - \sum_{i=1}^{s/2} g_i g_{s-i+1}\right], \quad s \text{ even}$$

$$\left[\frac{1}{\epsilon} f_s - \tfrac{1}{2} g^2 \frac{s+1}{2} - \sum_{i=2}^{\frac{s-1}{2}} g_i g_{s-i+1}\right], \quad s \text{ odd}$$

The method has the obvious advantage of being very straightforward and, if fine enough partitions are chosen, a reasonably faithful approximation is possible. However, because each solution depends on all the previous solutions, errors in the data mount up exponentially. Consequently, unless extremely accurate data is available or unless a method for adjusting the data is used, serious divergences in the solutions can occur. In general, then, caution must be used in utilizing this method.

Laplace Transform Analysis

In this approach the Auger transform is shown to be expressible as a convolution integral for which the formalism of Laplace transforms is directly applicable. To proceed, the Auger transform is taken out of its symmetric form by changing variables to $y = \zeta + \Delta$. This yields

$$f(\zeta) = \int_{\zeta}^{2\zeta} \bar{g}(y)\ \bar{g}(2\zeta - y)\ dy$$

Similarly, a change of variables to $y = \zeta - \Delta$ gives

$$f(\zeta) = \int_{o}^{\zeta} \bar{g}(y)\ \bar{g}(2\zeta - y)dy$$

which, when added to the previous result, gives

$$2f(\zeta) = \int_{o}^{2\zeta} \bar{g}(y)\ \bar{g}(2\zeta - y)dy \qquad (25)$$

This is precisely the form necessary to apply the convolution theorem of Laplace transforms[38] which states that if $w(t) = \int_{o}^{t} u(y)\ v(t - y)\ dy$ then $L[w(t)] = L[u(t)] \times L[v(t)]$. Application of this theorem to equation (25) results in

$$\bar{g}(t) = L^{-1}\left[\sqrt{L[2f(t/2)]}\ \right] \qquad (26)$$

$$= 2L^{-1}\left[\sqrt{F(2s)}\ \right]$$

with $F(s) = L[f(t)]$ and $t = 2\zeta$. Equation (26) constitutes a closed

form expression for the transition density dependent on a knowledge of the indicated Laplace transforms of the data. In applying this formalism in practice, one must suitably represent the data mathematically so that (1) its Laplace transform exists, (2) the square root of the resulting expression is obtainable and (3) the inverse transform operation can be handled in a satisfactory manner.

Two possible mathematical representations of the Auger data are considered: (1) power series and (2) linear segmentation. Power Series. The power series approach to utilizing eq. (26) is based upon the assumption that both the Auger data $f(\zeta)$ and the transition density $g(\zeta)$ can be expressed as power series of finite order. That is suppose

$$g(t) \cong \sum_{i=o}^{v} g_i \, t^i \tag{27}$$

and

$$f(\zeta) \cong \sum_{i=1}^{2v+1} a_i \, \zeta^i \tag{28}$$

The philosophy is to relate the empirically determined a_i's to the g_i's by use of eq. (26). Taking the Laplace transform of (26) and substituting in the power series representations yields

$$L[g(t)] = \sum_{i=o}^{v} g_i \frac{i!}{s^{i+1}} = \sqrt{\sum_{i=1}^{2v+1} \frac{a_i{}'i!}{s^{i+1}}} \qquad (29)$$

with

$$a_i{}' = \frac{a_i}{2^{i-1}}$$

Squaring both sides of (29) and defining for convenience $\gamma_i = g_i i!$ and $\lambda_k = a_k{}'k!$ it is found that

$$\left\{L\,[g(t)]\right\}^2 = \sum_{i=o}^{v} \sum_{\ell=o}^{v} \frac{\gamma_i \gamma_\ell}{s^{i+\ell+2}} \qquad (30)$$

$$= \sum_{i=1}^{v+1} \sum_{\ell=o}^{i-1} \frac{\gamma_\ell \gamma_{i-\ell-1}}{s^{i+1}} + \sum_{i=v+2}^{2v+1} \sum_{\ell=i-v-1}^{v} \frac{\gamma_\ell \gamma_{i-\ell-1}}{s^{i+1}}$$

$$= \sum_{k=1}^{2v+1} \frac{\lambda_k}{s^{k+1}}$$

It therefore follows from linear independence that

$$\lambda_k = \sum_{\ell=o}^{k-1} \gamma_\ell \gamma_{k-\ell-1} \quad \text{for} \quad 1 \leqq k \leqq v + 1 \tag{31}$$

$$\lambda_k = \sum_{\ell=k-v-1}^{v} \gamma_\ell \gamma_{k-\ell-1} \quad \text{for} \quad v + 2 \leqq k \leqq 2v + 1$$

Equations (31) are now each multiplied by the factor

$$\chi^{\beta(k+2\alpha-1)} = \chi^{\beta(\ell+\alpha)} \chi^{\beta(k-\ell-1+\alpha)}, \quad (\chi,\alpha,\beta \text{ real and } \chi > 0)$$

and all equations are added together.

$$\sum_{i=o}^{v} \gamma_i \chi^{\beta(i+\alpha)} = \left[\sum_{k=1}^{2v+1} \lambda_k \chi^{\beta(k+2\alpha-1)} \right]^{\frac{1}{2}}, \quad \text{for all } \chi > 0 \tag{32}$$

If the right hand side of (32), which is in principle known, is designated as H(x), then it is clear that (32) is solved for the γ_i's by fitting the "best" power series (the left hand side) to the function H(x). Once these γ_i's are found the transition density becomes, from (27),

$$\bar{g}(t) = \sum_{i=o}^{v} \frac{\gamma_i}{i!} t^i$$

Expression (32) is a linear equation and the problem of solving it, which

is tantamount to solving the Auger transform problem, can be handled by standard linear techniques although this is sometimes tedious. Alternatively, one can select a finite set of x's and convert (32) to a matrix equation of the form

$$\underline{\underline{X}}\,\underline{\gamma} = \underline{H}$$

which, if the inverse of X is obtainable, is easily solved

$$\underline{\gamma} = \underline{\underline{X}}^{-1}\,\underline{H} \tag{33}$$

In general, this is the most convenient approach although one is no longer sure that the solution is the best fit for all χ . When $\underline{\underline{X}}^{-1}$ is found for a particular order v this order inversion need never be computed again because $\underline{\underline{X}}^{-1}$ does not depend on the data. Solutions are obtained immediately upon the determination of $\underline{H}$ and multiplication by $\underline{\underline{X}}^{-1}$.

Another approach to finding the γ_i's is to recognize that for $\alpha = \beta = 1$, $\chi = \frac{1}{s}$ eq. (32) becomes

$$L\,[\bar{g}(t)] = \sum_{i=o}^{v} \gamma_i \frac{1}{s^{i+1}} = \left\{ L\left[\sum_{k=1}^{2v+1} a_k' t^i \right] \right\}^{\frac{1}{2}}$$

$$= 2 \left\{ \int_o^{\infty} e^{-2st} f(t)\, dt \right\}^{\frac{1}{2}}$$

The integral on the right hand side of (34) is done numerically and the resultant relation is solved by the methods already discussed. The advantage lies in the fact that this numerical integral can, in general, be found much more accurately than H(x) resulting in a more precise determination of the transition density. Further, since the right hand side of (34) does not depend on v (as does H(x)), v can be varied until a suitable result is obtained.

Generally the power series approach to solving the Auger transform problem is both mathematically and physically esthetic. Power series of finite order are usually very pleasant functions with which to work. However, satisfactory results are obtained only when the coefficients can be determined to several significant digits of accuracy, and in practice, this is difficult. In the discussion immediately following a different approach to representing the data is considered which has less demanding requirements of accuracy.

Linear Segmentation. Suppose that, similar to the Unfold analysis, the data is segmented into intervals spaced $\frac{\epsilon}{2}$ apart and in each interval the Auger curve is approximated by a straight line in such a manner that the resulting approximate function is continuous. This is illustrated in Figure 2.

It is easy to show by direct integration of eq. (20) that the transition density function necessary to produce such a curve is just the same function used in the Unfold approach, eq. (21) and (22). The Auger distribution function f in this approximation is given by

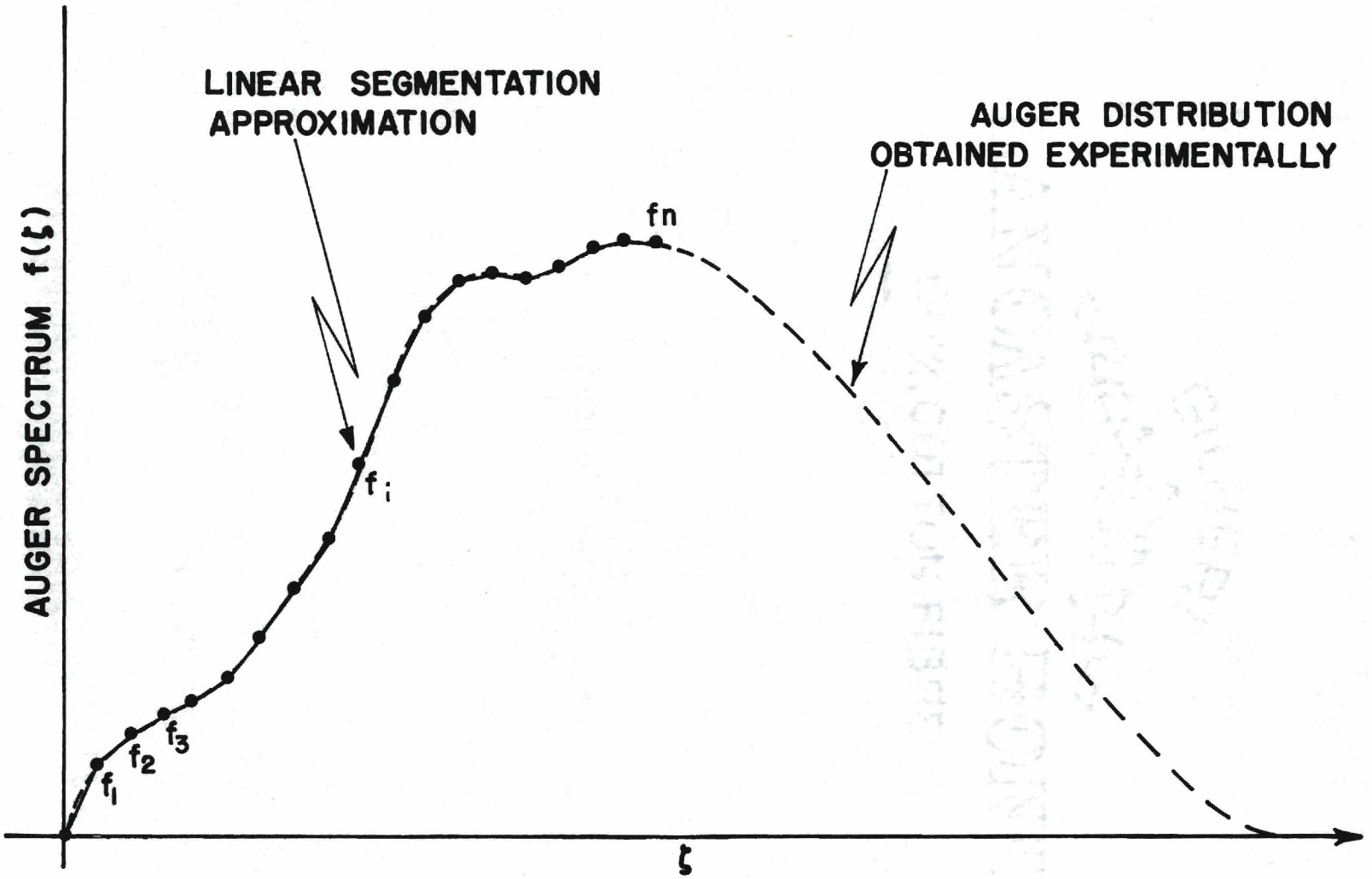

Figure 2. Linear Segmentation Representation of Auger Spectrum Data.

$$f(t) = \sum_{i=1}^{\infty} y_i(t)\ \delta_i(t) \tag{35}$$

where

$$y_i(t) = 2\,\frac{f_i - f_{i-1}}{\epsilon}\,\left(t - (i-1)\,\frac{\epsilon}{2}\right) + f_{i-1}$$

The f_i's are the end points of each linear segment sequentially ordered exactly as in the Unfold discussion.

Equation (35) is more conveniently expressed as

$$f(t) = \int_{t-\frac{\epsilon}{2}}^{t} \sum_{j=1}^{\infty} f_j \delta_j(r)\,dr \tag{36}$$

which can be easily verified. To utilize eq. (26) it is necessary to determine the Laplace transform of (36).

Therefore (with $\Delta = \epsilon/2$)

$$L\,[f(t)] = F(s) = L\,\left[\int_{o}^{t} h(r)\,dr - \int_{o}^{t-\Delta} h(r)\,dr\right]$$

$$\text{with}\quad h(r) = \sum_{j=1}^{\infty} f_j \delta_j(r)$$

and consequently

$$F(s) = \frac{1}{s} L[h(r)] - \frac{e^{-s\Delta}}{s} L[h(r)] \tag{37}$$

$$= \frac{e^{s\Delta} - 1}{s} \sum_{j=1}^{\infty} f_j e^{-js\Delta}$$

Finally, by taking the Laplace transform of (26) and utilizing (37) and (21), the Auger transform problem reduces to

$$\sum_{i=1} g_i e^{-is\varepsilon} = \left[\frac{2}{\varepsilon} \sum_{j=1}^{2n-1} f_j e^{-(j+1)s\varepsilon}\right]^{\frac{1}{2}} \tag{38}$$

where n is an integer such that for all $j \geq 2n$, $f_j = 0$. If x is set equal to $e^{-s\varepsilon}$, then equation (38) takes a form exactly like that of eq. (32) and, hence, all comments given there on solving such a system carry over. Equation (38) has the advantage of being expressed directly in terms of the g steps being sought. It is not necessary to fit a power series to the data and no factorials are present to complicate matters. In addition it is not usually necessary to know the value of the transition density histogram steps to the same accuracy required of the expansion coefficients in the power series approach. In fact, the only disadvantage of the method is associated with the difficulty of solving (38) for large n. In general, the order n is much larger here than in the

case of (32) and the normal methods for handling linear systems become much more tedious. For large n, for instance, the Gaussian elimination procedure is not reliable because of round-off errors inherent in digital computers.

Except for the difficulty just discussed, the linear segmentation approach is frequently the most accurate way to proceed -- especially if a good initial guess for the solution is available. In the next section a method for obtaining an approximate solution independent of the Laplace transform formalism is treated.

Self-Consistent Iterative Analysis

Recently it has been empirically shown[39,40] that the first derivative of the Auger spectrum obtained from ion neutralization and low energy electron studies of solid surfaces bears a striking resemblance to the transition density. In this section, this observation is put on a theoretically sound footing. Moreover, a self-consistent iterative technique, not unlike the Feynman perturbation expansion famous in field theory, based on the Auger spectrum derivatives is offered as a means of approximating the transition density.

Starting with equation (25), the first derivative with respect to the energy is taken $\left(\zeta \leqq \frac{\zeta_1}{2}\right)$

$$\frac{df(\zeta)}{d\zeta} = \bar{g}\ (2\zeta)\ \bar{g}(o) + \int_o^{2\zeta} \bar{g}(y)\ \bar{g}'(2\zeta - y)dy \qquad (39)$$

The primed notation above, as well as throughout this section, designates differentiation with respect to the argument. In terms of the transition density $\bar{g}$, equation (39) becomes

$$\bar{g}(2\zeta) = \frac{1}{\bar{g}(o)} \left\{ f'(\zeta) - \int_o^{2\zeta} \bar{g}'(y)\, \bar{g}(2\zeta - y)\, dy \right\} \tag{40}$$

$$\bar{g}(o) \neq 0$$

where the primed term in the integral has been reversed by an integration by parts. The self-consistent iterative procedure consists of inserting the entire right hand side of (40) into the integral on the right and expanding the result. Thus, in terms of $t = 2\zeta$, after one iteration

$$\bar{g}(t) = \frac{1}{\bar{g}(o)} \left\{ f'(t/2) - \left(\frac{1}{2\bar{g}(o)} \right)^2 \int_o^t f''\left(\frac{y}{2}\right) f'\left(\frac{t-y}{2}\right) dy \right. \tag{41}$$

$$\left. + \text{ Integrals involving } \bar{g} \text{ and } \bar{g}' \right\}$$

The next order term is obtained by once again using the right hand side of (40) and inserting this into the integrals in (41) involving $\bar{g}$ and $\bar{g}'$. Thus, after two iterations,

$$\bar{g}(t) = \frac{1}{\bar{g}(o)} \left\{ f'\left(\frac{t}{2}\right) - \left(\frac{1}{2\bar{g}(o)} \right)^2 \int_o^t f''\left(\frac{y}{2}\right) f'\left(\frac{t-y}{2}\right) dy \right. \tag{42}$$

$$+ \left(\frac{1}{2\bar{g}(o)} \right)^4 \int_o^t \int_o^y f''\left(\frac{x}{2}\right) \left[\tfrac{1}{2} f'\left(\frac{t-y}{2}\right) f''\left(\frac{y-x}{2}\right) \right.$$

$$+ f'' \left(\frac{t-y}{2}\right) f' \left(\frac{y-x}{2}\right)\Big] \, dxdy + \text{terms}$$

$$\text{of order } \left(\frac{1}{2\bar{g}(o)}\right)^6 \Big\}$$

Continuing in this manner, higher order terms can be obtained. However, as may seem apparent, the expressions become increasingly more complex.

The convergence of this expansion depends in part on the value of $\bar{g}(o)$. The value of $\bar{g}(o)$ is easily determined from (40)

$$\bar{g}(o) = \left[f'(o)\right]^2 \tag{43}$$

which is generally not zero. In fact, in practice, for a convenient choice of coordinates, $\bar{g}(o)$ is on the order of ten. Further, since the integrals are well behaved, the series often converges quickly and the first three terms are frequently sufficient to obtain a reasonable first approximation to the transition density. The primary disadvantage of the self-consistent iterative approach is that the first and second derivatives of the Auger data must be known and a method for calculating the integrals in eq. (42) must be available. Despite this, the formalism is very attractive since it is not necessary to sequentially solve any systems of equations. Moreover, the method is not dependent on the mathematical representation of the Auger data. Consequently, when $\bar{g}(o)$ is of suitable value, this approach has much to offer, especially if extremely accurate results are not required. It is also possible to use the

solution resulting from this method as a first guess in one of the Laplace transform analyses and thus serve to simplify those approaches.

Summary

The two electron Auger effect involving an inner level and the broad allowed region near the Fermi surface is quantum mechanically treated by a first order time dependent perturbation analysis. Solving for the anticipated Auger spectrum $f(\zeta)$ in terms of a band function $g(\zeta)$, the transition density, results in a fundamental equation designated as the Auger transform

$$f(\zeta) = \int_0^{\zeta} \bar{g}(\zeta + \Delta)\, \bar{g}(\zeta - \Delta) d\Delta \qquad (20)$$

with

$$\bar{g}(\zeta) = g(\zeta)\, \theta(\zeta_1 - \zeta) \; ; \quad \theta(\zeta_1 - \zeta) = \begin{cases} 1, & \zeta \leq \zeta_1 \\ 0, & \zeta > \zeta_1 \end{cases}$$

$g(\zeta)$ = (a term associated with exchange) x (a term involving the matrix element) x (the density of occupied states). (18′)

Three methods for obtaining an expression for the extended transition density function $\bar{g}(\zeta)$ are possible. (1) Unfold -- the transition

density function is assumed representable as a histogram and the Auger transform integral is converted to a sum. The analysis leads to a non-linear system of equations which can, however, be solved sequentially for the values of the histogram steps. The result is

$$g_1 = \sqrt{\frac{2f_1}{\epsilon}} \quad ; \tag{24}$$

$$g_2 = \sqrt{\frac{\epsilon}{2f_1}} \; \frac{f_2}{\epsilon} \quad ;$$

$$\vdots$$

$$g_s = \begin{cases} \sqrt{\dfrac{\epsilon}{2f_1}} \left[\dfrac{1}{\epsilon} f_s - \displaystyle\sum_{i=2}^{s/2} g_i g_{s-i+1} \right], & s \text{ even} \\[2ex] \sqrt{\dfrac{\epsilon}{2f_1}} \left[\dfrac{1}{\epsilon} f_s - \frac{1}{2} g^2_{\frac{s+1}{2}} - \displaystyle\sum_{i=2}^{(s-1)/2} g_i g_{s-i+1} \right], & s \text{ odd} \end{cases}$$

where the f_k's are Auger data points separated $\epsilon/2$ apart beginning with f_1 at $\zeta = \epsilon/2$. Each step is ϵ wide. (2) Laplace transform -- the Auger transform is expressible as

$$2f(\zeta) = \int_0^{2\zeta} \bar{g}(y)\, \bar{g}(2\zeta - y)\, dy \tag{25}$$

which has as its solution

$$\bar{g}(t) = 2L^{-1}\left[\sqrt{F(2s)}\right] \tag{26}$$

with $F(s) = L[f(t)]$ and $t = 2\zeta$. If f and g are assumed to be representable as power series of finite order $2v + 1$ and v respectively, then (26) transforms to a linear system

$$\sum_{i=o}^{v} \gamma_i \chi^{\beta(i+\alpha)} = \left[\sum_{k=1}^{2v+1} \lambda_k \chi^{\beta(k+2\alpha-1)}\right]^{1/2} \tag{32}$$

for all $\chi > 0$ (α, β, χ real and arbitrary).

which for selected χ can be put in the form

$$\underline{X}\,\underline{\gamma} = \underline{H}\,.$$

The transition density function is then given by

$$\bar{g}(t) = \sum_{i=o}^{v} \frac{\gamma_i}{i!} t^i\,.$$

If f and g are represented as in the Unfold approximation, then (26) transforms to a linear system

$$\sum_{i=1}^{n} g_i e^{-is\varepsilon} = \left[\frac{2}{\varepsilon}\sum_{j=1}^{2n-1} f_j e^{-(j+1)s\varepsilon}\right]^{\frac{1}{2}} \tag{38}$$

for all s

which again, for selected s, can be put in the form

$$\underline{\underline{X}}\,\underline{g} = \underline{H} .$$

In this case the transition density is given by

$$\bar{g}(t) = \sum_{i=1}^{n} g_i \delta_i(t) . \tag{21}$$

(3) Self-Consistent Expansion -- The derivative of (25) can be used to establish a new equation which is subject to an iterative expansion. Carrying out the expansion results in the following expression for the transition density

$$\bar{g}(t) = \frac{1}{\bar{g}(o)}\left\{f'\left(\frac{t}{2}\right) - \left(\frac{1}{2\bar{g}(o)}\right)^2 \int f''\left(\frac{y}{2}\right) f'\left(\frac{t-y}{2}\right) dy \right. \tag{42}$$

$$\left. + \left(\frac{1}{2\bar{g}(o)}\right)^4 \int_o^t \int_o^y f''\left(\frac{x}{2}\right)\left[\tfrac{1}{2} f'\left(\frac{t-y}{2}\right) f''\left(\frac{y-x}{2}\right) + f''\left(\frac{t-y}{2}\right) f'\left(\frac{y-x}{2}\right)\right] dxdy \right.$$

$$+ \text{ terms of order } \left(\frac{1}{2\bar{g}(o)}\right)^{6}\Big\}$$

All three approaches have certain advantages and disadvantages which are discussed in the chapter. The choice of which to use depends on the case at hand. It is often effective to combine the techniques for greater flexibility in analysis.

Thus far a detailed knowledge of the Auger spectrum has been assumed available. Indeed, it is possible to obtain magnified versions of the associated subsidiary maxima in the true secondary electron energy distributions. However, the question arises as to how much of this experimental spectrum is attributable to background. Further, since the measurements are obviously made external to the sample volume, one must also ask what is the effect on the distribution as the Auger electrons diffuse to the surface? The answer to these questions must rest on a theory of electron diffusion. Such a theory should additionally be able to predict the slow peak shape -- a prediction that could be used to measure the accuracy of the theory and determine the confidence with which it can be applied to Auger data analysis. In the next chapter, a general theory of electron diffusion is developed.

CHAPTER III

THE THEORY OF ELECTRON DIFFUSION

Electron diffusion is the transport and multiple scattering of excited electrons in a solid material. Such diffused electrons are termed secondary electrons if the exciting mechanism is a primary beam. Alternatively, such electrons would be identified as photo emission electrons if the exciting mechanism is a light source. In the theory presented here, the former is the case considered, although, with appropriate modifications, it should be possible to treat the latter case as well.

Theoretically the phenomenon of secondary electron emission is conveniently divided into two steps: (1) the production of the secondaries and (2) the diffusion mechanism. Whereas the factors in (1) are often reasonably well investigated, the effect of (2) is frequently overlooked or ignored. However, the highly interacting secondary electron is likely to suffer many inelastic collisions before emission as indicated by mean free path studies.[39] The result of these many scattering events is a piling-up of electrons in a very low energy range giving rise to a large, broad peak with a maximum somewhere between one and five electron volts. This has been named the "slow peak." Often, processes of interest, including the Auger phenomenon, occur in regions where the slow peak is not negligible. Further, the Auger electrons are subject to the identical loss mechanisms resulting in a distortion

of the true Auger spectrum. Consequently, any rigorous study of a secondary electron production mechanism must consider the diffusion problem.

In the first section of this chapter a general formalism is developed for the diffusion of electrons through solid matter. In the next two sections two of the important terms of the formalism are discussed: (1) the source or production of secondary electrons and (2) the processes by which they can be inelastically scattered into lower energy states. In the fourth section the effect of the secondary distribution as the electrons cross the surface boundary is treated. In the last section, for purposes of convenience, the essential results of the theory are summarized and the appropriate integrations performed so that it is possible to write an expression for the true secondary electron energy distribution.

General Formalism

In attempting to write down a dynamical equation governing the production and diffusion of secondary electrons, it is important to observe two points: (1) in any sample which is being continually bombarded by primary electrons there is expected to be a large number of internal secondary electrons; (2) because of their highly interacting nature, these secondaries will inelastically scatter frequently. These two considerations suggest that a statistical approach should be of value. Assuming each secondary electron in the crystal can be characterized by its position and momentum, a phase space ensemble is constructed in which all electrons with position between $\vec{r}$ and $\vec{r} + \vec{dr}$ and

momentum between $\vec{p}$ and $\vec{p} + \vec{dp}$ belong to that element of the ensemble labeled $\vec{r},\vec{p}$. The population density of electrons in this phase space cell at time t is designated $N(\vec{r},\vec{p},t)$ and, if the number of electrons in the cell is sufficiently large so that N can be treated satisfactorily as a continuous quantity, then N is governed by a continuity equation of the form

$$\frac{\partial N(\vec{r},\vec{p},t)}{\partial t} + \frac{\vec{p}}{m} \cdot \nabla N(\vec{r},\vec{p},t) = H(\vec{r},\vec{p},t) \tag{1}$$

where m is the electron mass and H is the non-conservative portion of the equation. Physically H represents the sources and sinks of secondary electrons within the phase space cell $\vec{r}$, $\vec{p}$ at time t.

There are three contributions to H. One, the source term $S(\vec{r},\vec{p},t)$, represents those secondary electrons which enter the phase space cell as a result of some physical excitation such as the Auger process. Another contribution to H comes about as a result of scattering. If $\lambda(\vec{p})$ is the mean free path, then

$$\frac{|\vec{p}|}{m} \quad \frac{N(\vec{r},\vec{p},t)}{\lambda(\vec{p})} \tag{2}$$

is the loss rate of the cell due to scattering. Likewise, the population can increase as a result of scattering into the cell. For this case the appropriate expression is a collision integral

$$\int \frac{|\vec{p}'|}{m} \frac{N(\vec{r},\vec{p}',t)}{\lambda(\vec{p}')} F(\vec{p},\vec{p}')\, d\vec{p}' \tag{3}$$

where $F(\vec{p},\vec{p}')$ is the probability that, given an electron at $\vec{p}'$, one will be found at $\vec{p}$ after scattering. $S(\vec{r},\vec{p},t)$ and expressions (2) and (3) constitute the three factors in H. Consequently, the dynamical equation governing electron diffusion is

$$\frac{\partial N}{\partial t} + \frac{\vec{p}}{m} \cdot \vec{\nabla} N = S - \frac{|\vec{p}|}{m} \frac{N}{\lambda} + \int \frac{|\vec{p}'|}{m} \frac{N(\vec{r},\vec{p}',t)}{\lambda(\vec{p}')} F(\vec{p},\vec{p}')\, d\vec{p}' \tag{4}$$

The rest of the treatment in this chapter will center around the proper application of this equation and its solution within the context of certain specified approximations.

Equation (4) can be simplified somewhat by considering the geometry of the experiment. The most common experimental geometry, and the one used in this work, has the primary electrons normally incident on a plane crystal surface which is considered to be of infinite extent. Further, it is consistent with the model to assume azimuthal symmetry. This is tantamount to ignoring the details of the crystal field, which is valid if the spatial dimensions of the phase space cell is large compared to atomic dimensions. This must be the case if it is assumed that there is a sufficient number of electrons in the phase space cell to treat its population density function N as a continuous variable. In

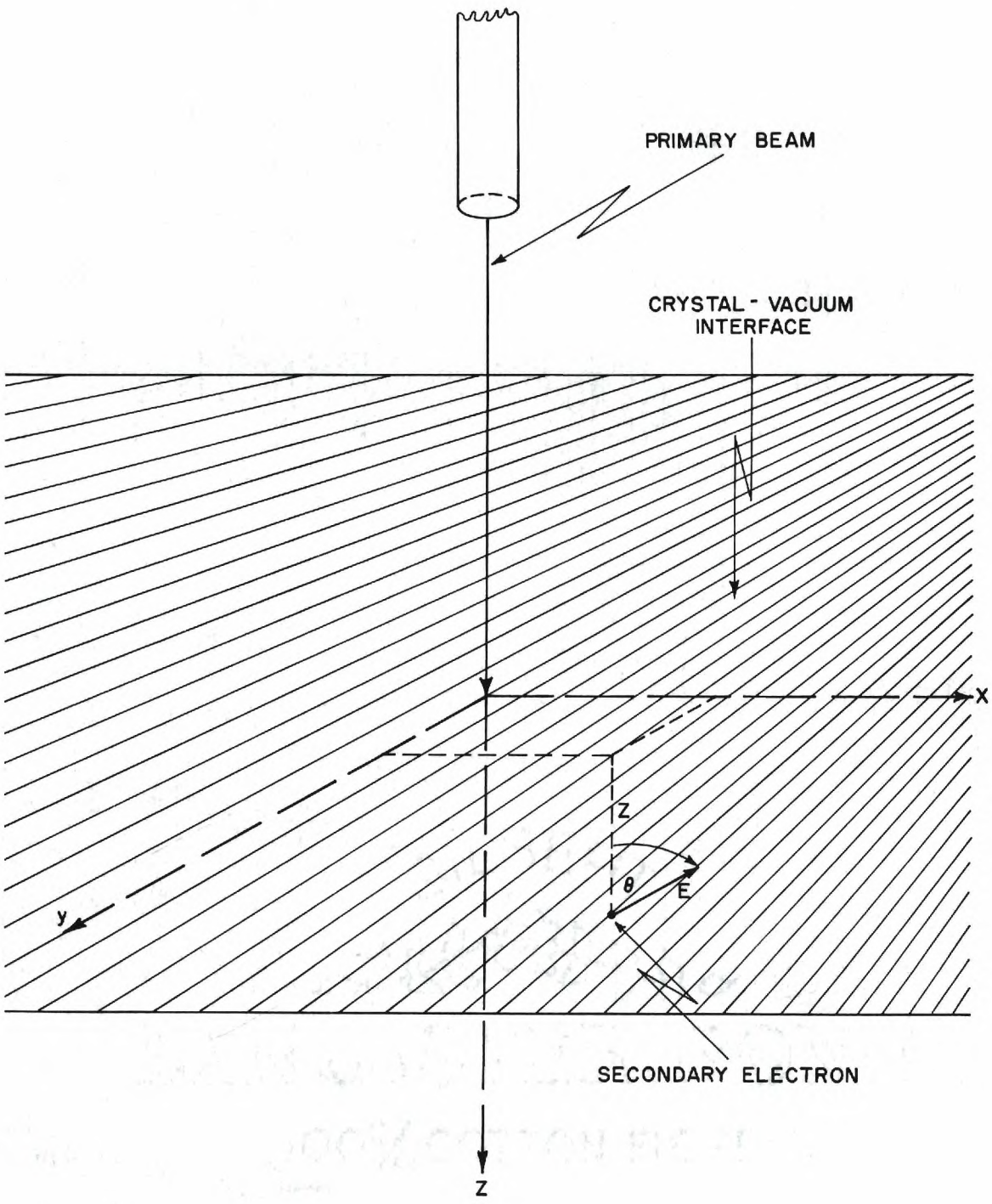

Figure 3. Typical Experimental Geometry Showing Coordinates and Energy of a Secondary Electron.

this same spirit, $\lambda(\vec{p})$ is assumed dependent only on the magnitude of $\vec{p}$ and is replaced by $l(E)$. Referring to Figure 3, the distance normal to the surface is taken as z, the angle that the momentum of the secondary electron makes with the normal as θ, and the energy as E (corresponding to the momentum magnitude $|\vec{p}|$). Thus, in the steady state case, equation (4) reduces to

$$-\frac{|\vec{p}|}{m}\nabla N(z, \cos\theta, E)\cos\theta = S(z, \cos\theta, E) - \frac{|\vec{p}|}{m}\frac{N(z, \cos\theta, E)}{l(E)} \qquad (5)$$

$$+\iint \frac{|\vec{p}'|}{m}\frac{N(z, \cos\theta', E')}{l(E')}F(\theta,E,\theta',E')dE'd\theta'.$$

The population function N, the source term S, and the scattering probability function F are now expanded in Legendre Polynomials.

$$N(z, \cos\theta, E) = \frac{1}{4\pi}\sum_{l=0}^{\infty}(2l+1)\,N_l(z,E)\,P_l(\cos\theta) \qquad (6)$$

$$S(z, \cos\theta, E) = \frac{1}{4\pi}\sum_{l=0}^{\infty}(2l+1)\,S_l(z,E)\,P_l(\cos\theta)$$

$$F(\theta, E, \theta', E') = F(\cos\Theta, E, E') = \frac{1}{4\pi}\sum_{l=0}^{\infty}(2l+1)\,F_l(E, E')\,P_l(\cos\Theta)$$

where Θ is the angle between $\vec{p}$ and $\vec{p}'$.

These expansions prove to be not only mathematically convenient but also physically meaningful. Expansion in Legendre Polynomials serves to segment the various functions of interest into components dependent on their angular distribution. Thus $N_0(z,E)$, for instance, is that portion of the internal secondary electron energy distribution which is isotropic; $N_1(z,E)$ belongs to the Cos θ group and so on. By investigating the population of each group inferences can be made concerning any preferential angular distribution.

The orthogonality of the Legendre Polynomials can be used to advantage. After substituting equations (6) into (5) both sides of (5) are multiplied by $P_k(\text{Cos}\,\theta)$ and integrated over the solid angle $\sin\theta d\theta d\varphi$. The result is

$$- \frac{|\vec{p}|}{m} \sum_{\ell} \frac{\partial N_\ell}{\partial z} (2\ell + 1) \int \frac{1}{2k + 1} [kP_{k-1} + (k+1)\, P_{k+1}]\, P_\ell \, d\Omega \qquad (7)$$

$$= 4\pi S_k - 4\pi \frac{|\vec{p}|}{m} \frac{N_k}{\ell}$$

$$+ \iiint dE'\, d\Omega'\, d\Omega \frac{|\vec{p}'|}{m\ell} \sum_{\ell} \sum_{i} (2\ell + 1)\, (2i + 1)\, N_\ell(z,E')F_i(E,E')P_\ell(\text{Cos}\,\theta')$$

$$P_i(\text{Cos}\,\Theta)\, P_\ell(\text{Cos}\,\theta)$$

If the substitution $\psi_k = \frac{|p| N_k}{m\ell(E)}$ is made and the following addition identity used,

$$P_i(\cos\Theta) = P_i(\cos\theta')\,P_i(\cos\theta) + 2\sum_{m=1}^{i}\frac{(i-m)!}{(i+m)!}P_i^m(\cos\theta)\,P_i^m(\cos\theta)\cos(\varphi'-\varphi)$$

where $P_i^m(\cos\theta)$ are the associated Legendre functions, the diffusion equation finally becomes

$$\psi_k(z,E) = \frac{\ell(E)}{2k+1}\left[k\frac{\partial\psi_{k-1}}{\partial z} + (k+1)\frac{\partial\psi_{k+1}}{\partial z}\right] \tag{8}$$

$$+ S_k(z,E) + \int_E^\infty F_k(E,E')\,\psi_k(z,E')dE'$$

Equations (8) are a set of coupled integro-differential equations which are in general very cumbersome. Note, however, that if the z dependence is rather weak the equations uncouple and become much simplified. In the current work this is probably a reasonable approximation. Because of the heavy screening generally present in the materials studied, one would expect the scattering potentials involved in the electron diffusion to be effective only over short distances. Such an argument was used in the introduction of the transition density earlier. Consequently, the volume within the screening length of the surface is much less than the total volume of interest. It is then likely that little error will be made if the z-dependence in (8) is ignored. Wolff,[17] using the technique of Weymouth,[40] has solved (8) for simple choices of S and F and found that the solutions differ very little from that of the z-independent equations. Thus, in this approximation, equations (8)

become

$$\psi_k(E) = \int_E^\infty F_k(E,E')\ \psi_k(E')\ dE' + S_k(E) \tag{9}$$

Equations (9) are solved by assuming solutions of the form

$$\psi_k(E) = \int_{E_a}^{E_b} G_k(E,E'')\ S_k(E'')dE'' \tag{10}$$

where G_k is a Green's function. By substituting (10) into (9) a condition on the form of G_k can be obtained.

$$G_k(E,E'') = \delta(E-E'') + \int_E^\infty G_k(E,'E'')\ F_k(E,E')dE' \tag{11}$$

where $\delta(E-E'')$ is the familiar Dirac distribution. Note that the Green's function depends only on the scattering function $F_k(E,E')$. Hence once the F_k's are enunciated, the Green's functions can be found and used in (10) with any applicable source function to derive the secondary distribution.

The general formalism is developed; however, an analytical investigation of the appropriate source functions S(E) and the scattering or loss functions F(E,E') still remains. This is the context of the next

two sections. In the section pertaining to the loss mechanisms the required Green's functions are obtained.

Secondary Electron Source Functions

In order to use equation III-10 to obtain the secondary electron distribution interior to the crystal the appropriate source terms and Green's functions, expressed in Legendre polynomial expansions, must be known. In this section the former are discussed.

There are two important mechanisms which give rise to secondary electrons. From the work of the last chapter it is clear that the Auger process is a source of secondary electrons. Another process, and perhaps the more important, is single electron excitations resulting from electron-electron collisions. In this case the primary beam interacts in a Coulombic fashion with the crystal electrons and some are excited to available states above the fermi level leaving a hole in the fermi sea. In semiconductors such a process is often called pair production because the hole can, in many respects, be treated like a positive electron. Pair production and the Auger process are the only two mechanisms of secondary electron creation that will be considered.

The Auger source function was actually derived in the last section. It is the self-convolution of the transition density. However, this expression gives no information as to the absolute magnitude of the effect. Further, the true shape of the Auger distribution is unknown, even empirically, because of the effect of electron diffusion. These troublesome points not withstanding, the calculation will be continued assuming that the true distribution f(E) is known. In the applications the amplitude

is empirically estimated and the true distribution is adjusted so that, after the result of diffusion, experimental agreement is obtained. Further, it is assumed that the Auger distribution is spherically symmetric in the laboratory frame of reference. That this is the case may seem reasonable by recalling that the Auger mechanism is a two-electron process. The Auger electron has no way of "knowing" in which direction the primary beam, i.e., the z axis, is oriented. With no direct experimental information available, isotropic production is probably a reasonable choice.

The calculation of the source function for pair production is more involved. The correct calculation was actually first done by Streitwolf[16] in 1959. However, the derivation is repeated briefly on the following pages. This is done for several reasons: (1) the result is important to the work presented here and a knowledge of the origin of the expression is valuable, (2) Streitwolf's paper is in German and an English translation is not conveniently available, and (3) Streitwolf's presentation and notation are not ideally suited for the current application.

Summary of Streitwolf's Energy Excitation Function Calculation

Suppose that $P(\vec{k},\vec{k}',\vec{p},\vec{p}')$ is the transition probability per unit time and volume that a primary electron of momentum $\vec{p}$ will interact with a crystal electron of momentum $\vec{k}$ and will be found after scattering with momenta $\vec{p}'$ and $\vec{k}'$ respectively. The excitation function of crystal electrons to momentum $\vec{k}'$ is then given by

$$S'(k') = 2 \int_{\substack{\text{occupied} \\ \text{states}}} d^3\vec{k} \int_{\substack{\text{unoccupied} \\ \text{states}}} d^3\vec{p}' \; P(\vec{k},\vec{k}',\vec{p},\vec{p}') \tag{12}$$

where the factor of two takes into account spin degeneracy. If only the final energy of the excited crystal electron is of interest, then one has for the source function

$$S(E') = k'^2 \frac{dk'}{dE'} \int d\Omega_{\vec{k}'} \, S'(\vec{k}') \tag{13}$$

where $E' = E(k')$.

The hamiltonian for this process is

$$H = H_0 + H_1 = H_0 + \frac{c^2}{\epsilon|\vec{R}-\vec{r}|} e^{-\lambda|\vec{R}-\vec{r}|} \tag{14}$$

with

$$H_0 = -\frac{\hbar^2}{2m} (\nabla_{\vec{R}}^2 + \nabla_{\vec{r}}^2) + V(\vec{r})$$

λ = screening parameters

ϵ = dielectric constant

where $\vec{R}$ and $\vec{r}$ are the position vectors of the primary and crystal electrons respectively. The wave functions for the H_0 Hamiltonian are expressed

$$|\vec{k},\vec{p}\rangle = \psi_{\vec{k}}(\vec{r})\ \psi_{\vec{p}}(\vec{R}) \tag{15}$$

where

$$\psi_{\vec{p}}(\vec{R}) = (2\pi)^{-3/2}\ e^{i\vec{p}\cdot\vec{R}}$$

and

$$\psi_{\vec{k}}(\vec{r}) = (2\pi)^{-3/2}\ e^{i\vec{k}\cdot\vec{r}}\ U_{\vec{k}}(\vec{r})$$

The term $U_{\vec{k}}(\vec{r})$ is the familiar Bloch function. The transition probability as given by first order time dependent perturbation theory has the form

$$P = \frac{2\pi}{\hbar}\ |\langle\vec{k}',\vec{p}'|H_1|\vec{k},\vec{p}\rangle|^2\ \delta(E_{\vec{k},\vec{p}'} - E_{\vec{k},\vec{p}}) \tag{16}$$

The matrix element, after performing the R integration, is

$$\langle\vec{k}',\vec{p}'|H_1|\vec{k},\vec{p}\rangle = (2\pi)^{-6}\ \frac{4\pi e^2}{\epsilon(q^2+\lambda^2)} \int_{\substack{\text{crystal}\\\text{volume}}} U^*_{\vec{k}'}\ U_{\vec{k}}\ e^{i(\vec{k}-\vec{k}'+\vec{q})\cdot\vec{r}}\ d\vec{r}^3$$

$\vec{q} = \vec{p}-\vec{p}'$ = momentum transferred

The Bloch functions are now expanded in plane waves (Fourier series)

$$U_{\vec{k}'}^{*} U_{\vec{k}} = \sum_{\vec{t}} I(\vec{k}',\vec{k};\vec{t})\ e^{2\pi i \vec{t} \cdot \vec{r}}$$

in which

$$I(\vec{k}',\vec{k};t) = \frac{1}{V_R} \int_{V_R} U_{\vec{k}}^{*} U_{\vec{k}}\ e^{-2\pi i \vec{t} \cdot \vec{r}}\, d^3\vec{r} \qquad (17)$$

V_R = volume of reciprocal lattice unit cell

Using these expressions, (16) becomes

$$P = \frac{me^4}{\epsilon^2 2\hbar^2 \pi^3 p (q^2+\lambda^2)^2} \sum_{\vec{t}} |I|^2\, \delta^3(\vec{k} - \vec{k}' + \vec{q} + 2\pi\vec{t})\ \delta(E_{\vec{k}',\vec{p}'} - E_{\vec{k},\vec{p}}) \qquad (18)$$

Expression (18) has been normalized to the primary current density

$$j_p = (2\pi)^{-3} \frac{\hbar p}{m}$$

Using (18) and (12) the source function (13) becomes

$$S(E') = \frac{m^2e^4}{\epsilon^2\pi^3\hbar^4p} \sum_{\vec{t}} \int d^3\vec{k} \int d^3\vec{p}' \int d\Omega_{\vec{k}'} \frac{|I|^2}{(q^2+\lambda^2)^2} \delta^3(\vec{k}-\vec{k}'+\vec{q}+2\pi\vec{t}) \, \delta(E_{\vec{k}'},\vec{p}'-E_{\vec{k}},\vec{p}) \tag{19}$$

Performing the integration over the final primary momentum p' one obtains

$$S(E') = \frac{2m^3e^4k'}{\epsilon^2\pi^3\hbar^6p} \sum_{\vec{t}} \int\int d^3\vec{k} d\Omega_{k'} \frac{|I|^2}{(q^2+\lambda^2)^2} \delta(k'^2+p'^2-k^2-p^2)$$

For the integration over the solid angle $d\Omega_{k'}$, it is convenient to define a new quantity

$$\vec{C}_{\vec{t}} = \vec{p} + \vec{k} + 2\pi\vec{t}$$

Using this as the polar axis, the integration over the polar angle can be performed and yields (see Appendix A)

$$S(E') = \frac{m^3e^4}{\epsilon^2\pi^3\hbar^6p} \sum_{\vec{t}} \int \frac{d^3\vec{k}}{|\vec{C}_{\vec{t}}|} \int_0^{2\pi} \frac{|I|^2}{(q^2+\lambda^2)^2} d\varphi \tag{20}$$

In order to proceed it is necessary to set $I = 1$, $\vec{t} = 0$, and $\lambda = 0$. For the $\vec{t} = 0$ case, it is easy to see from (17) that I is equal to or close to unity when (1) $\vec{q}$ is small or (2) the crystal electrons are assumed free. Even if these two requirements do not strictly hold, I

may still be close to unity. In (17) the excited state can be reasonably assumed to be of plane wave form. Essentially all that is ignored then is the dependence of the integral on $\vec{k}$. Since the integration is over a reciprocal cell in which the function is basically oscillatory, the assumption of constant I with value one should not introduce serious errors. Further, the $\vec{t} \neq 0$ case (phonon assisted processes) is generally ignored because, as shown by Streitwolf, it contributes less than $\frac{1}{2}$ per cent to the total excitation function. A similar argument holds for $\lambda = 0$. The per cent change in the result by varying λ from zero to a reasonable screening length is small. This however is not true in the $\vec{t} \neq 0$ case.

With these values for I, $\vec{t}$, and λ the azimuthal integration in (20) yields (see Appendix B)

$$S(E') = \frac{2m^2e^4}{\epsilon^2\pi^2\hbar^6 p} \int d^3\vec{k}\, \frac{p^2(k^2+k'^2) - 2(\vec{p}\cdot\vec{k})^2 + k^2(k^2-k'^2)}{(k'^2-k^2)^3|\vec{p}-\vec{k}|^3}$$

The final integration over the initial crystal electron states (the fermi sphere) can be done in closed form (see Appendix C). Thus

$$S(E') = \frac{e^4 k_F^3}{\epsilon^2 3\pi E_p (E' - E_F)^2} \tag{21}$$

is the desired energy excitation function. A similar result has been obtained by Baroody,[15] and Dekker and Van der Ziel[11] but both had to approximate that $\vec{k} \ll \vec{p}$. No such approximation is required in (21).

This completes the summary of Streitwolf's calculation.

Angular Dependence

The angular dependence in the excitation function can be obtained by putting (18) into (12) and doing the indicated integrations. The result for I = 1, $\vec{t} = 0$ and $\lambda = 0$ is

$$S'(\vec{k}') = \frac{m^2 e^4}{\pi^2 \hbar^4 p} \frac{p^2 k'^2 - (\vec{p}\cdot\vec{k}')^2 - (k'^2 - k_F^2)(\vec{p}-\vec{k})^2}{|\vec{p}-\vec{k}'|^3 (k'^2 - k_F^2)^2} \tag{22}$$

$$\text{for} \quad |\vec{k}'\cdot(\vec{p}-\vec{k}')| \leq k_F |\vec{p}-\vec{k}'|$$

$$= 0 \text{ otherwise}$$

The stipulation on the relation above indicates that S′ must be non-negative. Further, the integration of this equation over the appropriate angles must yield (21). For the polar angle on the interval $(0,\pi)$ S′ is non-negative between the zeroes of the numerator. Thus the angular excitation must be

$$S(E',\theta) = \frac{e^4 k_F^3}{3\pi\epsilon^2 E_p (E'-E_F)} \frac{a + b\cos\theta - \cos^2\theta}{\frac{1}{6}(b^2+4a)^{3/2}} \tag{23}$$

where

$$a = \frac{k_F^2}{k'^2} - \frac{k'^2 - k_F^2}{p^2}$$

$$b = \frac{2(k'^2 - k_F^2)}{pk'}$$

Note that the integration of this function over $\sin\theta\, d\theta$ between the zeroes $\cos\theta = \frac{b + \sqrt{b^2+4a}}{2}$ and $\cos\theta = \frac{b - \sqrt{b^2+4a}}{2}$ yields (21). $S(E',\theta)$ is now expanded in Legendre polynomials.

$$S_0(E') = \frac{e^4 k_F^3}{3\pi\epsilon^2 E_p (E'-E_F)^2} \tag{24}$$

$$S_1(E') = S_0(E') \frac{2b(a - \frac{b^2}{4})}{b^2 + 4a}$$

$$S_2(E') = S_0(E') \frac{6[\frac{a^2}{5} - \frac{a}{3} + \frac{ab^2}{2} + \frac{3b^3}{8} - \frac{3b^4}{10} - \frac{b^2}{12}]}{b^2 + 4a}$$

$$\vdots$$

$$S(E',\theta) = \frac{1}{4\pi} \sum_{\ell=0}^{\infty} (2\ell + 1)\, S_\ell(E')\, P_\ell(\cos\theta)$$

These equations for the coefficients in the expansion of the angular energy excitation function are extremely complicated, and except for $S_0(E')$, their use in equation III-10 is mathematically

prohibitive. They can, however, be simplified by considering two very important cases. These are (1) $p \gg k' \sim k_f$ (low energy secondaries) and (2) $p \gg k' \gg k_f$ (high energy secondaries).

Case 1: Low Energy Secondaries. In this case, it is easy to show that

$$a \rightarrow 1$$

$$b \rightarrow 0$$

Therefore,

$$S_1(E') \rightarrow 0 \tag{25}$$

$$S_2(E') \rightarrow S_0(E')(-1/5)$$

Case 2: High Energy Secondaries. In the limit of high energy secondary electrons the parameters a and b both tend to zero. Therefore,

$$S_1(E') \rightarrow 0 \tag{26}$$

$$S_2(E') \rightarrow S_0(E')(-1/2)$$

The contributions from the higher order coefficients are

ignored. It should be mentioned that the results (25) are the same as those used by Stolz.[19] In the high energy case, however, equations (26) differ from those of Guba[20] and Grinchak[21] who considered (22) incorrectly.

As has already been stated these two sets of source functions are used in equation III-10 to obtain the internal secondary distribution. One set, equations (25), is used for low energy secondaries and the second set, equations (26), is used for high energies. Thus the limits in equation III-10 for the former case are $E_a = E_F$, the fermi energy, to $E_b = E_m$, some upper bound. This upper bound is set at 100 ev or the primary energy, whichever is smaller. In the latter case, E_a = 100 ev and E_b = 150 ev or $E_p/2$, whichever is larger. This case is not considered when $E_p < 150$ ev.

At this time the choices of the limits may appear a bit arbitrary other than the fact that they correspond roughly to the E' energies mentioned in (25) and (26). The choices will seem more concrete after a discussion of the appropriate scattering and loss mechanisms - the topic of the next section.

Scattering and Loss Mechanism Green's Functions

In the last section, the appropriate source functions to be used in equation III-10 were discussed. In this section the loss mechanisms will be considered and the corresponding Green's functions will be obtained. The Green's functions are found by solving equation III-11 for a particular choice of the scattering function $F_k(E,E')$. The applicable scattering functions are therefore discussed first.

There are several ways by which a secondary electron can lose energy as it cascades through the crystal. One way is clearly pair production. In this case a secondary electron has a "collision" with a crystal electron, exciting it to some level in the conduction band, and thereby loses some energy and changes direction - i.e., it is scattered into a new momentum state. There is, in addition, another loss mechanism that turns out to be of significant importance in the case of semiconductors. This is plasmon creation. A secondary electron of sufficient energy can contribute to the collective oscillations of the valence electron by plasmon excitation and be subsequently scattered into a new momentum state. It is this method, as shall be seen in the applications, which actually predominates in semiconductors and leads to satisfactory theoretical explanation of the observed distributions.

An investigation of the screened Coulomb interaction reveals that, in the case of electron-electron collisions, the scattering is spherically symmetric in the center of mass system up to about 100 ev (for an appropriately chosen cutoff distance) after which it is more accurately described by Rutherford scattering.[17] It is clear that the modification of the scattering symmetry from a spherical behavior to a Rutherford behavior is a smooth monotonic transition. However, such an ideal description is very difficult to achieve theoretically. Therefore, a cutoff energy ($\sim$ 100 ev) is defined above which the scattering is strictly Rutherford and below which the scattering is strictly spherical.

The case of low energy ($<$ 100 ev) initial secondaries is

considered first. For the propositon of pure spherical scattering the problem reduces to an exercise in kinematics. Assuming the crystal electron is at rest with respect to a scattering particle of energy E′, the energy of the secondary after the interaction is given strictly by

$$E = E' \cos^2 \Theta \tag{27}$$

where Θ is the angle between the initial and final momentum vectors. Thus the scattering function is given by

$$F(\cos \Theta, E, E') = \frac{2}{4\pi} \delta(E - E' \cos^2 \Theta) 4 \cos \Theta \tag{28}$$

The factor $4 \cos \Theta$ is the Jacobian of the transformation from the center of mass to laboratory angles. The normalization $2/4\pi$ is such that

$$\int_0^{E'} \int_0^{2\pi} \int_0^{\pi/2} F(\cos \Theta, E, E') \sin \Theta \, dE d\Theta d\varphi = 2 \tag{29}$$

The normalization to two instead of unity, first recognized by Wolff, is crucial and amounts to a cognizance of the fact that for every particle which scatters, there are two electrons in the cascade after the collision. This is termed electron multiplication. As required by the formalism, $F(\cos \theta, E, E')$ must be expanded in Legendre polynomials. Thus

$$F_\ell(E, E') = \int d\Omega F(\cos \Theta, E, E') \, P_\ell(\cos \Theta) \tag{30}$$

$$= 2\pi \int_0^{\pi/2} \frac{2}{4\pi} \delta(E-E' \cos^2\Theta)\, 4 \cos\Theta\, P_\ell(\cos\Theta) \sin\Theta\, d\Theta$$

$$= \frac{2}{E'} P_\ell\left(\sqrt{\frac{E}{E'}}\right)$$

This is the result which must be used in equation III-11 to obtain the Green's function. With the above choice for $F_\ell(E,E')$, III-11 is solved by use of the Mellin transform. The results for $\ell = 0$ and $\ell = 2$ (the only non-vanishing cases being considered) are (see Appendix D)

$$G_o(E,E'') = \begin{cases} 2\dfrac{E''}{E^2} + \delta(E-E'') & ;\quad E'' \geq E \\ 0 & ;\quad E'' < E \end{cases} \tag{31}$$

$$G_2(E,E'') = \begin{cases} \dfrac{2}{\sqrt{E''E}} \cos\left[\dfrac{\sqrt{3}}{2} \ln\left(\dfrac{E''}{E}\right)\right] + \delta(E-E'') & ;\quad E'' \geq E \\ 0 & ;\quad E'' < E \end{cases}$$

With these Green's functions, integration of equation III-10 is essentially all that need be done to obtain an expression for the internal secondary electron energy distribution in the case of low energy secondaries scattered by crystal electrons. This operation, however, will be postponed until all contributions to the secondary distribution can be

included.

The above Green's functions, which are based on the assumption of pure spherical scattering, are not applicable if the secondary electron is energetic enough for the scattering to be considered Rutherford. Consequently, instead of (28), for this case the correct scattering function is given by

$$F(\cos\Theta, E, E') = \frac{\alpha^2}{E'^2} \frac{\cos\Theta}{\sin^4\Theta} \delta(E - E'\cos^2\Theta) \tag{32}$$

where Θ, the laboratory angle, has the same significance as before. The quantity α is equal to $e^2/2$.

The expression (32) is not yet normalized. If one attempts to do so by means of equation (29), the integral is found to diverge. This problem is overcome by restricting consideration to large energy losses per collision. Actually, this is probably not a serious restriction since those electrons which lose large amounts of energy and are scattered into low energy states are just those electrons which contribute to the slow peak. Investigation of the delta function in (32) indicates that this case corresponds to large angle scattering ($\Theta \sim \frac{\pi}{2}$). Expanding $\sin^{-4}\Theta$ in this limit and keeping only the first two terms, (32) becomes, after proper normalization

$$F(\cos\Theta, E, E') = \frac{1}{\pi} \cos\Theta \, (1 + 2\cos^2\Theta) \, \delta(E - E'\cos^2\Theta) \tag{33}$$

Proceeding in the by-now-standard way, the Legendre polynomial expansion coefficients of (33) are

$$F_\ell(E,E') = \frac{1}{E'}\left(1+2\frac{E}{E'}\right) P_\ell\left(\sqrt{\frac{E}{E'}}\right) \tag{34}$$

This expression is put in equation III-11 and the Green's function solved for by the Mellin transform.

$$G_o(E,E'') = \begin{cases} \dfrac{1}{E\sqrt{2}}\left[4\sinh\left(\sqrt{2}\,\ln\dfrac{E''}{E}\right) + 3\sqrt{2}\cosh\left(\sqrt{2}\,\ln\dfrac{E''}{E}\right)\right] \\ \qquad + C_o\delta(E-E'') \;; \quad E'' \geq E \\ 0 \;; \quad E'' < E \end{cases} \tag{35}$$

$$C_o = \frac{2}{3\sqrt{2}-2}$$

$$G_2(E,E'') = \begin{cases} \dfrac{1}{E''}\left[\dfrac{4}{5}\left(\dfrac{E}{E''}\right)^{1.15} + \left(\dfrac{E''}{E}\right)^{0.6}\left\{5.8\cos\left(\ln\left(\dfrac{E''}{E}\right)^{0.7}\right)\right.\right. \\ \qquad \left.\left. - 3.8\sin\left(\ln\left(\dfrac{E''}{E}\right)^{0.7}\right)\right\}\right] + C_2\delta(E-E'') \;; \quad E'' \geq E \\ 0 \;; \quad E'' < E \end{cases}$$

$$C_2 = \frac{3.63 - 1.6 \cosh 1.4\pi}{(3.63 - 1.6 \cosh 1.4\pi)^2 + 0.14^2 \sinh 1.4\pi}$$

These are the Green's functions to be used in equation III-10 for high energy secondaries (> 100 ev). Thus for single electron or pair production type losses, a secondary is scattered by successive Rutherford type collisions (use (35) and (26) in (10)) until it falls below 100 ev at which time it participates in the cascade by spherically symmetric type collisions (use (31) and (25) in (10)).

Attention is now directed to the situation of secondary scattering due to plasmon creation. As was mentioned earlier, this turns out to be an important contribution as might be expected if mean free path lengths are considered. Based on Quinn's[41] expression for the mean free path to plasmon scattering in the free electron approximation, it appears that for many semiconductors the plasmon mean free path is at least an order of magnitude less than that for pair production. The effective cross section for plasmon production has been calculated by D. Pains[42] for the case of small angle scattering (or $E' \gg \hbar w_p$),

$$d\sigma = \frac{d\Omega}{2\pi N \sigma_o} \frac{E' - E}{E'\left[\sin^2 \Theta + \left(\frac{E'-E}{2E'}\right)^2\right]} \qquad (36)$$

where Θ is the scattering angle. The scattering function is then

$$F(\mu_s \Theta, E, E') = \frac{(E'-E)\,\delta(E-E'\mu_s^2\Theta)}{2\pi\, 0.9\, E'\left[\sin^2\Theta + \left(\frac{E'-E}{2E'}\right)^2\right]} \tag{37}$$

where the normalization is now unity because electron multiplication does not apply. The coefficients of the expansion of the scattering function (37) are obtained in the form

$$F_\ell(E,E') = \frac{2\cdot 2\, P_\ell\left(\sqrt{\frac{E}{E'}}\right)}{E'\sqrt{\frac{E}{E'}}\left(5-\frac{E}{E'}\right)} \tag{38}$$

The solution of III-11 by means of the Mellin transform results in the following expression for the Green's functions.

$$G_o(E,E'') = \begin{cases} \frac{1}{E''}\left[18.2\left(\frac{E''}{E}\right)^{5.5} - 0.58\left(\frac{E''}{E}\right)^{-1.1}\right] \\ \qquad + 0.25\,\delta(E-E'') \quad ; \quad E'' \geq E \\ 0 \quad ; \quad E'' < E \end{cases} \tag{39}$$

$$\frac{1}{E''}\left[42.7\left(\frac{E''}{E}\right)^{3.2} - 7.1\left(\frac{E''}{E}\right)^{1.4} - 0.28\left(\frac{E''}{E}\right)^{-1.7}\right] + 0.13\,\delta(E-E'') \quad ; \quad E'' \geq E$$

$$G_2(E,E'') = \qquad\qquad (36)$$

$$0 \quad ; \quad E'' < E$$

Because of the requirement in (36) that $E' \gg \hbar w_p$, these Green's functions should strictly be used only for high energy secondaries. However, if the correct source function is used, satisfactory agreement can be obtained for secondaries with energy as low as $2\hbar w_p$.

In this section the means by which secondary electrons can lose energy have been discussed. Scattering functions and their corresponding Green's functions are now established. Thus, everything that is needed to calculate the internal secondary electron energy distribution N(E) is available. However, experimentally the distribution is measured external to the sample interior and it might be anticipated that the distribution is modified as it crosses the surface boundary. This is indeed the case and prompts the derivation of an expression for the external distribution in the next section.

Escape Across the Surface Boundary

In the previous sections of this chapter the necessary formalism to predict theoretically the internal secondary electron distribution has been enunciated. However, experimental observations are clearly of the external distribution. Such an experimentally measurable distribution can be related to a good approximation to the internal distribution

by taking into account the surface barrier created by the presence of a work function.

Imagine a perfectly smooth planar surface being approached from within by an electron of momentum $\vec{p}$. As the electron crosses the boundary, the normal component of momentum will be modified by an amount depending on the work function. The tangential component, however, is continuous. If E is the energy of the electron interior to the crystal and E′ its energy externally, then the two following relations must hold

$$E' = E - W \tag{40}$$

$$E' \sin^2\beta = E \sin^2\theta \tag{41}$$

where W is the energy level of the work function, θ and β the angles the electron makes with the normal internally and externally respectively. It follows then that

$$\cos^2\beta = \frac{E \cos^2\theta - W}{E - W} \tag{42}$$

and hence

$$\sin \beta d\beta = \frac{E}{E - W} \frac{\cos \theta}{\cos \beta} \sin \theta d\theta \, . \tag{43}$$

Now the external distribution $j(E',\beta)$ is related to the internal

distribution $N(E,\theta)$ by the equation

$$j(E',\beta)dE' \sin\beta d\beta = N(E,\theta)\sqrt{\frac{2E}{m}}\,\cos\theta\, dE \sin\theta\, d\theta . \qquad (44)$$

This is easily seen by considering the fact that $N(E,\theta)$ is the number of secondaries per unit volume in the crystal and the factor $\sqrt{\frac{2E}{m}}\cos\theta$, which is just the normal component of velocity, takes care of the rate at which the secondaries reach the surface. Using (44) and (43) it is possible to write the energy-angular distribution law for external secondaries,

$$\frac{j(E',\beta)}{j(E',0)} = \frac{N(E,\theta)}{N(E,0)}\cos\beta \qquad (45)$$

with

$$\cos\beta = \sqrt{1 - \frac{E}{E-W}\sin^2\theta} \quad . \qquad (46)$$

Not all secondaries reaching the surface can contribute to the external distribution. This is because there is a critical angle θ_o, depending on the energy and less than $\pi/2$, for which electrons striking the surface at a greater angle of attack can not overcome the surface potential barrier. The critical angle θ_o is determined from (40) by setting $\beta = \pi/2$; thus

$$\cos\theta_o = \frac{W}{E} . \tag{47}$$

Recognition of this limiting factor is important when integrating over all angles to get the total external contribution at energy E′. Recall that

$$N(E,\theta) = \frac{1}{4\pi} \sum_{\ell=0}^{\infty} (2\ell + 1)\, N_\ell(E)\, P_\ell(\cos\theta)$$

Thus the external distribution takes the form

$$j(E',\beta)dE' \sin\beta d\beta = \frac{1}{4\pi}\sqrt{\frac{2E}{m}} \sum_{\ell=0}^{\infty} (2\ell+1)\, N_\ell(E)\, P_\ell(\cos\theta) \cos\theta \sin\theta\, d\theta\, dE$$

If J(E′) is the total external contribution in the energy interval E′,E′+dE′, then

$$J(E') = \frac{1}{4\pi}\sqrt{\frac{2E}{m}} \sum_{\ell=0}^{\infty} (2\ell+1)\, N_\ell(E) \int_0^{2\pi} \int_0^{\theta_o} P_\ell(\cos\theta) \cos\theta \sin\theta\, d\theta d\varphi \tag{48}$$

$$= \frac{1}{2}\sqrt{\frac{2(E'+W)}{m}} \sum_{\ell=0}^{\infty} (2\ell + 1)\, N_\ell(E'+W) \int_{\sqrt{\frac{W}{E'+W}}}^{1} X\, P_\ell(X)dX$$

Since it has been established that $\ell = 0$ and $\ell = 2$ are the only non-vanishing cases being considered, (48) can be written more explicitly. Consider the integral on the right

$$\ell = 0: \quad \int_{\sqrt{\frac{W}{E'+W}}}^{1} X\, P_0(X)dX = \tfrac{1}{2}\,\frac{E'}{E' + W}$$

$$\ell = 2: \quad \int_{\sqrt{\frac{W}{E'+W}}}^{1} X\, P_2(X)dX = \tfrac{1}{4}\left[\tfrac{3}{2}\left(1 - \frac{W^2}{(E'+W)^2}\right) - \frac{E'}{E' + W}\right]$$

The experimentally observable distribution thus takes the form

$$J(E') = \tfrac{1}{4}\sqrt{\frac{2(E'+W)}{m}}\left\{\frac{E'}{E'+W}\, N_0(E'+W)\right. \tag{49}$$

$$\left. - \tfrac{5}{2}\, N_2(E'+W)\left[\tfrac{3}{2}\left(1 - \frac{W^2}{(E'+W)^2}\right) - \frac{E'}{E'+W}\right]\right\}$$

Hence, once N_0 and N_2 are found the external secondary electron energy distribution is obtained from (49). N_0 and N_2 are secured by solving III-10 with the appropriate source and Green's functions. In the next section the theory developed throughout this chapter is reviewed and summarized for future reference. Integration of equation III-11 for the source and Green's functions discussed in the previous two sections is also carried out.

Summary and Integration of Distribution Equations

The electron diffusion formalism is based on a Boltzmann transport equation of the following form:

$$\frac{\partial N(\vec{r},\vec{p},t)}{\partial t} + \frac{\vec{p}}{m} \cdot \nabla N_{(\vec{r},\vec{p},t)} = \tag{4}$$

$$- \frac{|\vec{p}|N(\vec{r},\vec{p},t)}{m} + S(\vec{r},\vec{p},t) + \int |p'| \frac{N(\vec{r},\vec{p}',t)}{m\lambda(p')} F(\vec{p},\vec{p})d\vec{p}$$

The first term on the right describes the rate of secondary loss from the phase space cell at $\vec{r},\vec{p}$ at time t as a result of scattering; the second describes the rate of secondary creation; and the third the rate of gain due to scattering into the cell. $F(\vec{p},\vec{p}')$ is the scattering function giving the probability that an electron at $\vec{p}'$ will be found at $\vec{p}$ after a collision.

Equation (4) can be simplified somewhat if attention is restricted to the steady state case and if the common geometry of electrons incident normally on a planar surface is included. The resulting expression is then expanded in spherical harmonics, and, by including the previously mentioned assumptions concerning the crystal field and surface effects, equation (4) becomes

$$\psi_k(E) = \int_E^\infty F_k(E,E')\ \psi_k(E')dE' + S_k(E);\ k = 0,\ 1,\ 2,\ \ldots \tag{9}$$

where

$$\psi_k(E) = \frac{|\vec{P}| N_k(E)}{m\ell(E)} \quad .$$

$F_k(E,E')$ and $S_k(E)$ are the expansion coefficients of the scattering and source functions respectively. Solutions to this integral equation are of the form

$$\psi_k(E) = \int G_k(E,E'') \, S_k(E'') \, dE'' \tag{10}$$

with the Green's functions condition

$$G_k(E,E'') = \delta(E-E'') + \int_E^\infty G_k(E',E'') \, F_k(E,E') \, dE' \tag{11}$$

Solution (10) then depends on the source function directly and the scattering mechanism through the Green's function condition. The various source and scattering mechanisms appropriate to the present work are as follows:

Source Functions

1. Single electron excitations
2. Auger electrons

Scattering Functions

1. Single electron collisions
   a. low energy (< 100 ev) - spherically symmetric scattering assumed

b. high energy (> 100 ev) - Rutherford scattering assumed

2. Plasmon creation

The applicable source functions include the Auger process and pair production. For the Auger process the self-convolution F(E) is used as the zeroth order source coefficient with all other terms vanishing (the Auger process is assumed to be isotropic). In the low energy range (< 100 ev), the pair production source functions were shown to be

$$S_o^{(1)}(E') = \frac{e^4 k_F^3}{3\pi\epsilon^2 E_p (E'-E_F)^2} \tag{25}$$

$$S_2^{(1)}(E') = -\frac{1}{5} S_o^{(1)}(E')$$

with higher order terms being ignored. In the high energy region (> 100 ev)

$$S_o^{(2)}(E') = \frac{e^4 k_F^3}{3\pi\epsilon^2 E_p (E'-E_F)^2} \tag{26}$$

$$S_2^{(2)}(E') = -\frac{1}{2} S_o^{(2)}(E')$$

Again the higher order terms are ignored.

The electron scattering mechanisms considered were electron-

electron collisions and plasmon creation. The expansion coefficients of these scattering functions were found to be

$$F_\ell^{(1)}(E,E') = \frac{2}{E'} P_\ell\left(\sqrt{\frac{E}{E'}}\right) ; \quad \text{(low energy electron scattering)} \tag{30}$$

$$F_\ell^{(2)}(E,E') = \frac{1}{E'}\left(1 + 2\frac{E}{E'}\right) P_\ell\left(\sqrt{\frac{E}{E'}}\right) ; \quad \text{(high energy electron scattering)} \tag{34}$$

$$F_\ell^{(3)}(E,E') = \frac{2.2\, P_\ell\left(\sqrt{\frac{E}{E'}}\right)}{E'\sqrt{\frac{E}{E'}}\left(5 - \frac{E}{E'}\right)} ; \quad \text{(plasmon creation; } E' \gg \hbar\omega_p\text{)} \tag{38}$$

The corresponding Green's functions, which are dependent only on the scattering mechanism, are obtained by solving equation III-11 by means of the Mellin transform. They are

$$G_o^{(1)}(E,E'') = \begin{cases} 2\dfrac{E''}{E^2} + \delta(E-E'') ; & E'' \geq E \\ 0 ; & E'' < E \end{cases} \tag{31}$$

$$G_2^{(1)}(E,E'') = \begin{cases} \dfrac{2}{\sqrt{E\,E''}} \cos\left[\dfrac{\sqrt{3}}{2} \ln\left(\dfrac{E''}{E}\right)\right] + \delta(E-E'') ; & E'' \geq E \\ 0 ; & E'' < E \end{cases}$$

$$\frac{1}{E''}\left[42.7\left(\frac{E''}{E}\right)^{3.2} - 7.1\left(\frac{E''}{E}\right)^{1.4} - 0.28\left(\frac{E''}{E}\right)^{-1.7}\right]$$

$$+ 0.13\,\delta(E-E'') \;;\quad E'' \geq E$$

$$G_2^{(3)}(E,E'') =$$

$$0 \qquad ;\quad E'' < E$$

With these Green's functions and source functions, equation III-10 can be integrated to give the internal secondary distribution. This is now done for the six possible combinations.

Case 1: Low energy secondaries scattered by electron collisions.

$$\psi_k^{(1)}(E) = \frac{|\vec{P}|N_k^{(1)}(E)}{m\ell_{pp}(E)} = \int_{E_F}^{E_m} G_k^{(1)}(E,E'')\, S_k^{(1)}(E'')dE''$$

$$N_o^{(1)}(E) = \ell_{pp}(E)\gamma\left\{\frac{2}{E^2}\left[\ln\frac{E_m-E_F}{E-E_F} + E_F\left(\frac{1}{E-E_F} - \frac{1}{E_m-E_F}\right)\right]\right. \tag{50}$$

$$\left. + \frac{1}{(E-E_F)^2}\right\}$$

$$N_2^{(1)}(E) = -\frac{1}{5}\ell_{pp}(E)\,\gamma\left\{\frac{1}{(E-E_F)^2} + \frac{4}{E^2}\sum_{n=o}^{\infty}\frac{(2n+3)(n+1)}{(2n+3)^2+3}\right. \tag{51}$$

$$\frac{1}{E\sqrt{2}}\left[4\sinh\left(\sqrt{2}\,\ln\frac{E''}{E}\right)+3\sqrt{2}\,\cosh\left(\sqrt{2}\,\ln\frac{E''}{E}\right)\right]$$

$$+ C_o\delta(E-E'') \quad ; \quad E'' \geq E$$

$$G_o^{(2)}(E,E'') = \tag{35}$$

$$0 \quad ; \quad E'' < E$$

$$C_o = \frac{2}{3\sqrt{2}-2}$$

$$\frac{1}{E''}\left[0.8\left(\frac{E}{E''}\right)^{1.15}+\left(\frac{E''}{E}\right)^{0.8}\left\{5.8\cos\left(0.7\ln\frac{E''}{E}\right)\right.\right.$$

$$\left.\left.-3.8\sin\left(0.7\ln\frac{E''}{E}\right)\right\}\right]+C_2\delta(E-E'') \quad ; \quad E'' \geq E$$

$$G_2^{(2)}(E,E'') =$$

$$0 \quad ; \quad E'' < E$$

$$C_2 = \frac{3.63 - 1.6\cosh 1.4\pi}{(3.63 - 1.6\cosh 1.4\pi)^2 + 0.14^2\sinh 1.4\pi}$$

$$\frac{1}{E''}\left[18.2\left(\frac{E''}{E}\right)^{5.5} - 0.58\left(\frac{E''}{E}\right)^{-1.1}\right]$$

$$+ 0.25\,\delta(E-E'') \quad ; \quad E'' \geq E$$

$$G_o^{(3)}(E,E'') =$$

$$0 \quad ; \quad E'' < E$$

$$\times \left[\left(\frac{E}{E_m} \right)^{3/2} \left(\frac{E_F}{E_m} \right)^n \left\{ \frac{\sqrt{3}}{2n+3} \sin \left(\frac{\sqrt{3}}{2} \ln \frac{E_m}{E} \right) \right. \right.$$

$$\left. \left. - \cos \left(\frac{\sqrt{3}}{2} \ln \frac{E_m}{E} \right) \right\} + \left(\frac{E_F}{E} \right)^n \right] \Bigg\}$$

E_F = fermi energy, $E_m = \min(100 \text{ ev}, E_p)$

$$\gamma = \frac{\sqrt{2m}\, e^4 k_F^3}{6\pi E_p \sqrt{E}} \tag{52}$$

Case 2: High energy secondaries scattered by electron collisions.

$$\psi_k^{(2)}(E) = \frac{|\vec{P}| N_k^{(2)}(E)}{m \ell_{pp}(E)} = \int_{E_{min}}^{E_{max}} G_k^{(2)}(E, E'')\, S_k^{(2)}(E'')\, dE''$$

$$N_o^{(2)}(E) = \sqrt{2}\, \ell_{pp}(E)\, \gamma \left\{ \frac{1}{E E_{max}} \left[10 \sinh \left(\sqrt{2} \ln \frac{E_{max}}{E} \right) \right. \right. \tag{53}$$

$$\left. + 7\sqrt{2} \cosh \left(\sqrt{2} \ln \frac{E_{max}}{E} \right) \right] - \frac{1}{E E_{min}} \left[10 \sinh \left(\sqrt{2} \ln \frac{E_{min}}{E} \right) \right.$$

$$\left. \left. + 7\sqrt{2} \cosh \left(\sqrt{2} \ln \frac{E_{min}}{E} \right) \right] + \frac{C_o}{(E - E_F)^2} \right.$$

$$C_o = \frac{2}{3\sqrt{2} - 2}$$

$$N_2^{(2)}(E) = -5\,\ell_{pp}(E)\,\gamma\left\{\frac{E^{1.15}}{3.15}\left(\frac{1}{E_{max}^{3.15}} - \frac{1}{E_{min}^{3.15}}\right)\right. \tag{54}$$

$$+\frac{0.52}{E^2_{max}}\sin\left[\ell n\left(\frac{E_{max}}{E}\right)^{0.7}\right] + \frac{4.3}{E^2_{max}}\cos\left[\ell n\left(\frac{E_{max}}{E}\right)\right]^{0.7}$$

$$-\frac{0.52}{E^2_{min}}\sin\left[\ell n\left(\frac{E_{min}}{E}\right)^{0.7}\right] - \frac{4.3}{E^2_{min}}\cos\left[\ell n\left(\frac{E_{min}}{E}\right)^{0.7}\right]$$

$$\left. +\frac{C_2}{(E-E_F)^2}\right\}\;;\quad C_2 = \frac{3.63 - 1.6\cosh 1.4\pi}{(3.63 - 1.6\cosh 1.4\pi)^2 + 0.14^2 \sinh 1.4\pi}$$

$$N_k^{(2)}(E) = 0 \quad \text{if} \quad E_p < 150 \text{ ev}$$

$E_{min} = 100$ ev, $E_{max} = \max\,(150 \text{ ev}, E_p/2)$

Case 3: Low energy secondaries scattered by plasmon creation

$$\psi_k^{(3)}(E) = \frac{|\vec{P}| N_k^{(3)}(E)}{m\ell_{p\ell}(E)} = \int_{2E_{p\ell}}^{E_m} G_k^{(3)}(E,E'')\ S_k^{(1)}(E'')dE''$$

$$N_o^{(3)}(E) = 2\ell_{p\ell}(E)\ \gamma \left\{5.2\left[E_m^{3.5} - (2E_{p\ell})^{3.5}\right]\frac{1}{E^{5.5}}\right. \tag{55}$$

$$\left. + 0.19\left[\frac{1}{E_m^{3.1}} - \frac{1}{(2E_{p\ell})^{3.1}}\right]E^{1.1} + \frac{0.25}{(E-E_F)^2}\right\}$$

$$N_2^{(3)}(E) = \tfrac{1}{2}\,\ell_{p\ell}(E)\ \gamma \left\{39\left[E_m^{1.2} - (2E_{p\ell})^{1.2}\right]\frac{1}{E^{3.2}}\right.$$

$$+ 11.8\left(\frac{1}{E_m^{0.6}} - \frac{1}{(2E_{p\ell})^{0.6}}\right)\frac{1}{E^{1.4}} + 0.07\left(\frac{1}{E_m^{3.7}} - \frac{1}{(2E_{p\ell})^{3.7}}\right)E^{1.7}$$

$$\left. + \frac{0.13}{(E-E_F)^2}\right\}$$

Case 4: High energy secondaries scattered by plasmon creation.

$$\psi_k^{(4)}(E) = \frac{|\vec{P}| N_k^{(4)}(E)}{m\ell_{p\ell}(E)} = \int_{E_{min}}^{E_{max}} G_k^{(3)}(E,E'')\ S_k^{(2)}(E'')\ dE''$$

$$N_o^{(4)}(E) = N_o^{(3)}(E) \quad \text{with } E_{max} \text{ and } E_{min} \text{ replacing } E_m \text{ and } 2E_{p\ell} \text{ respectively} \tag{57}$$

$$N_2^{(4)}(E) = -2N_2^{(3)}(E) \quad \text{with } E_{max} \text{ and } E_{min} \text{ replacing } E_m \text{ and } 2E_{p\ell} \text{ respectively} \tag{58}$$

Case 5: Low energy Auger electrons scattered by both mechanisms.

When an Auger spectrum is present with average energy less than 100 ev, the following expression is to be used.

$$N_o^{(5)}(E) = K \int_E^{E_u} f(E'')[\ell_{pp}(E)\, G_o^{(1)}(E,E'') + \ell_{p\ell}(E) G_o^{(3)}(E,E'')]\, dE'' \tag{59}$$

where K is an adjustable constant and E_u is the upper limit of the Auger spectrum (f is non-zero only over the spectral region E_ℓ, E_u). The $G_o^{(3)}(E,E'')$ term is included only if the Auger spectrum is of energy greater than twice the plasma excitation energy. Assuming this to be the case

$$N_o^{(5)}(E) = K \left\{ \left[\ell_{pp}(E) + \frac{\ell_{p\ell}(E)}{4} \right] f(E) + \frac{2\ell_{pp}(E)}{E^2} \int_E^{E_u} E'' f(E'')\, dE'' \right. \tag{60a}$$

$$\left. + \ell_{p\ell}(E) \int_E^{E_u} \frac{f(E'')}{E''} \left[18.2 \left(\frac{E''}{E}\right)^{5.5} - 0.58 \left(\frac{E''}{E}\right)^{-1.1} \right] dE'' \right.$$

The last two integrals are done numerically. Consistent with the deconvolution approach of the last chapter, this is usually done by the trapezoidal technique.

Unlike the $N_k^{(i)}(E)$ contributions discussed previously, the amplitude of $N_o^{(5)}(E)$ is uncertain because of a lack of a knowledge about the intensity of f(E). Consequently when reconstructing a true secondary distribution theoretically the amplitude is included empirically through the parameter K. That is, K, rather than based on theoretical considerations, is adjusted so that the results of the theory most nearly agree with experiment.

As will be done later, it is often the purpose of a diffusion theory analysis to determine the "true" Auger spectrum rather than just predict a secondary distribution based on an Auger spectrum obtained elsewhere. There are two ways to approach such a problem. One way is to build up a true secondary distribution theoretically except for the Auger contribution and then adjust f(E) in (60) point by point starting with E_u and working toward E_ℓ until the theoretical and experimental curves match over the Auger region. To do this one must assume a value for K. Alternatively, it is possible to determine the "true" Auger spectrum by assuming a trapezoidal rule for (60) and attempting to invert the equation. $N_o^{(5)}(E)$ is determined empirically by subtracting out all other possible contributions. It is possible to do this but again K must be assumed. If it is difficult to estimate K from the data (as is often the case) one can accomplish the same task by estimating where the spectrum falls to zero (that is, estimating both E_u and E_ℓ). It is not difficult to show that this is the same as estimating

K. Carrying out this inversion results in the following expression for the "true" Auger distribution in the trapezoidal approximation:

$$f(E_u - n\Delta E) = f_n = \frac{N_o^{(5)}(E_u - n\Delta E = E_n) - \frac{2\Delta E}{E_n}\sum_{i=1}^{n-1} f_i E_i - \frac{\Delta E}{\lambda_1}\sum_{i=1}^{n-1}\frac{f_i}{E_i}F(E_i, E_n)}{\frac{4\gamma_1 + 1}{4\lambda_1} + \frac{\Delta E}{E_n}\left(1 + \frac{8.8}{\lambda_1}\right)} \tag{60b}$$

$$E_n = E_u - n\Delta E \; ; \quad \lambda_1 = \frac{\ell_{p\ell}(E)}{\ell_{pp}(E)}$$

$$F(E_i, E_n) = 18.2\left(\frac{E_i}{E_n}\right)^{5.5} - 0.6\left(\frac{E_i}{E_n}\right)^{-1.1}$$

Case 6: High energy Auger electrons scattered by both mechanisms.

If the Auger spectrum has an average energy greater than 100 ev then the following is applicable:

$$N_o^{(6)}(E) = K\int_E^{E_u} f(E'')\left[\ell_{pp}(E)G_o^{(2)}(E,E'') + \ell_{p\ell}(E)G_o^{(3)}(E,E'')\right]dE'' \tag{61}$$

$$N_o^{(6)}(E) = \left[C_o \ell_{pp}(E) + \frac{\ell_{p\ell}(E)}{4} \right] f(E) \tag{62}$$

$$+ \frac{\ell_{pp}(E)}{E\sqrt{2}} \int_E^{E_u} f(E'') \left[4 \sinh\left(\sqrt{2} \ln \frac{E''}{E}\right) + 3\sqrt{2} \cosh\left(\sqrt{2} \ln \frac{E''}{E}\right) \right] dE''$$

$$+ \ell_{p\ell}(E) \int_E^{E_u} \frac{f(E'')}{E''} \left[18.2 \left(\frac{E''}{E}\right)^{5.5} - 0.58 \left(\frac{E''}{E}\right)^{-1.1} \right] dE''$$

$$C_o = \frac{2}{3\sqrt{2} - 2}$$

Again the integrals are done numerically and all comments made in the previous case carry over.

The total internal distribution is therefore given by

$$\eta(E) = \sum_k \sum_i \lambda_{ki} N_k^{(i)}(E) P_k(\cos\theta) \tag{63}$$

where the normalizing factors λ_{ki} contain information dependent on the material and $P_k(\cos\theta)$ are the familiar Legendre polynomials. The k expansion in (63) is empirically found to converge rapidly and it is sufficient to consider k = 0, 1, 2 only.

Experimentally, however, one does not observe $\eta(E)$, the internal secondary electron energy distribution, but rather an external current which is a function of the energy $J(E')$ where E' denotes the external energy of an electron which, because of the work function, had energy $E(\neq E')$ internal to the sample. Careful consideration of the effect on the internal distribution as it crosses the surface boundary and is collected leads to the following theoretical expression for the external secondary electron energy distribution experimentally observed.

$$J(E') = \delta \left\{ \frac{E'}{E' + W} \sum_i \lambda_{oi}(E)\, N_o^{(i)}\, (E' + W) \right. \tag{64}$$

$$\left. - \frac{5}{2}\left[\frac{3}{2}\left(1 - \frac{W^2}{(E' + W)^2}\right) - \frac{E'}{E' + W} \right] \sum \lambda_{2i}(E) N_2^{(i)} (E' + W) \right\}$$

where

$$\delta = 1/2 \sqrt{\frac{E' + W}{2m}}$$

and W = energy of the vacuum level.

Equation (64) can be evaluated as soon as certain values are given as input information.

Input Information

1. Primary electron energy
2. Conduction band bottom
3. Work function
4. Fermi level
5. Auger spectrum (spectra) and amplitude(s)
6. Mean free paths

This expression (equation (64)) concludes the discussion of the theory of electron diffusion. All the physical equations necessary to analyze the experimental true secondary electron energy distributions for the Auger spectrum and to compare the theoretical true secondary distributions with the experimental findings have been established. It is now time to turn to the problem of obtaining experimental distributions. Correspondingly the experimental instrumentation is discussed in the next chapter.

CHAPTER IV

EXPERIMENTAL INSTRUMENTATION

Throughout the discussion thus far it has been implicitly assumed that the Auger and true secondary electron energy spectra data were experimentally realizable. It is now time to consider the problem of acquiring such data by discussing the experimental requirements.

Apparatus

The principal piece of apparatus used to obtain the data is a modified Varian low energy electron diffraction (LEED) system capable of energy analyzing backscattered electrons (Fig. 4). The details of this instrument have been discussed extensively elsewhere.[45] Consequently, the current presentation will be limited to a brief description of the general system with emphasis on those particular elements specifically related to accumulating Auger and true secondary distribution data.

For purposes of discussion, the general system apparatus can be conveniently divided into three segments: (1) the ultrahigh vacuum arrangement, (2) the test or sample chamber and (3) the electronic signal processing configuration.

Vacuum System

In order to achieve and maintain atomically well defined crystal surfaces, it is necessary to perform the experiments in a high vacuum -- nominally 10^{-9} torr (one torr = one mm of Hg). To obtain such pressures it is essential to utilize special equipment and to observe proper vacuum procedures.

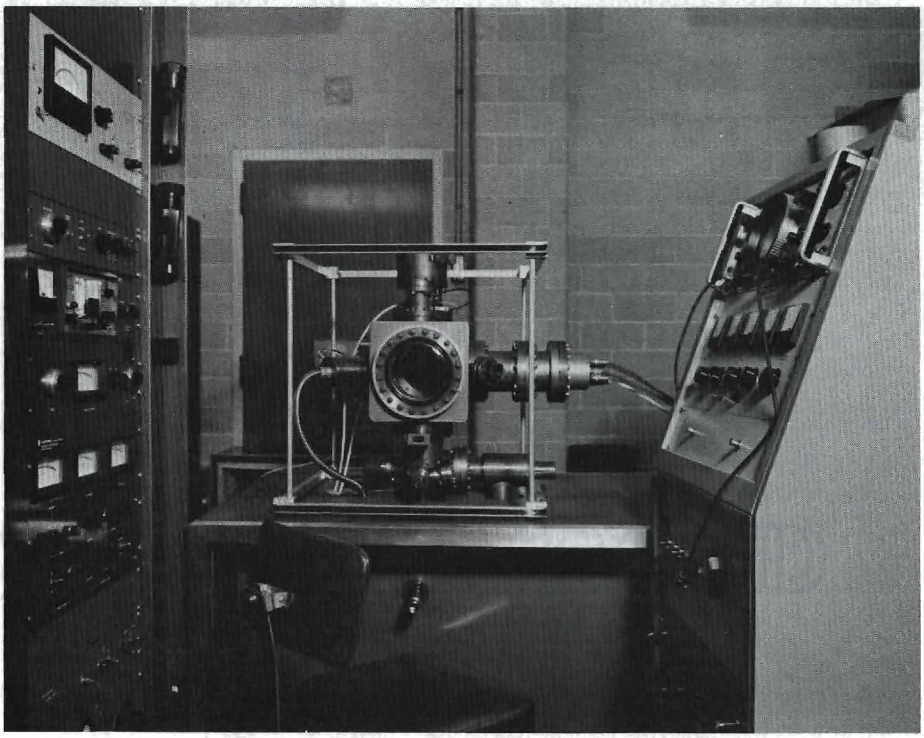

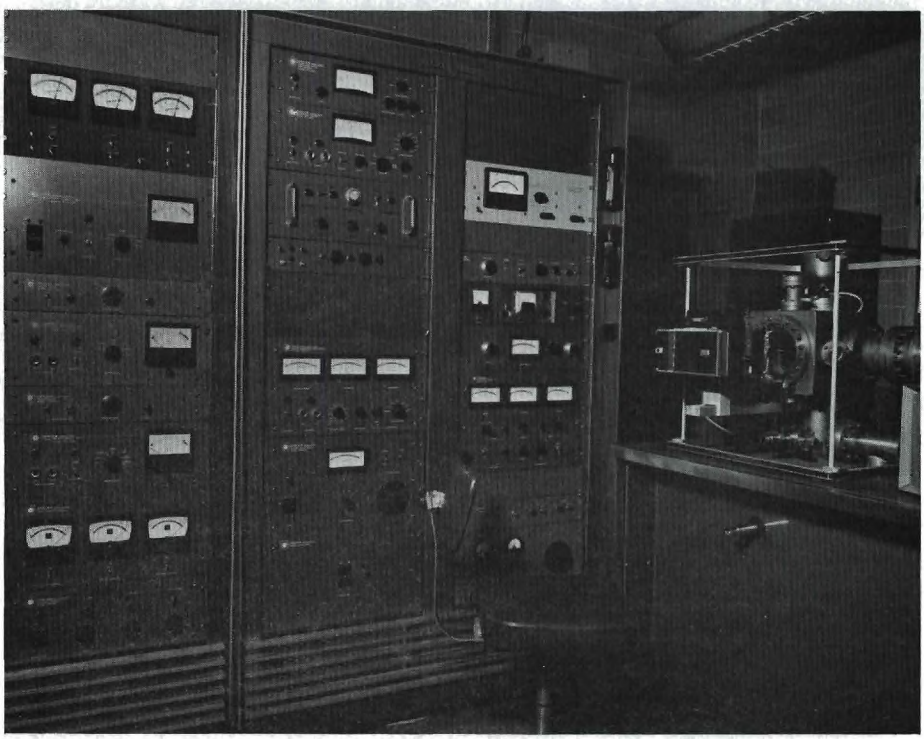

Figure 4. Photographs of Experimental Apparatus.

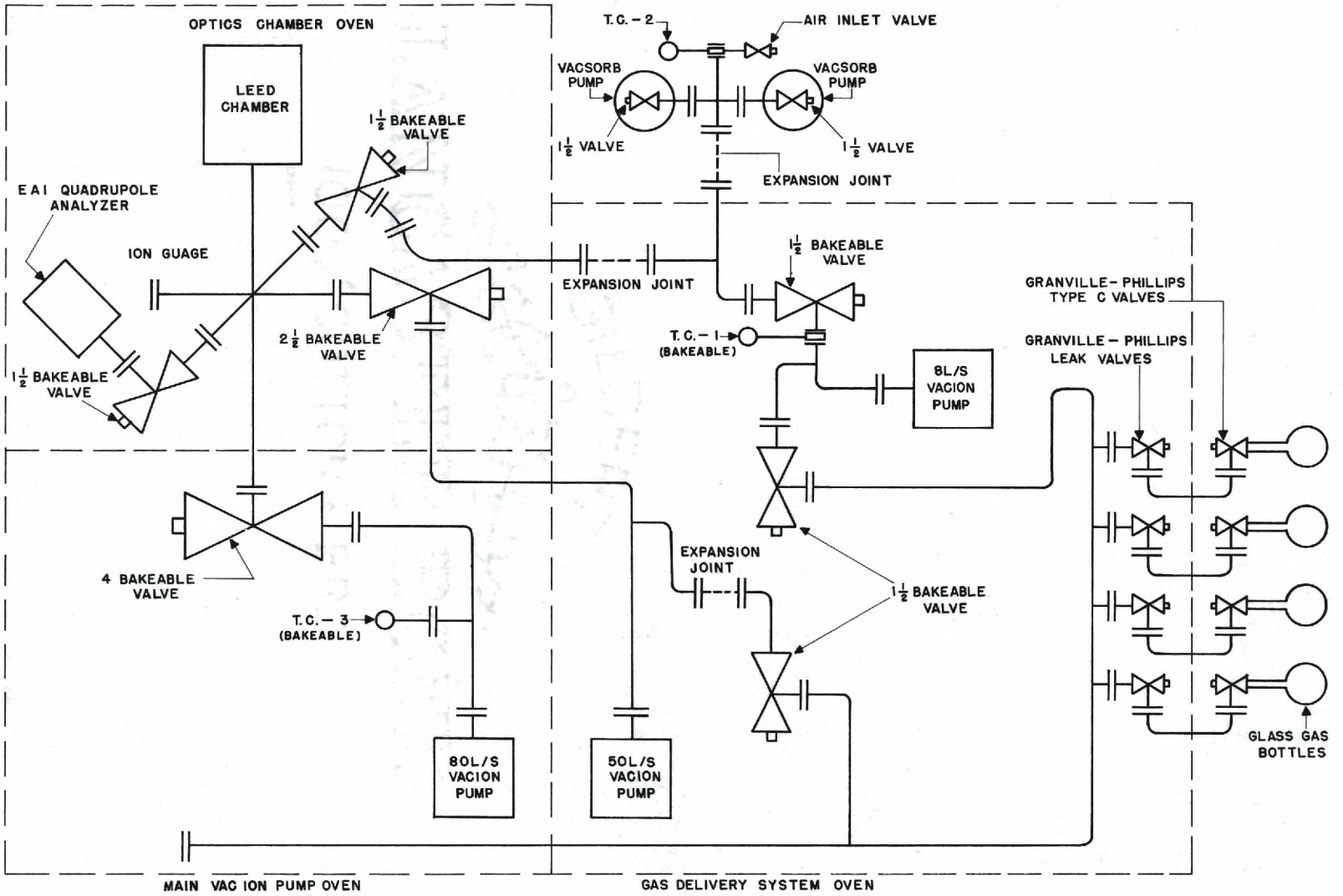

Figure 5. Schematic Diagram of LEED Vacuum System.

Equipment. The vacuum system is shown schematically in Figure 5. All tubing in the system is stainless steel connected by flanges with copper gaskets. The system employs three pump types: (1) cryogenic molecular sorption, (2) ion and (3) titanium sublimation. The cryogenic pumps use a synthetic zeolite core which, when cooled to liquid nitrogen temperatures, adsorbs gases readily. The ion pumps utilize strong electric and magnetic fields to ionize residual gases and accelerate them to titanium plates in which the molecules are buried. Finally, the titanium sublimation unit operates on the principle that fresh titanium adsorbs gases. A large current is periodically passed through a titanium rod, subliming the outer few layers of it, and continually recoating the pump walls. The ion pumps and the titanium sublimation unit are each supported by appropriate commercially available electronics which supply the necessary voltages and currents.

In addition to the tubing and pumps, the vacuum system is equipped with several valves, both manual and automatic. The primary function of the manual valves is to isolate various segments of the vacuum system for the purposes of performing certain experiments and changing samples. The automatic valves, on the other hand, are used for admitting gases in controlled amounts into the system so that their reaction with the crystal may be observed. These automatic valves along with the pure gas reservoirs and delivery tubes leading to the sample chamber are collectively known as the gas delivery system. As before, the motors and power supplies for these automatically controlled valves are commercially available.

The final element of the vacuum system is the ovens used for con-

ducting bake-out operations. Heating elements capable of 250 degrees centigrade or more are located in the ion pump area and the gas delivery system. In addition, a removable clam-shell type oven is available for baking the sample chamber. Associated with the oven electronics are safety circuits for detecting temperature and pressure which turn off the ovens if the prescribed limits of these parameters are exceeded (250°C and 10^{-5} torr).

Procedures. The procedures necessary to attain satisfactory pressures in the sample chamber are probably most easily illustrated by describing a typical sample changing operation.

Assuming the system to be at high vacuum, the first step is to valve off those portions of the system which need not come up to atmospheric pressure. Any pumps not in these areas are shut off. After opening the valve between the test chamber and the cryogenic chemical pump area, the system is slowly brought to room pressure in a dry nitrogen atmosphere. These higher pressures are monitored by thermocouple gauges. The crystal manipulator is then removed and the new sample properly installed. During this operation the opening created by the absence of the manipulator flange is covered with lint free paper to prevent dust particles from settling in the system. A slight positive pressure of dry nitrogen is maintained. After selecting a new copper gasket and cleaning it and the flanges with methanol, the sample holder assembly is replaced and bolted in position in a uniform manner. The dry nitrogen supply is valved off. The cryogenic pumps are then chilled to liquid nitrogen temperature (taking approximately one-half hour) and the system is "roughed" down to about five microns (5×10^{-3} torr).

After having valved off the cryogenic pumps, those ion pumps which have been at atmosphere are put in the "start" mode and turned on. All remaining valves are opened. With the ion pumps started the pressure soon falls into the 10^{-7} torr range at which time the ion pumps are put in the "protection" mode. After turning on the sublimation unit and degassing (if necessary) the titanium filaments, the system is ready for bake-out.

For bake-out it is necessary to remove the Helmholtz coils (to be described) from around the test chamber and any other temperature sensitive electronics in the vicinity. The clam-shell oven is positioned and plugged into the controller circuit. The oven timing controls are then set (usually twelve hours for the test chamber and 8-9 hours for the pumps and gas delivery system) and the ovens turned on. After bake-out the system is allowed to cool to room temperature during which time the Helmholtz coils and other necessary facilities are replaced. The final pressures, read on a standard ionization gauge, are generally on the order of 5×10^{-10} torr.

Test Chamber

With a high vacuum achieved it is now possible to conduct experiments all of which are performed in the test chamber. The test chamber is a stainless steel enclosure of approximately cubic geometry with dimensions 9" by 9" by $9\frac{1}{2}$" and containing numerous flanges for greater flexibility. On the side that shall be called the front is a viewing port for visual control and LEED pattern observation. Directly to the rear of the viewing port is the electron optics containing a three grid analyzer, fluorescent screen/collector and a low energy electron gun

capable of delivering approximately one microamp to the crystal surface. Mounted from the top is the crystal manipulator capable of rotation about a vertical axis and translation along this same axis. The sample is normally positioned directly in front of the electron gun and at normal incidence to the electron beam. On the side of the chamber, to the observer's left, is the ion bombardment unit for the purpose of surface cleaning by inert ion impact. To the right is the quadrupole assembly for analysis of residual gases within the test chamber.

Electronics

Surrounding the sample chamber is a pair of Helmholtz coils which serve to cancel stray magnetic fields in the target region. The appropriate magnetic field is created by adjusting the coil current until the beam exhibits a straight line of flight from the gun to the viewing port which is capable of fluorescing.

Returning consideration to the electron optics, there are normally two modes of operation when conducting electron scattering investigations. One is the observation of diffraction patterns which result from coherent Bragg reflection of electrons from the single crystal surface. To observe such patterns, the analyzer is set with the second, or suppressor, grid at a retarding potential such that only the elastically reflected electrons are passed. The first and third grids are grounded for field isolation purposes. A potential of approximately five kilovolts is put on the screen resulting in post acceleration of the passed electrons to energies capable of exciting the phosphors on the fluorescent screen. The result is a diffraction pattern visible on this screen.

For the purposes of obtaining energy distribution curves the five

kilovolt screen potential is replaced by a nominal 225 volt collector potential and the suppressor grid is programmed with a ramp voltage operating between cathode potential and ground. Superimposed on this slowly changing ramp is a small ac modulation on the order of one volt peak to peak. This ripple imparts an ac component to the collected current which is proportional to the change in the number of electrons collected divided by the constant magnitude of the ripple. If the ripple can be considered small in comparison with the total energy scale, this ac component is just the derivative of the collected current -- the energy distribution.

The ramp voltage is supplied by a voltage programmer which is driven by the x-axis of the xy recorder. The ac ripple (nominally 150 cps) is supplied either by an audio oscillator or the reference terminals from a phase sensitive lock in amplifier. This lock in amplifier is additionally used to detect the ac component (first harmonic) of the collected current. If the second derivative of the collected current is desired, one simply locks in on the second harmonic.[46] A block diagram of the electronic configuration is shown in Figure 6.

Data Accumulation

The acquisition of data in practice proceeds in an automatic mode with the xy recorder as the driving mechanism. The type of data being taken and the anticipated strength of the signal dictate the various instrument settings such as amplification, filtering, voltage per inch scale and speed of plotting. Although a certain amount of testing is required to find the optimum settings for any particular study, it can generally be stated that the more detailed readings are taken with larger

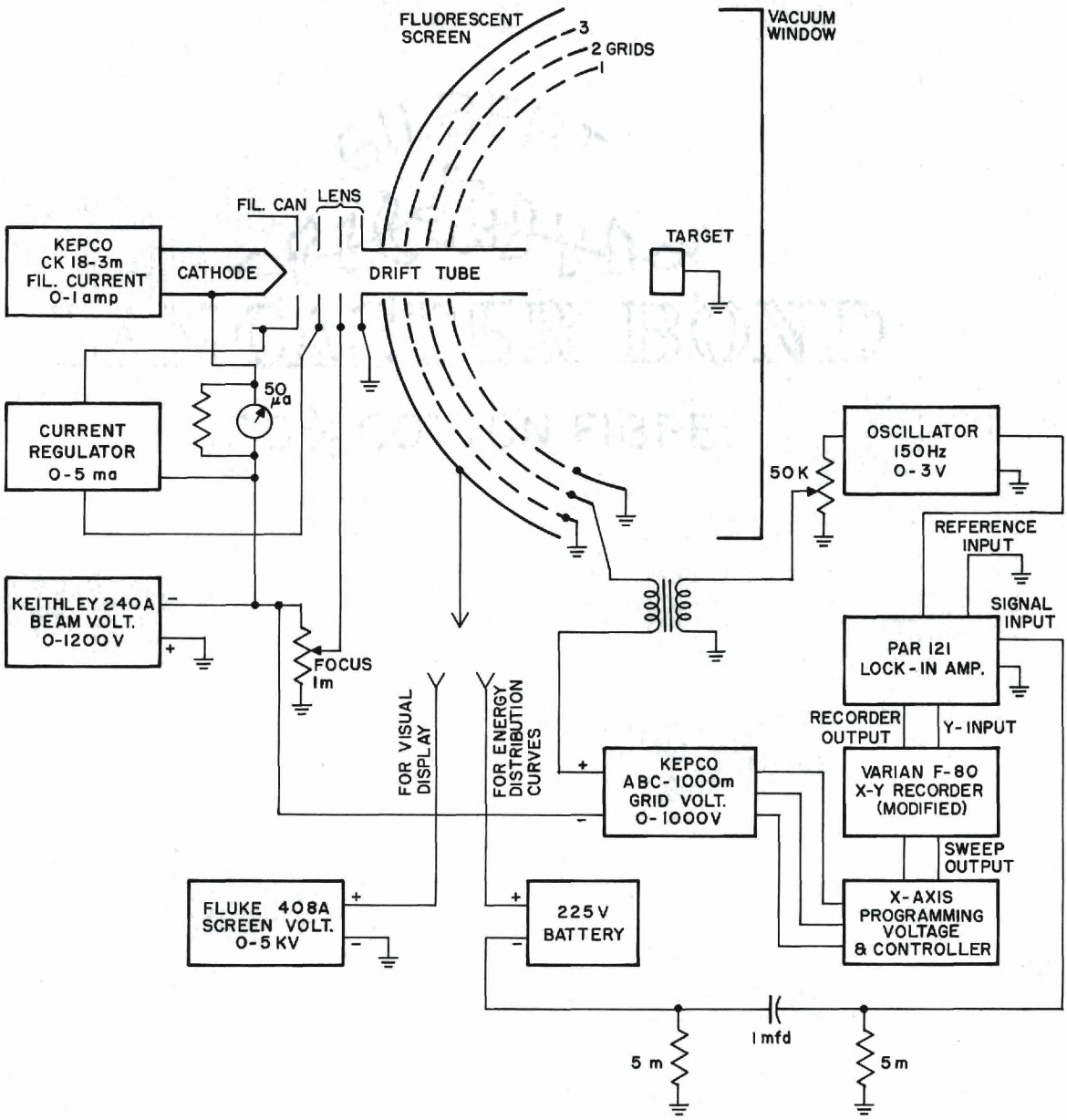

Figure 6. Diagram of LEED Optics and Electronics for Obtaining Diffraction Patterns and Electron Energy Distribution Curves.

amplification and filter settings and smaller voltage per inch and plot speeds than usual so as to enhance the statistics. There are various controls available to the experimenter. From the standpoint of practicality in accumulating data, complete control of the x and y coordinate scales is essential. The abscissa factor is regulated by the x-axis controller which has incremental choices of $\frac{1}{2}$, 1, 2, 3, 4, 5, 10, 15, 20, 25, 50, 75, 80, 85, 90, 95, 100, and 125 volts/inch plus one continuously adjustable selection. The continuous selector must be recalibrated at each new setting but its availability allows one to select some unusual scale factor which might be desirable for a particular experiment. The ordinate scale is controlled by the lock in amplifier. The collector current is put into a pi filter network (two resistors and a capacitor) and the voltage developed across the second resistor is read by the lock in amplifier. The filter is for the purpose of eliminating the dc portion of the signal so that a maximum ac signal can be put into the lock in amplifier without overloading it. For weaker signals larger resistances are used. Nominally five to ten megohm resistors are used with a one-tenth to one microfarad capacitor. For signals which still must be amplified a great deal, the integration or signal averaging time on the lock in amplifier is increased from its nominal value of one second. So as not to lose resolution the plotting time must be slowed down proportionately. A typical plotting time for an average distribution curve is fifteen minutes, although the modified recorder can plot at speeds which vary the total time from two and one-half minutes to two and one-half hours. The longer times are often necessary to acquire statistically accurate Auger data. This is also

the case when taking second derivative or second harmonic data. The second harmonic is generally very weak and extraction of accurate data requires longer time constants to average the noise to an acceptable level.

Noise is not the only source of error in the data. One element of uncertainty is the primary beam energy. There is a Gaussian spread about the desired energy of the beam which has been estimated to have a standard deviation on the order of two-tenths of an electron volt. Similarly the three grid analyzer has resolution limitations. In this case, the grid resolution standard deviation is a function of electron energy -- being smaller at lower voltages. It has been shown that the standard deviation varies linearly with electron energy starting close to zero at zero energy and going to several electron volts at 1000 ev electron energy.[45] In effect, the resolution limitations smooth the data -- i.e., neighboring points in the distribution are weighted and averaged by an equation of the form

$$f(x) = \int_{\alpha}^{\beta} F(x')G[x', x, \sigma(x')]dx'$$

where x and x′ represent the independent variables of the distribution function, α and β are the upper and lower limits on the independent variable of the energy distribution F and G is a resolution function whose analytic form depends on the experimental apparatus. Generally it is sufficient to assume that G can be represented by a Gaussian of characteristic resolution width σ.[47] Such smoothing can obscure any "fine

structure" if it is present but the general trend of the curve should be satisfactorily represented. Since fine structure (millivolt fluctuations) is not of interest in the current work and since it has often proven necessary to purposely smooth the Auger data to obtain satisfactory deconvolutions,[48] the experimental apparatus poses for the most part no serious limitations with respect to resolving power in the investigations reported here. On the other hand, if it is desired to investigate the details of a spectrum whose signal is down several orders of magnitude (empirically, larger than four orders of magnitude) from the fundamental, then a better electron gun and analyzer system, such as the electrostatic system,[49,50,51] is necessary.

The results obtained with the apparatus described in this chapter are presented next. Included with the results are experimental points which are peculiar to the particular sample being studied such as cleaning and preparation of the sample.

CHAPTER V

RESULTS

The combined experimental and theoretical results of Auger spectra and true secondary electron investigations on silicon, germanium and graphite are presented in this chapter. Because of the varied approaches needed to study each material, they are treated separately herein although common points of analysis among the materials studied are not repeated. Comparisons and contrasts are deferred until the next chapter.

Silicon

Preparation

A six millimeter by ten millimeter by one millimeter silicon crystal with a (111) orientation on the broad face was obtained from Dr. G. W. Simmons who had already prepared the crystal for LEED studies. Further preparation was therefore unnecessary in this case although there are several preparation methods available in the literature (see ref. 52 for example). Once in the vacuum system, the silicon surface was atomically cleaned by repeated Argon ion bombardment treatments (each treatment averaging 45 minutes with a one microampere ion current and 300 volt ions). After five such treatments the pattern shown in Figure 7 was obtained. A representative energy distribution from this surface is also shown. The characteristic losses adjacent to the elastic peak are due to excitation of plasma oscillations within the valence electron gas by primary electrons. Electron losses to such a collective phenomenon are

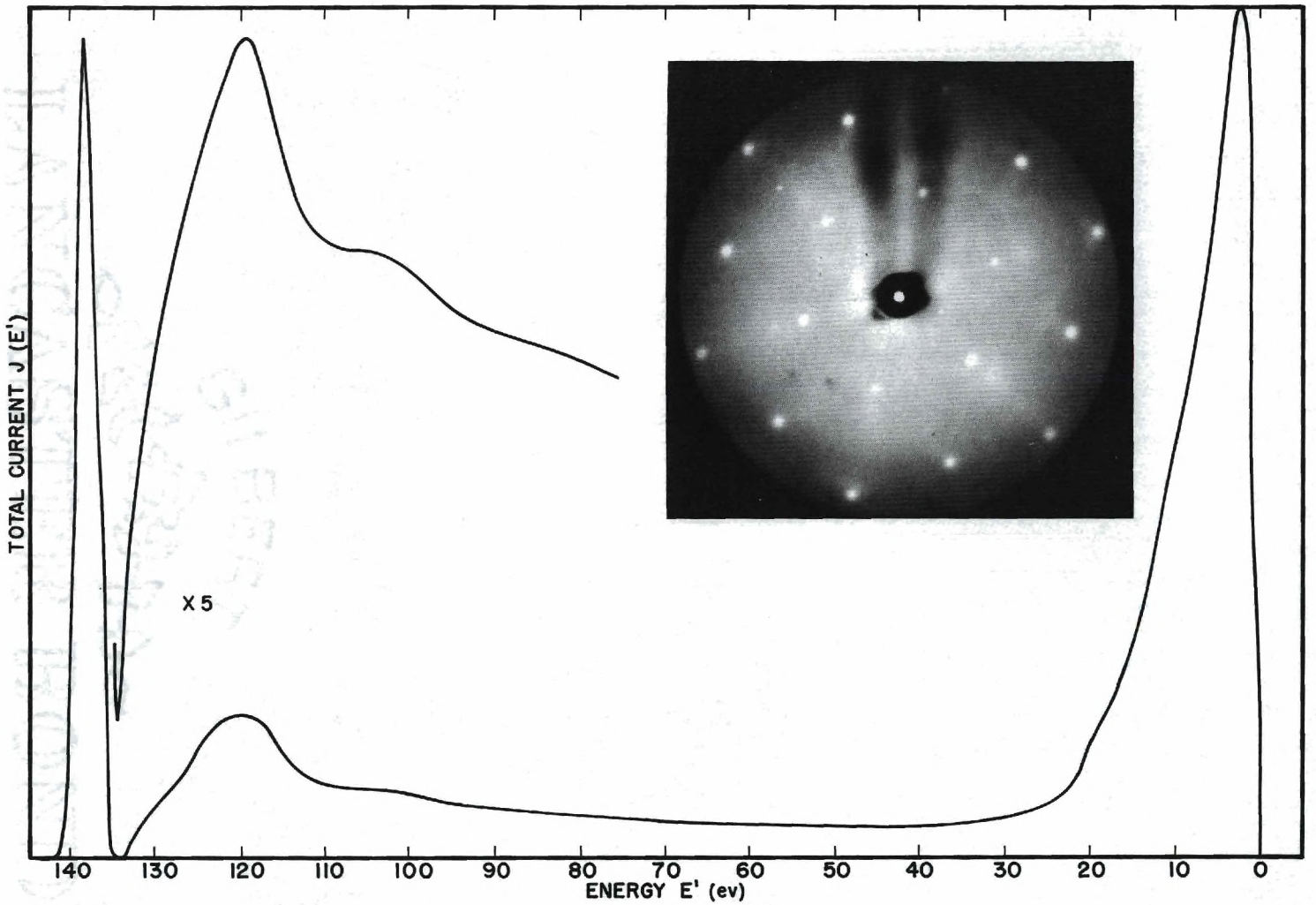

Figure 7. LEED Pattern and Energy Distribution Curve for the Clean (111) Surface of Silicon at a Primary Energy of 140 Electron Volts.

of extreme importance and have been observed in all materials studied. There have been numerous studies of the solid state plasma phenomenon. Therefore it will not be treated here but results will be used as needed.

Auger and True Secondary Distributions

Based on x-ray data the $L_{2,3}$ level in silicon lies some 100 electron volts below the vacuum level. It is therefore expected that an Auger spectrum involving this shell and the valence band should occur in the 100 volt energy range of an energy distribution resulting from primary electrons of energy greater than 100 ev. However, discernible results were not visible below a primary energy of 200 ev. This is probably due to a rapid falling off of the cross section for ionization by way of the L shell. Figure 8 shows the true secondary portion of the electron energy distribution from a clean silicon surface for a primary energy of 1000 ev. The Auger distribution which occurs at roughly the expected energy region is seen to be rather prominent. Nonetheless the background and distortion effects discussed earlier are quite apparent and cannot be ignored.

Analysis of these results proceeds qualitatively as follows. Numerous (10 to 20) curves of the Auger spectrum and true secondary distribution are taken for a given surface condition (clean for example) . The distributions are normalized to the same area and averaged to minimize any spurious effects. The experimental points thus obtained in the Auger region are then read into a computer program which evaluates equation III-64 and adjusts the Auger spectrum in such a manner that agreement is obtained between the theoretical and experimental results. The

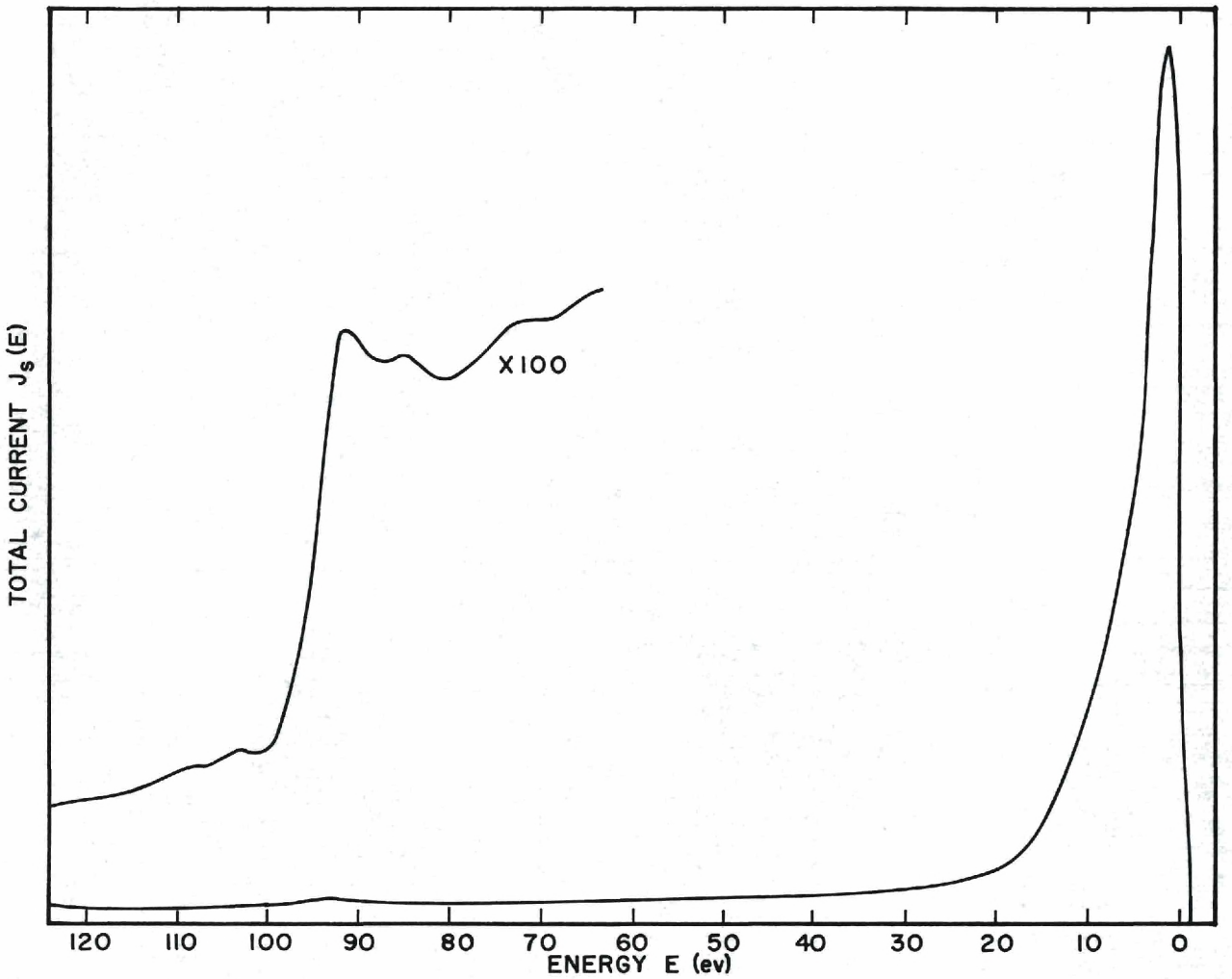

Figure 8. True Secondary Energy Distribution From Silicon (111) Surface with 1000 Volt Primaries Showing the LVV Auger Peak.

distribution thus obtained is considered to be the "true" Auger spectrum and is to be used to solve for the transition density. Confidence as to the accuracy and applicability of the theory is established by comparing the predicted slow peak with the empirical observations.

Analysis of Secondary Distribution

In order to illustrate the above procedure the analysis for silicon is now presented. Starting with the averaged experimental data, the "true" Auger distribution is found by requiring consistency between the theory and experiment. This is performed by a computer procedure as mentioned above in which each point along the Auger spectrum is considered sequentially starting with the high energy limit and varied so that subsequent to the operation of diffusion agreement is attained with the experimental results.

There are two basic steps in accomplishing the objective of obtaining the "true" Auger spectrum. Step one involves subtraction of the background and step two corrects for the inelastic scattering of the Auger electrons. In order to carry out Step one it is recognized that there are five contributions which give rise to the observed true secondary electron energy distribution. These are just the five cases discussed in Chapter III. One of these is the Auger contribution which is just the part needed to go on to Step two. In order to subtract from the data the contribution of the other four cases (low energy and high energy singly excited electrons scattered by electron collisions and plasmon creation) equation III-64 is evaluated for these cases.

$$J(E') = \delta \left\{ \frac{E'}{E' + W} \sum_i \lambda_{oi}(E)\, N_o^{(i)}\, (E' + W) \right. \qquad \text{(III-64)}$$

$$\left. - \frac{5}{2}\left[\frac{3}{2}\left(1 - \frac{W^2}{E' + W)^2}\right) - \frac{E'}{E' + W} \right] \sum \lambda_{2i}(E) N_2^{(i)} (E'+W) \right\}$$

where

$$\delta = 1/2 \sqrt{\frac{E'+ W}{2m}}$$

and

$$W = \text{energy of the vacuum level} \quad .$$

In these calculations for silicon $l_{pp}(E)$ is assumed to be a constant 270Å[53] and $l_{pl}(E) \sim 10$Å.[43] The λ's are given values such that each contribution is commonly normalized for silicon if the mean free paths were the same but weighted proportionately toward the smaller value for differing mean free paths as in the case here. The fermi level occurs at 4.45 ev with respect to a zero of energy which is determined by the following considerations. During the diffusion process new secondary electrons are constantly being created by the elevation of crystal electrons within the fermi volume to higher vacant states. The closer an electron is to the fermi surface the more likely it is to be affected. Not as much energy is needed to excite it to an unoccupied level. To

formally take such a matter into consideration would be extremely difficult. Thus in the same spirit embodied in the theory thus far, an effective penetration of the fermi volume below the surface is imagined. This penetration depth level is taken as the zero of energy. Electrons below this point form the "hard core" and are assumed not to participate in a way described by the theory of Chapter III. If the fermi level is taken at the midpoint of the band gap as is expected for a pure intrinsic semiconductor at zero degrees Kelvin and the penetration depth is five electron volts below the bottom of the conduction band, then for a band gap of 1.1 ev the fermi level occurs at 4.45 ev as mentioned. The choice of penetration depth is hardly more than an educated guess based on a review of Kane's work.[54] However, the results are not overly sensitive to the choice and a nominal value of five volts below the bottom of the conduction band seems to be a good choice for the semiconductors studied. In metals, on the other hand, one would choose the bottom of the conduction band as the zero of energy.

With a calculated expression for $J(E')$ for cases one through four the Auger contribution is obtained by subtracting this $J(E')$ from the experimental data which have been digitalized so that this can be done automatically. There is one complication with this operation: the experimental data and the calculated $J(E')$ which is to be subtracted from the data to give the Auger contribution are not in the same units. The experimental data is in arbitrary units because of the extreme difficulty in an absolute calibration of the experimental equipment. Consequently, before the subtraction operation defined above can be logically carried out it is necessary to multiply (or divide) one curve or the

other by a factor so that they will be suitably expressed. This factor can be determined if one point outside the Auger region is known -- the two curves can then be matched at this point. Although straightforward, experience has shown that this is difficult to accomplish accurately in practice. There is, however, an alternative way to proceed which has proven to be satisfactory and is now incorporated as an automatic part of the computer program. The logic revolves around the requirement that the "true" Auger spectrum finally obtained by the analysis must be zero at E_u and E_ℓ as defined. If both E_u and E_ℓ (the limits of the Auger spectrum) can be determined from the experimental data (or at least estimated with reasonable accuracy) then the desired factor is determined uniquely. The procedure operates as follows: a value for the desired factor, call it κ, is estimated (if one has no idea what the factor may be, a completely arbitrary choice will work just as well). Thus, for example, suppose it is assumed that the theoretically obtained $J(E')$ for cases one through four should be multiplied by two in the case of silicon. Then $J(E')$ is multiplied by this factor (two), subtracted from the experimental data to obtain a trial Auger contribution which is in turn solved for the trial "true" Auger spectrum. This last step is done, again in the case of silicon, by the use of equation III-60b.

$$f(E_u - n\Delta E) = f_n = \frac{N_o^{(5)}(E_u - n\Delta E = E_n) - \frac{2\Delta E}{E_n^2}\sum_{i=1}^{n-1} f_i E_i - \frac{\Delta E}{\lambda_1}\sum_{i=1}^{n-1}\frac{f_i}{E_i}F(E_i, E_n)}{\frac{4\gamma_1 + 1}{4\lambda_1} + \frac{\Delta E}{E_n}\left(1 + \frac{8.8}{\lambda_1}\right)} \qquad \text{(III-60b)}$$

$$E_n = E_u - n\Delta E \; ; \quad \lambda_l = \frac{\ell_{pl}(E)}{\ell_{pp}(E)}$$

$$F(E_i, E_n) = 18.2 \left(\frac{E_i}{E_n}\right)^{5.5} - 0.6 \left(\frac{E_i}{E_n}\right)^{-1.1}$$

with $$N_0(E) = \frac{E' + W}{E'} \text{ (data - factor x } J(E')_{1-4})$$

Equation III-60b is applicable not only to silicon but also for any material which has the Auger spectrum of interest at less than 100 ev. If $f(E_\ell)$ turns out to be zero then the correct factor was chosen. If $f(E_\ell)$ is positive then n should be larger and vice versa. Therefore n is adjusted until $f(E_\ell)$ is zero. The computer program does this by altering n in steps of unity until the closest digit is found, then altering in steps of 1/10 until the closest value to one decimal is found and so on. When the proper n is determined the "true" Auger spectrum is printed out and punched on computer cards for the purpose of transition density analysis by a subsequent program. The "true" Auger spectrum determined in this way for silicon is shown in Figure 9 where E_u and E_ℓ are chosen as 100 ev and 40 ev respectively.

If the "true" Auger spectrum is known either from an independent study or from a previous analysis as above, it can be used in the theoretical prediction of the true secondary electron energy distribution. This, of course, is done by evaluating III-64 for the various cases and the appropriate choice of values for the parameters. Thus for the case of silicon the results which are shown in Figure 10 are obtained from III-64 for the following parametric values: l_{pl} = 10Å, l_{pp} = 270Å, pri-

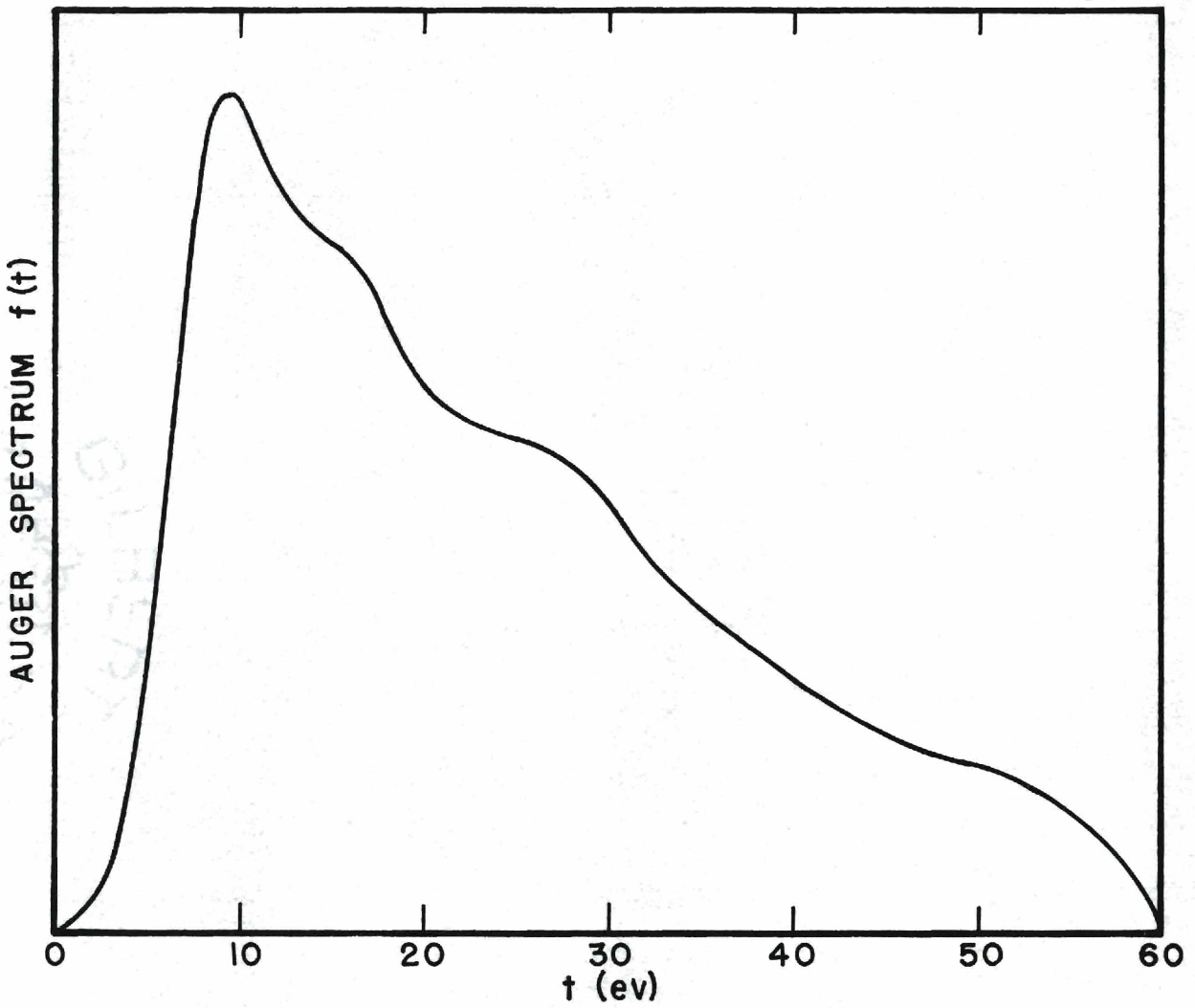

Figure 9. The Auger Spectrum for Silicon (111) After Correcting for the Effects of Background and Inelastic Scattering Distortion.

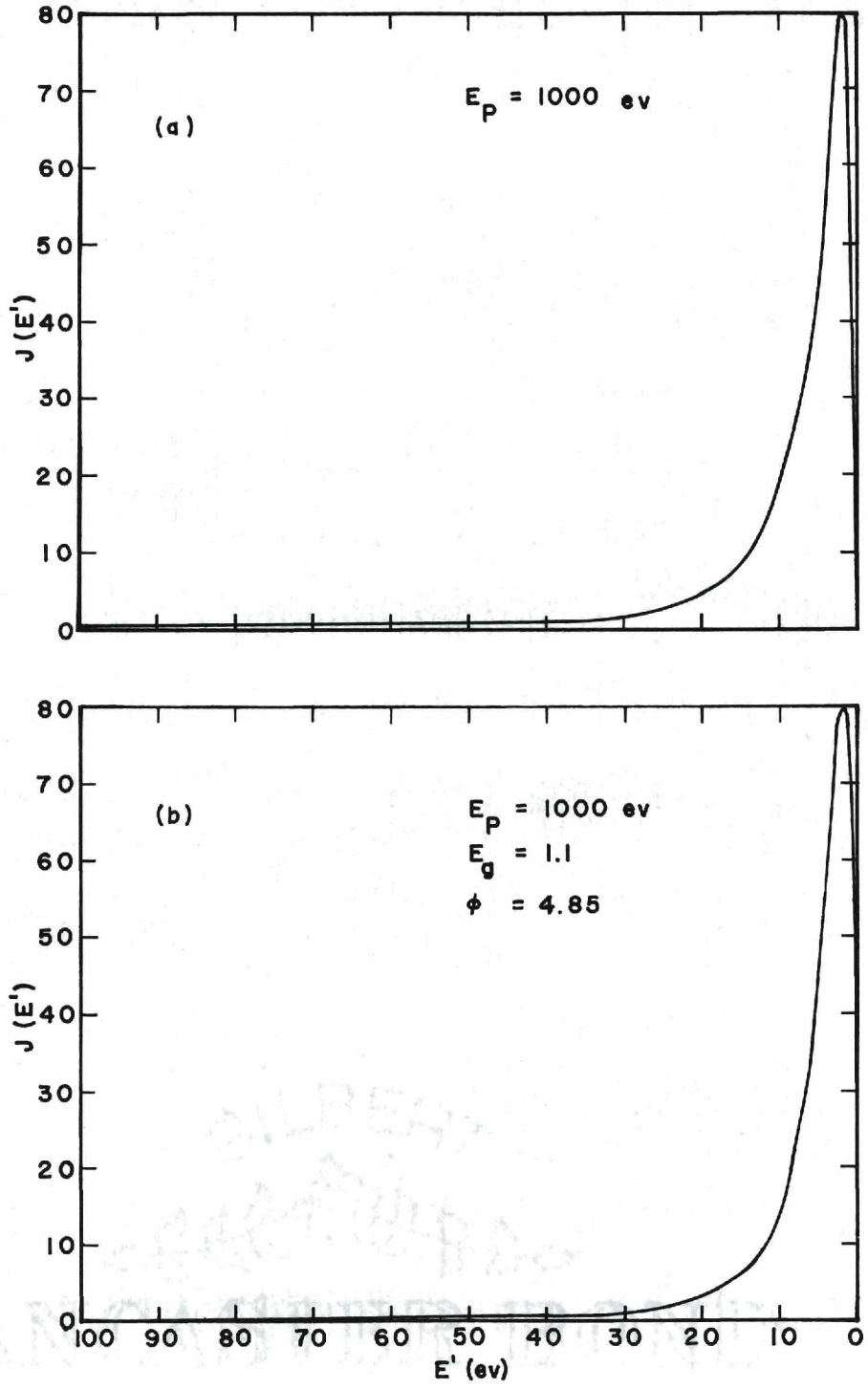

Figure 10. True Secondary Distributions From Silicon
(a) Experimentally Obtained with 1000 ev Primaries
(b) Theoretically Predicted Distribution for Same Primary Energy

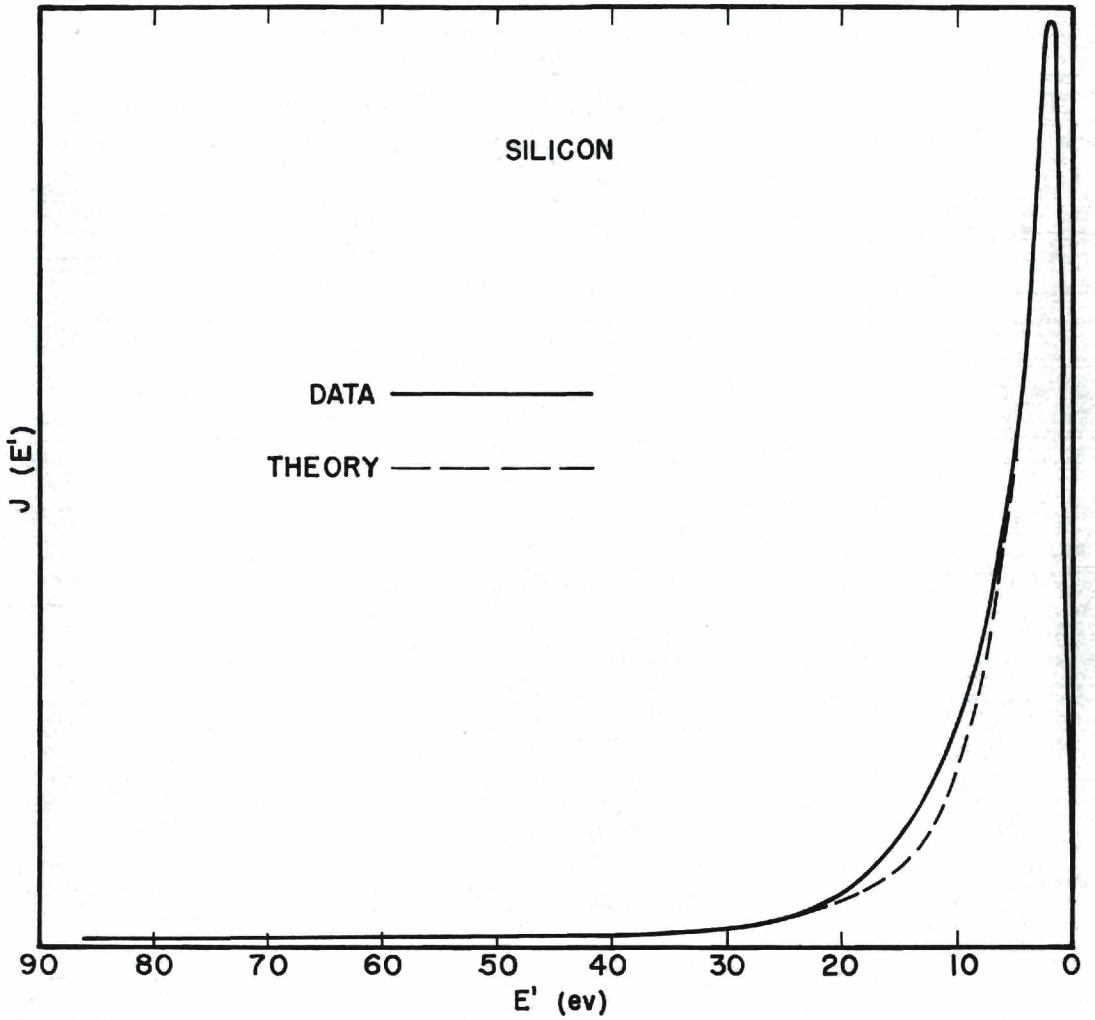

Figure 11. Comparison of the True Secondary Distributions Obtained Experimentally and Theoretically for the Case of Silicon (111) with 1000 ev Primaries.

mary energy E_p = 1000 ev, work function φ = 4.85 ev,[55] band gap E_g = 1.1 ev, and plasma energy E_{pl} = 16 ev. Other parameters used which hold for most other materials as well are cutoff energy E_m = 100 ev (most energetic low energy electron), high energy minimum E_{min}=100 ev, high energy maximum $E_{max} = E_p/2$ = 500 ev and the number of terms kept in the infinite series in $N_2^{(1)}(E)N_{max}$ = 10. In Figure 11 the theoretical results are compared with the experimental findings after adjusting them to a common maximum. The fit appears satisfactory implying that the diffusion theory has not ignored any important effects for the case of silicon. Similar results will be shown to hold for germanium. It should be mentioned that the contribution to the distribution from the N_2 terms is about ten per cent of the total suggesting that only about one per cent is being ignored by keeping only the first three terms of the Legendre Polynomial expansion.

Auger Spectrum Analysis

As shown above the result of the diffusion theory analysis is the predicted true secondary spectrum and the internal Auger spectrum. Using the formalism developed in Chapter II it is possible to analyze this Auger spectrum to obtain an expression for the transition density. In this section such an analysis is presented for silicon. The approach is given in sufficient generality to be directly applicable in the analysis of other materials and, consequently, is not repeated when offering the results for the other materials studied.

A typical analysis -- and the analysis for silicon -- proceeds in the following steps.

(1) An expression for the "true" Auger distribution is obtained using the diffusion theory analysis described above.

(2) The self-consistent derivative expansion is applied to the

distribution to obtain an approximate solution. For purely qualitative considerations, one could stop at this step although a knowledge of the errors of the method should be known.

(3) The Unfold technique is also utilized to obtain an approximate solution. In general this approximate solution is better than that of (2) but there is more labor involved in obtaining results. Again a knowledge of possible errors is important.

(4) Comparison is made between the results of (2) and (3) and a final estimated solution is established based on a knowledge of the possible errors generated by methods (2) and (3).

(5) This new estimate is put into one of the Laplace transform methods and, if necessary, refined until a result consistent with estimated experimental limitations is obtained.

These five steps are now discussed in detail in the following paragraphs.

Having obtained the Auger spectrum by the method of the last section the derivative expansion, based on equation II-42, is employed first.

$$g(t) = \frac{1}{g(o)}\left\{f'\left(\frac{t}{2}\right) - \left(\frac{1}{2g(o)}\right)^2 \int_o^t f''\left(\frac{y}{2}\right) f'\left(\frac{t-y}{2}\right) dy \right. \qquad \text{(II-42)}$$

$$\left. + \left(\frac{1}{2g(o)}\right)^4 \int_o^t \int_o^y f''\left(\frac{x}{2}\right)\left[\tfrac{1}{2}\, f'\left(\frac{t-y}{2}\right) f''\left(\frac{y-x}{2}\right)\right.\right.$$

$$+ f''\left(\frac{t-y}{2}\right)f'\left(\frac{y-x}{2}\right)\Big]dxdy + \ldots\Big\}$$

$$g(o) = \sqrt{f'(o)}$$

It is clear from the expression that the solution does not depend directly on a choice of the mathematical representation for the Auger distribution f(t). However, because it must be possible to estimate the first and second derivatives of f(t) it is sometimes convenient to express the spectrum as some polynomial expansion. Since it is used elsewhere in the analysis, a power series expansion is often a desirable choice. This is not always sufficient justification to use the power series representation however. In situations where it is difficult to express the Auger spectrum accurately as a power series other representations such as Fourier expansion or linear segmentation can be successfully and easily used. The Auger spectrum can be written in terms of a power series as

$$f(\zeta) = \sum_{i=1}^{n} f_i \zeta^i \qquad (1)$$

where the f_i's are chosen so as to yield a least squares fit to the data. For silicon a reasonably faithful representation is obtained for n = 21. A linear segmentation approach is also possible for silicon. In this case the Auger spectrum is partitioned into 0.5 ev intervals and the

value of the y-coordinate is recorded in a manner identical to the linear segmentation discussion of Chapter II. The derivative at the end of the ith partition is expressed

$$f_i' = \frac{f_{i+1} - f_{i-1}}{2\Delta} \tag{2}$$

where Δ is the partition width. The second derivative is expressed

$$f_i'' = \frac{f_{i+1} - 2f_i + f_{i-1}}{\Delta^2} \tag{3}$$

At i = 0 these expressions are not valid. The first and second derivative at zero is estimated by assuming the second derivative to be the same as f_1'' and the first derivative is written

$$f_o' = f_1' - \Delta f_1'' \tag{4}$$

The necessary integrations in II-42 are performed using the trapezoidal rule. It is typically convenient to rescale the energy axis so that $o \leq t \leq 1$ for all t. Such a step often guarantees the convergence of the expansion. The evaluation of expression II-42 for the polynomial and linear segmentation representations results in the approximate silicon transition density solution shown in Figure 12.

Note the tendency of the solution to go negative for greater

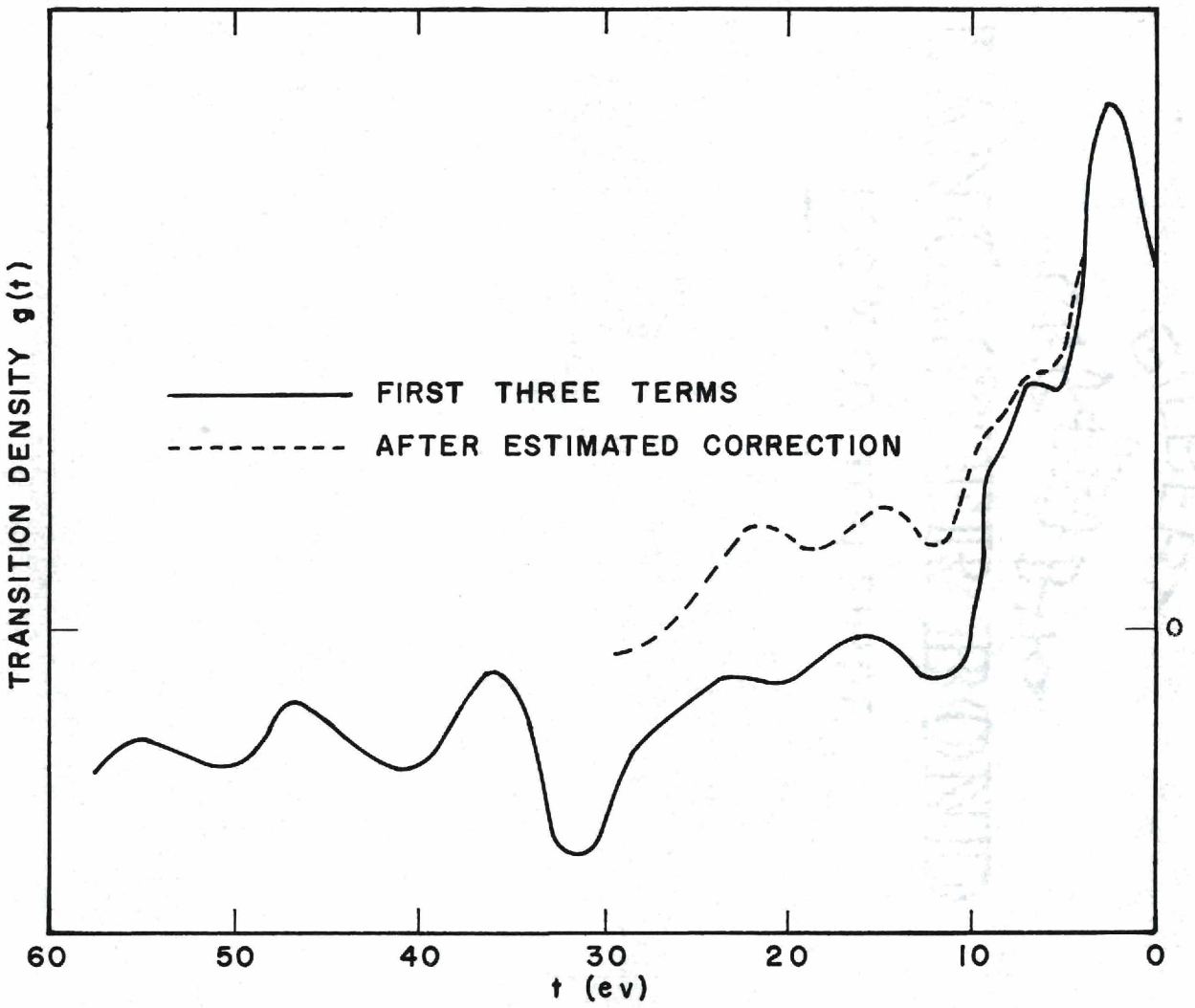

Figure 12. Transition Density for Silicon (111) Obtained by the Self Consistent Derivative Analysis.

values of the band energy ζ. This unphysical tendency seems to result from the dominance of the first term in the series. It is possible, however, to make a qualitative correction to the approximate solution and thereby obtain a better estimate of the transition density. The successively higher terms in this expansion for the extended transition density are just higher order convolutions of the Auger spectrum first and second derivatives. A smoothing effect is likely. Thus, most of the important structure of the transition density is expected to be contained in the first few terms. The sum of all terms ignored should have the general character of a rather smooth curve starting at zero and monotonically changing as ζ approaches ζ_1. From the definition of the extended transition density function $\bar{g}(\zeta)$, the solution is expected to be identically zero for values of ζ greater than ζ_1. Since ζ_1 is known to assume a value equal to one-half the Auger spectrum spread, ζ_1 is obtained through a knowledge of the Auger distribution. The correction to the approximate solution is such that the solution will be approximately zero on the interval $[\zeta_1, 2\zeta_1]$. Moreover, the error exhibited by the solution on this interval is expected to be more or less the same as on the interval $[o, \zeta_1]$. Now expression II-42 is not strictly correct on the interval $[\zeta_1, 2\zeta_1]$ because the discontinuity at ζ_1 has not been explicitly considered. Taking this into account results in a delta function which, when integrated, gives an additional term on the right of II-42. The additional term is

$$- \frac{1}{g(o)} \Big(g(t - \zeta_1) g(\zeta_1) \Big) \; ; \; t > \zeta_1 \qquad (5)$$

Using this an expression for $\bar{g}(t)$ on $[\zeta_1, 2\zeta_1]$ can be obtained and used as an estimate of the error in the solution due to the omission of the higher order terms. If desired, a new estimated transition density can be obtained by adding the negative of the results on $[\zeta_1, 2\zeta_1]$ to the solution obtained on $[o, \zeta_1]$. Once corrected the amount of uncertainty in the new estimate of the transition density is anticipated to be at most twice the amplitude of the average structure in the $[\zeta_1, 2\zeta_1]$ interval. The results of such an operation for silicon are shown in Figure 12.

The next step in the analysis of the Auger spectrum data is to return to the original distribution and obtain a solution by use of the Unfold technique which was discussed in Chapter II. As required by the method, the analysis begins by dividing the data into n equally spaced divisions and recording the "y" coordinate of the data at each division point. For silicon a partition of $\Delta\zeta = 0.5$ ev is selected. The solution, which is in the form of a histogram, is obtained by evaluating each of equations II-24.

$$g_1 = \sqrt{\frac{2f_1}{\epsilon}} \qquad \text{(II-24)}$$

$$g_2 = \sqrt{\frac{\epsilon}{2f_1}} \; \frac{f_2}{\epsilon}$$

.

.

.

$$\sqrt{\frac{\epsilon}{2f_1}}\left[\frac{1}{\epsilon}f_s - \sum_{i=2}^{s/2} g_i g_{s-i+1}\right], \quad s \text{ even}$$

$$g_s =$$

$$\sqrt{\frac{\epsilon}{2f_1}}\left[\frac{1}{\epsilon}f_s - \frac{1}{2}g^2_{\frac{s+1}{2}} - \sum_{i=2}^{(s-1)/2} g_i g_{s-i+1}\right], \quad s \text{ odd}$$

Because of the sensitivity of the solution to the initial points, wild oscillations often begin to dominate the solution as ζ approaches ζ_1. This can usually be satisfactorily reconciled by employing a three-point smoothing program. Thus each data point is replaced by $f_i = \frac{f_{i-1} + f_i + f_{i+1}}{3}$. Equations II-24 are then re-evaluated. When necessary, this smoothing procedure is repeated twice more. On occasion it is found that the resulting solution still does not behave in a satisfactory manner. In such instances, improvement in the solution is usually obtained by truncating the first point or two from the data and proceeding from there as the new zero. (Recall that there is a finite uncertainty in the choice of E_u). This is especially effective if the original $f'(0)$ is small. In the rare case when this is still not sufficient, the data points in the vicinity of the origin can be replaced by a "smooth" function such as $f(\zeta) = \zeta^2$. This is usually restricted to the first several partitions (generally < 1 ev).[27] For silicon it is necessary to truncate the first two points as well as smooth the data. The solution for the transition density in silicon by the method of Unfolding is given in Figure 13. This is to be compared with the result obtained earlier by the self-consistent iterative technique. Based on a

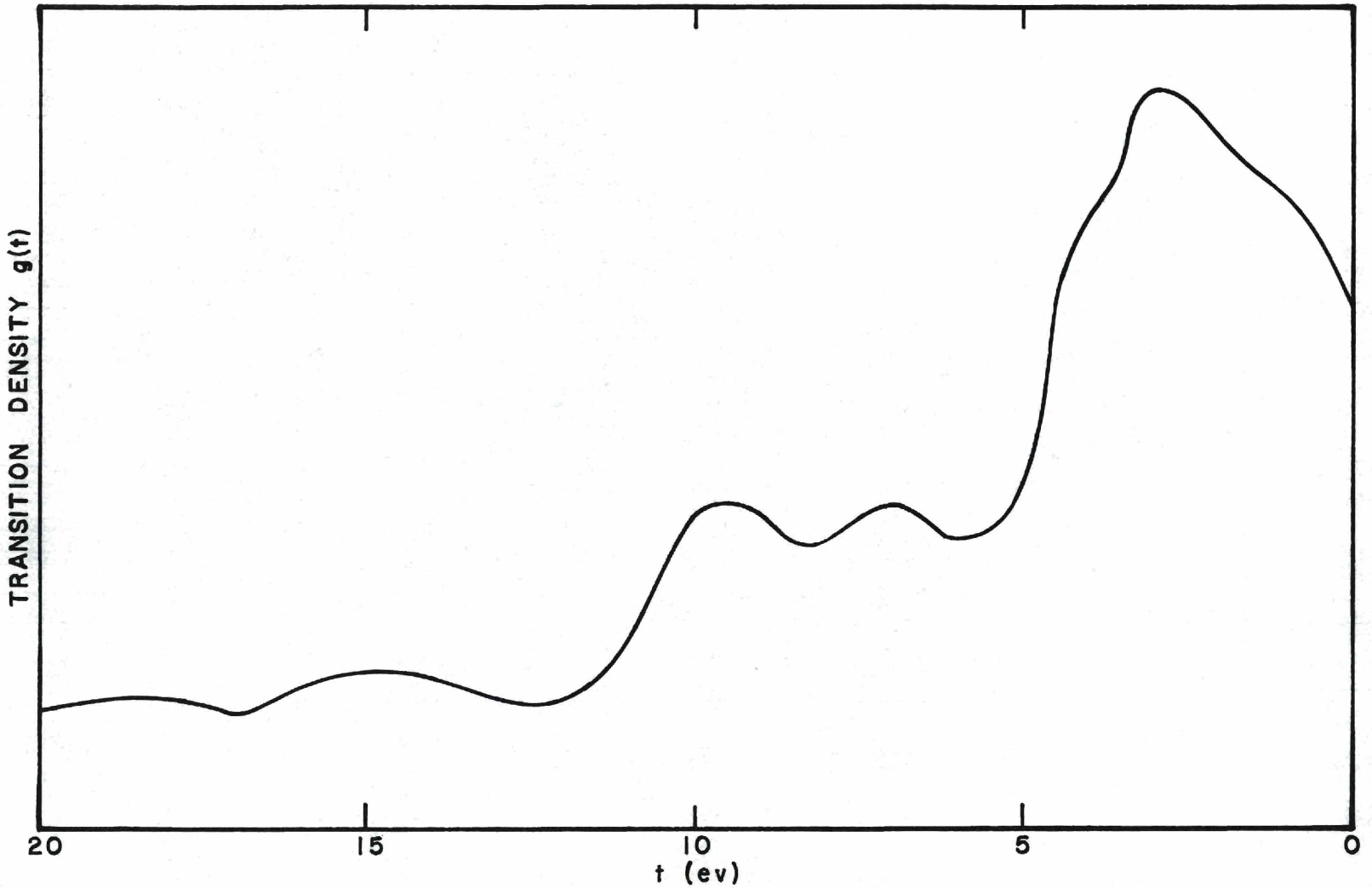

Figure 13. Transition Density Solution for Silicon (111) Obtained by the Unfold Approximation.

comparison of these two, a probable solution can be inferred.

Generally speaking, there is no cut and dry method for the inference of this probable solution. However, an understanding of the possible sources of error in the two estimates can serve as a guide. The following statements can be made about the two types of transition density analysis considered thus far.

(1) Both methods tend to be accurate for small ζ although the Unfold is generally superior.

(2) The self-consistent derivative expansion method tends to overlook the fine structure as well as be somewhat less than the correct value for ζ approaching ζ_1.

(3) The Unfold technique averages around the correct value but tends to break into unphysical oscillations for ζ approaching ζ_1.

Based on these considerations the result shown in Figure 14 is selected as the probable solution for the transition density of clean silicon (111).

The final step in the analysis is a check on this transition density solution by use of one of the Laplace transform methods. The easiest of these methods to apply is usually the linear segmentation approach although the others are not significantly more difficult. For the linear segmentation method equation II-38 is used.

$$\sum_{i=1}^{n} g_i e^{-is\epsilon} = \left[\frac{2}{\epsilon}\sum_{j=1}^{2n-1} f_j e^{-(j+1)s\epsilon}\right]^{\frac{1}{2}} \qquad \text{(II-38)}$$

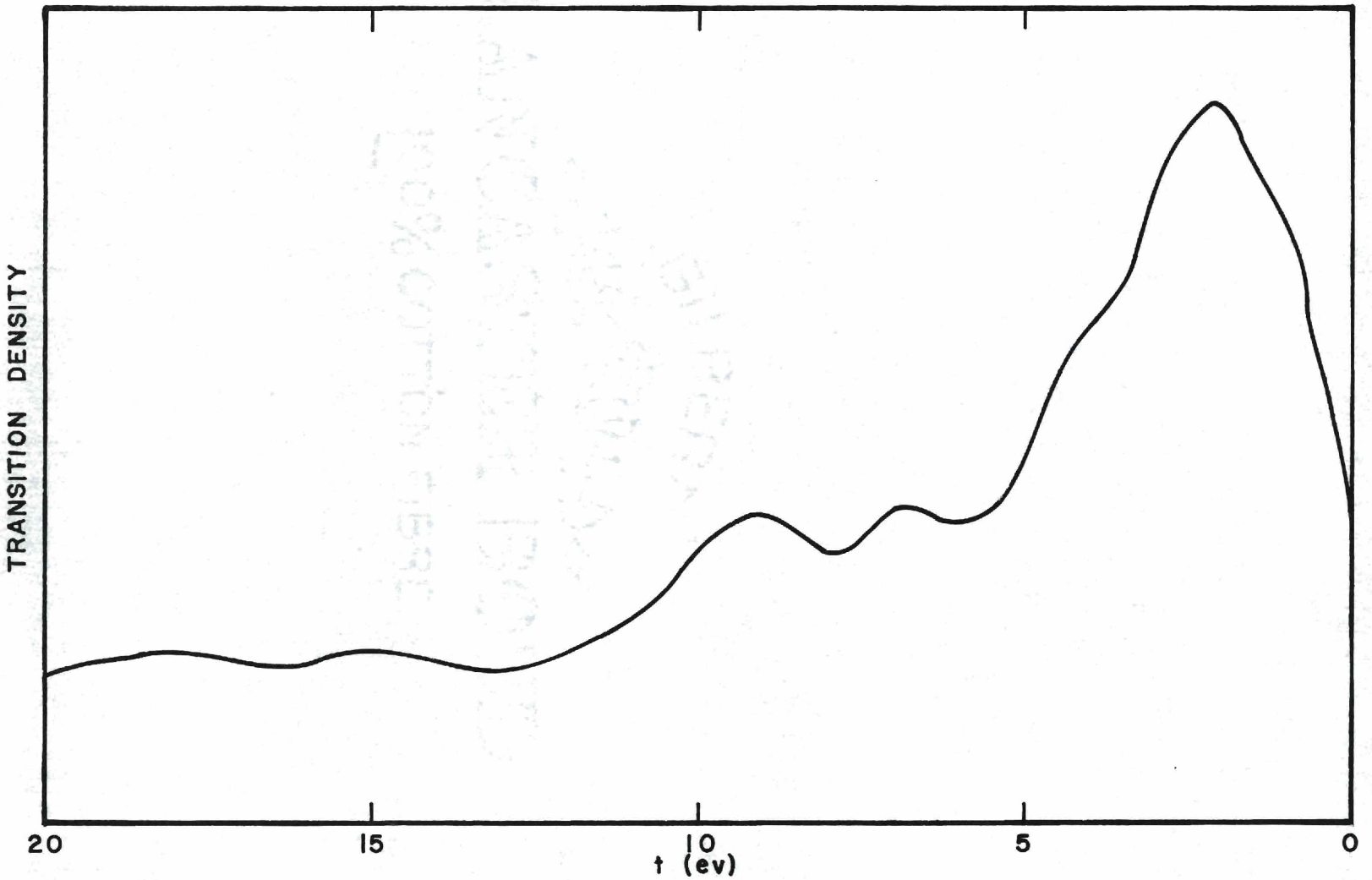

Figure 14. Final Transition Density Solution for Silicon (111) Found to be Consistent with All Methods of Analysis.

The estimated solution from above is divided into n segments -- the ith segment having the value g_i. The left hand side of the equation is then evaluated for the various values of s. For mathematical convenience, these values of s are generally chosen so that $\exp(-s\varepsilon)$ falls in the interval (1,2) although this is by no means essential. The result is some function of s. Similarly the right hand side is evaluated using the data points. A probable experimental error is associated with each of the data points so that the result of evaluating this side of the equation is not a line but a band of values. If the trial solution used generates a function of s (the left side of equation II-38) which falls in the allowed band, then the solution is considered satisfactory. If not, the transition density function is modified until this condition is met. This is done by modifying g_n first in such a manner that the solution moves toward the allowed band; then g_{n-1} is adjusted and so on. This procedure begins with g_n because the methods used to estimate the trial solution are most likely to be in error for ζ near ζ_1. A similar philosophy is employed when utilizing one of the other two Laplace transform formulations as a check. For silicon with a value of $n = 30$ and a ten per cent margin of error in the data, the estimated solution produces a function of s which falls within the ten per cent band and hence no further adjustments are necessary (Fig. 15).

Silicon With Oxygen Contamination

While carrying out the necessary experimental work it was observed that the Auger spectrum from silicon is sensitive to surface conditions (Fig. 16). To investigate this observation further, the silicon crystal was reacted with O_2 at a pressure of 5×10^{-7} torr for fifteen minutes.

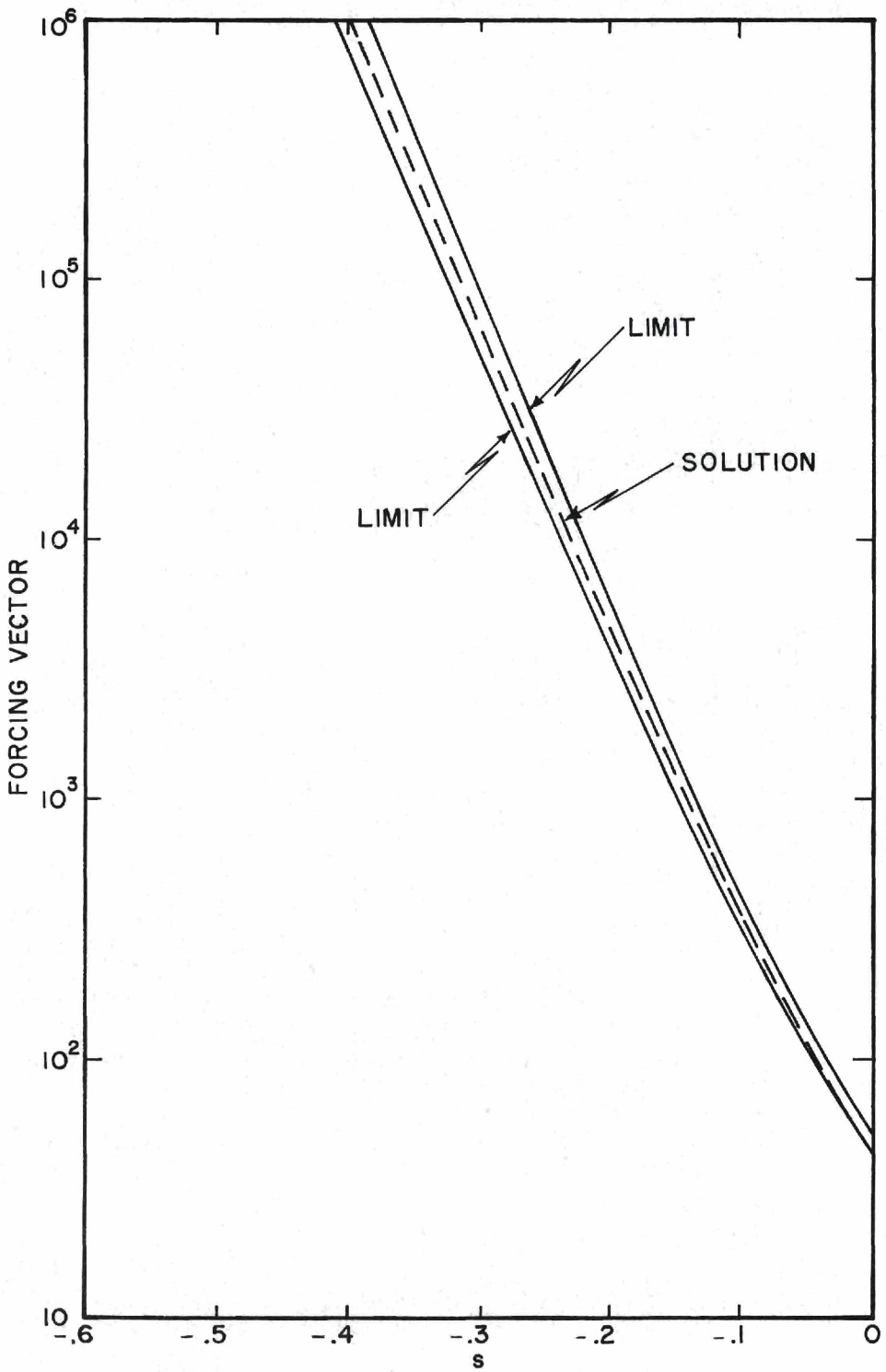

Figure 15. Plot of the Forcing Vector Generated by the Solution in Terms of the Laplace Frequency Variable Compared with the Experimentally Determined Allowable Limits.

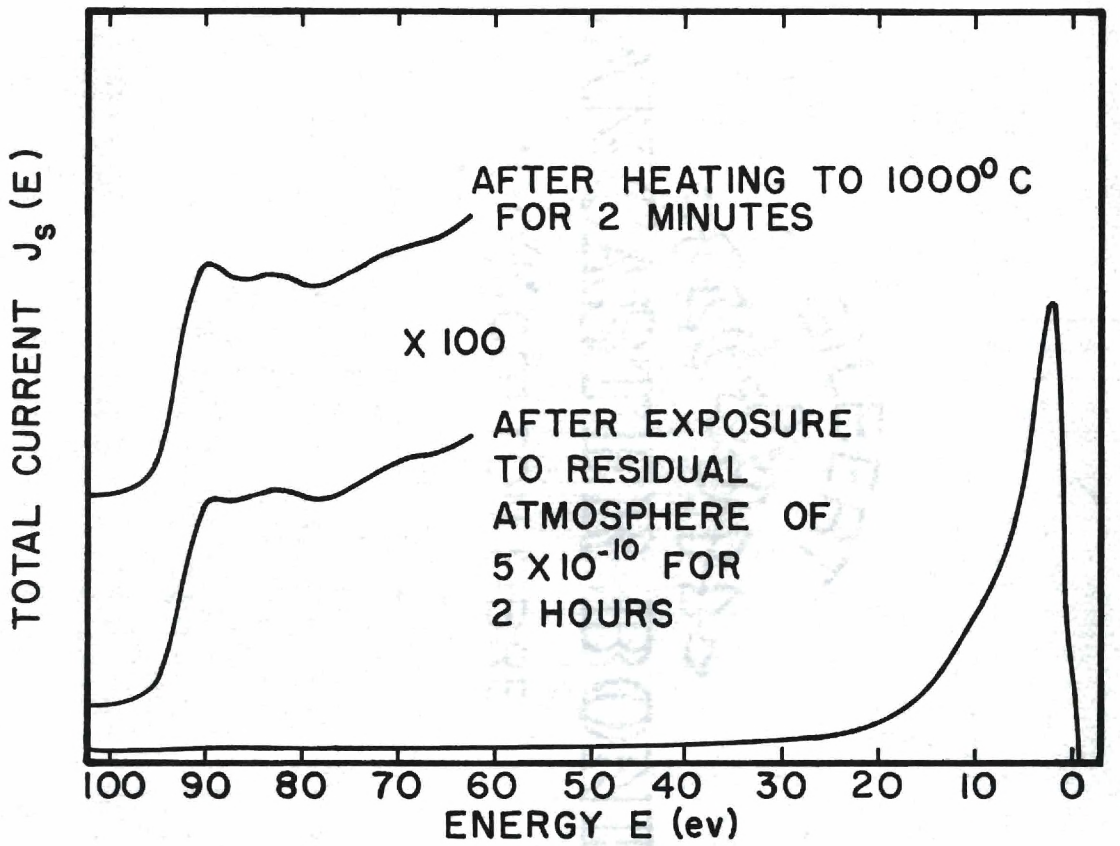

Figure 16. Comparison of the Silicon (111) Auger Spectrum From a Slightly Contaminated Sample with That From a Clean Surface.

For two of the fifteen minutes the crystal was heated to 600 degrees Centigrade. After returning to a background pressure of 1×10^{-9} torr, a diffraction pattern like that of Figure 17 was observed. The surface is clearly contaminated. Electron energy distribution measurements and diffusion theory analysis results in a characteristic Auger distribution somewhat different from that of the clean system (Fig. 18). All measurements were taken with the same instrument settings as the clean silicon data so that direct comparisons could be made. Likewise, the transition density analysis proceeded in a manner identical to that reported above. The results seen in Figure 19 are to be compared with the transition density for the clean Si(111) surface.

Germanium

Preparation

Several germanium single crystals oriented along the (111) and (100) surfaces were obtained from Dr. F. Jona of IBM Watson Research Center. Each crystal had been mechanically cut to approximately $\frac{1}{4}$" x 3/8" x 3/32". The preparation of the samples for the electron scattering studies was carried out in three steps. First, the sample was mechanically polished by hand using a medium nap polishing cloth and a 0.3 micron followed by a 0.1 micron polishing solution. The germanium crystal was then chemically etched using the technique given by Tegart.[56] Finally, the sample was polished using the sodium hypochlorite procedure described by Reisman and Rohr.[57] All samples were quenched in methyl alcohol before insertion into the vacuum system. After Argon ion bombardment of the germanium surface in a manner similar to the silicon treatment satisfactory diffraction patterns characteristic of the (111) and (100) structures were obtained.

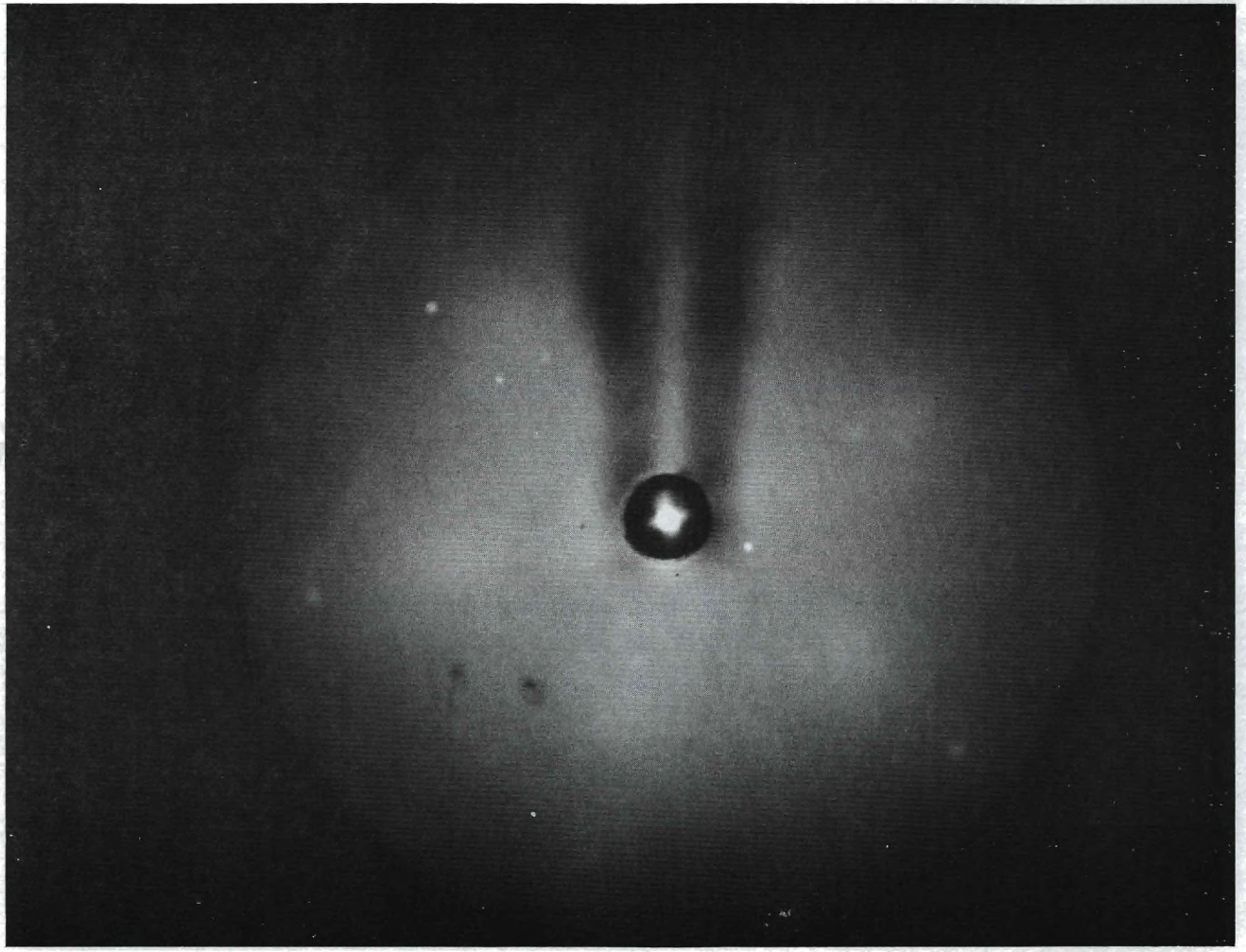

Figure 17. LEED Pattern From Silicon (111) Surface Heavily Contaminated with Oxygen.

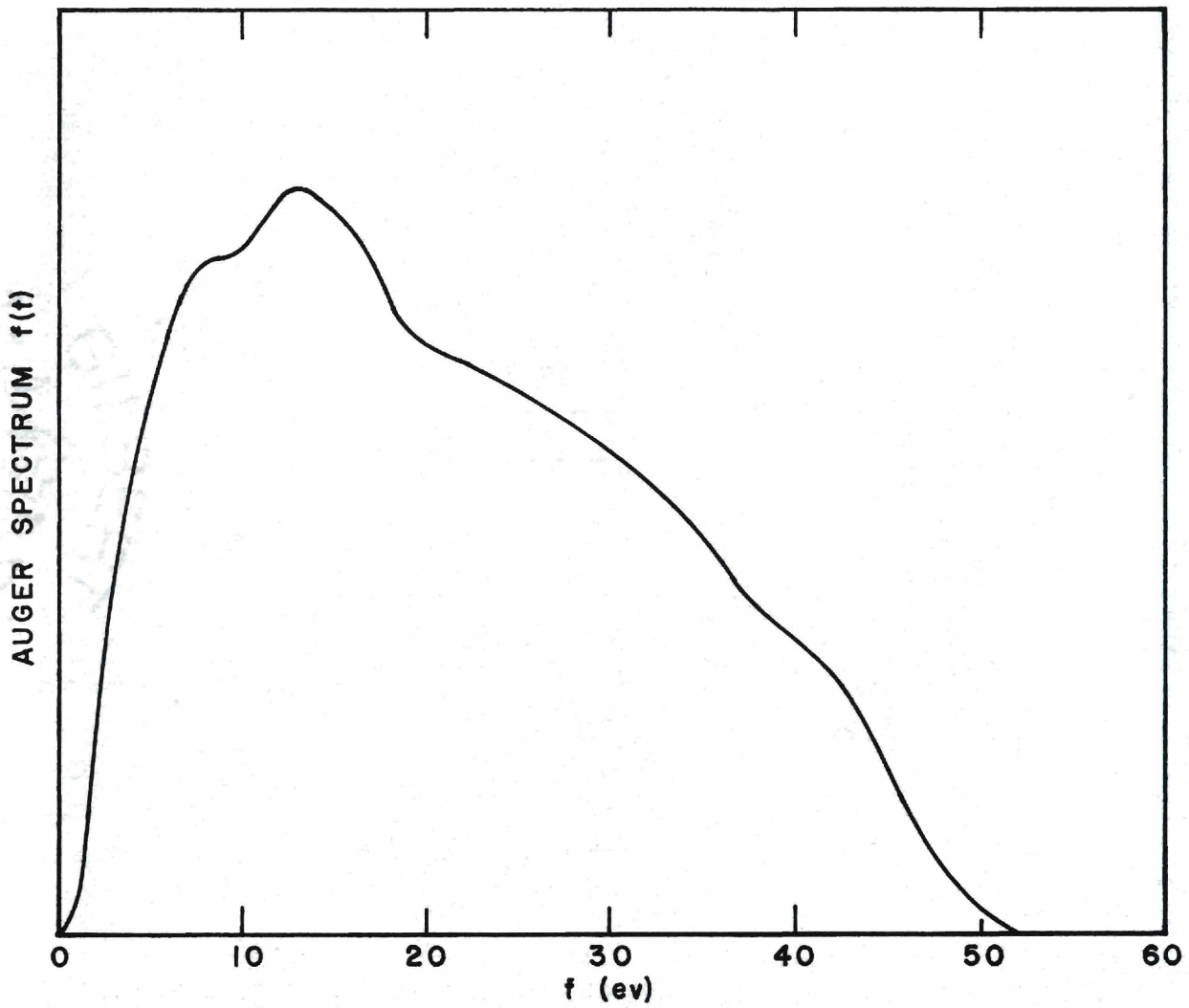

Figure 18. Corrected Auger Spectrum Resulting From Oxygen Contaminated Silicon (111) Surface.

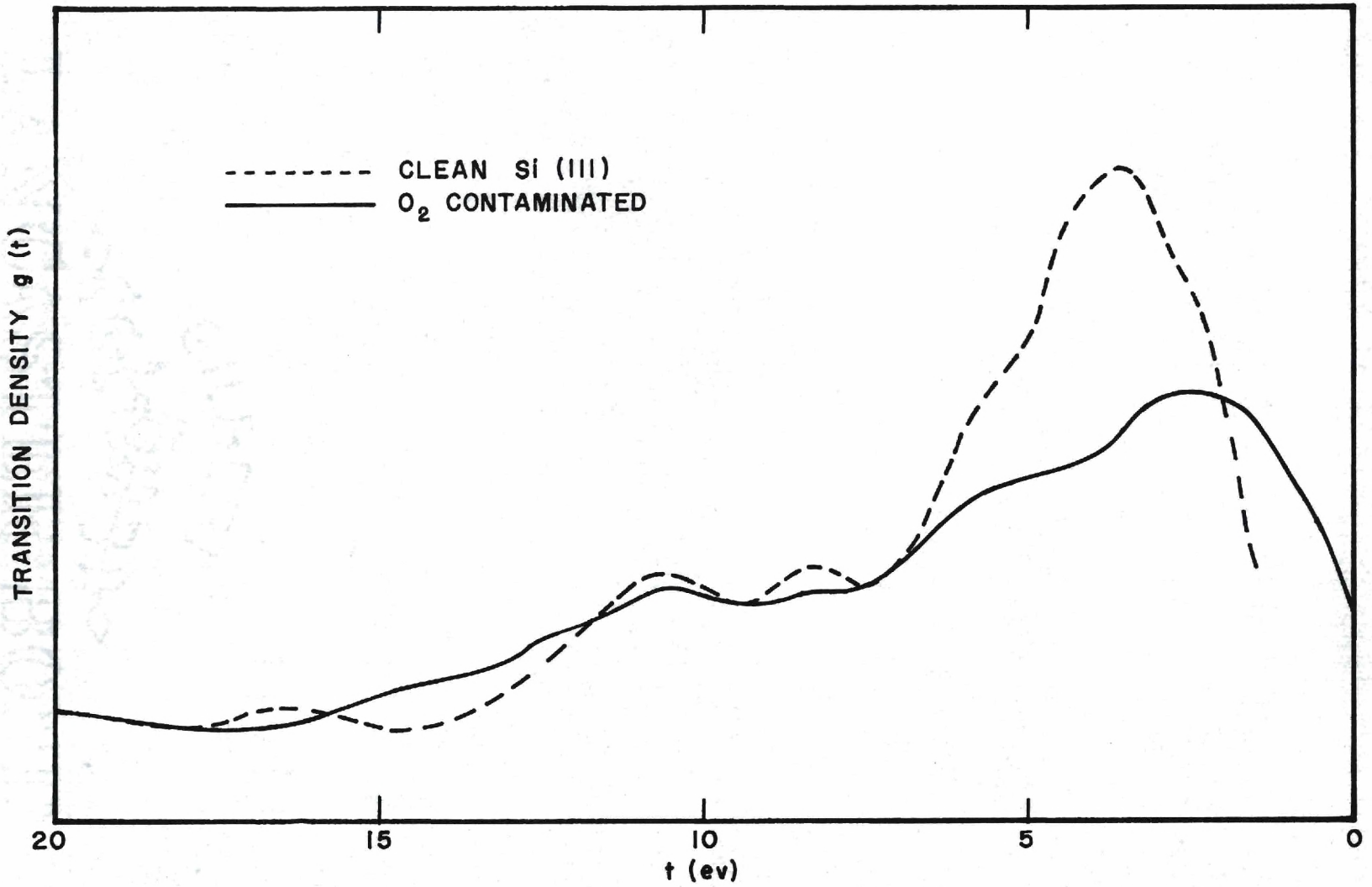

Figure 19. Transition Density for Oxygen Contaminated Silicon (111) Surface Compared with Clean Surface Results.

Auger Spectrum and Transition Density

Germanium is the element following silicon in group IV of the periodic chart and hence the K, L, and M levels are all filled. Auger processes involving the valence band and any one of these low lying levels are possible. However, because of energy limitations with the experimental apparatus only the M shell interaction was observed. According to characteristic x-ray data,[58] the M shell has five sublevels: one at about - 175 ev, two about - 110 ev, and two about - 30 ev. Although evidences of Auger spectra arising from these three regions were observed ($\sim$ - 140 ev, - 90 ev, - 50 ev) only the Auger spectrum originating from the highest M level was sufficiently strong to obtain satisfactory data. The Auger spectra resulting from diffusion theory analysis (Figures 20 and 21) for the (100) and the (111) surfaces are shown in Figure 22. The values used for the various parameters in the diffusion theory were the same as silicon except for the work function φ = 4.5 ev, band gap E_g = 0.85 ev, and primary energy E_p = 950 ev. The transition density solutions obtained by the methods already described are shown in the next figure.

Graphite

The third and final system to be considered is the basal plane of single crystal graphite.[59] Also a member of group IV, the hexagonal layered carbon structure has properties which resemble both semiconducting and metallic materials. The conduction and valence bands touch at one point only (the Γ or K = 0 point) according to Corbato's calculation[60] and thus the system can be viewed as a zero band gap semiconductor. Nonetheless, there is generally a sufficient number of electrons thermally

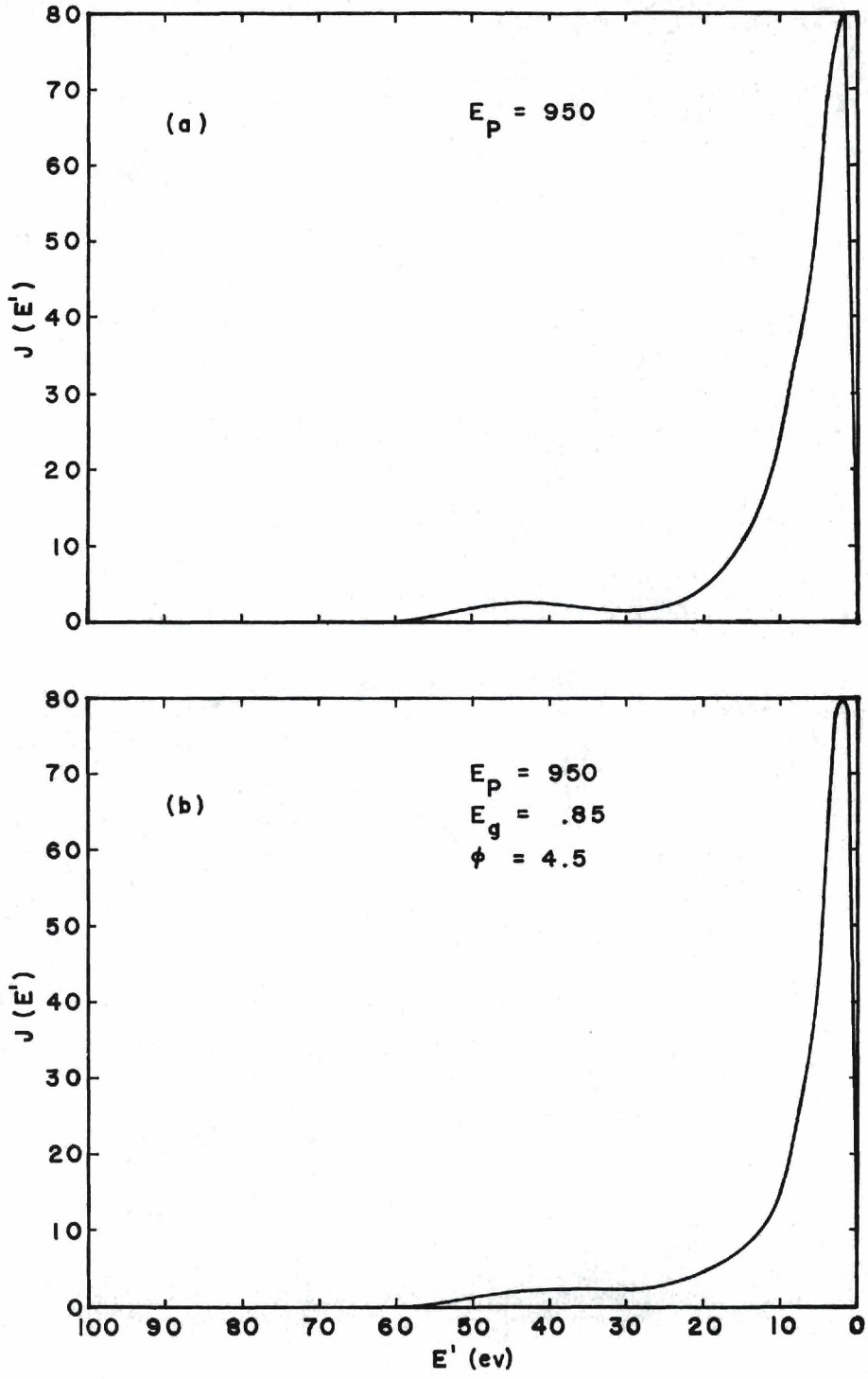

Figure 20. True Secondary Energy Distributions in Germanium (a) Experimental Results for 950 Electron Volt Primaries (b) Theoretical Results

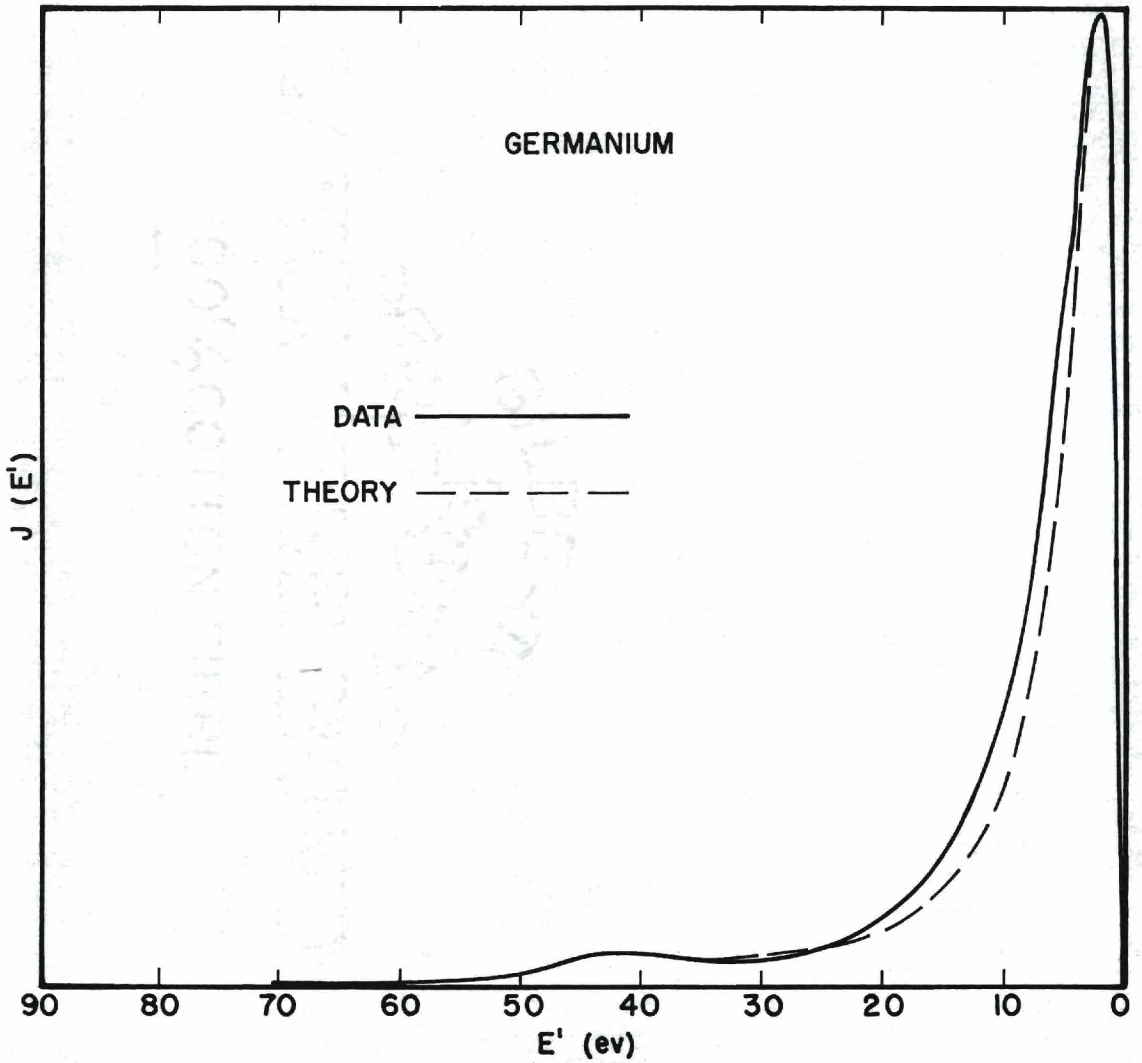

Figure 21. Comparison of the Theoretical and Experimental Results for the True Secondary Electron Energy Distribution From Germanium.

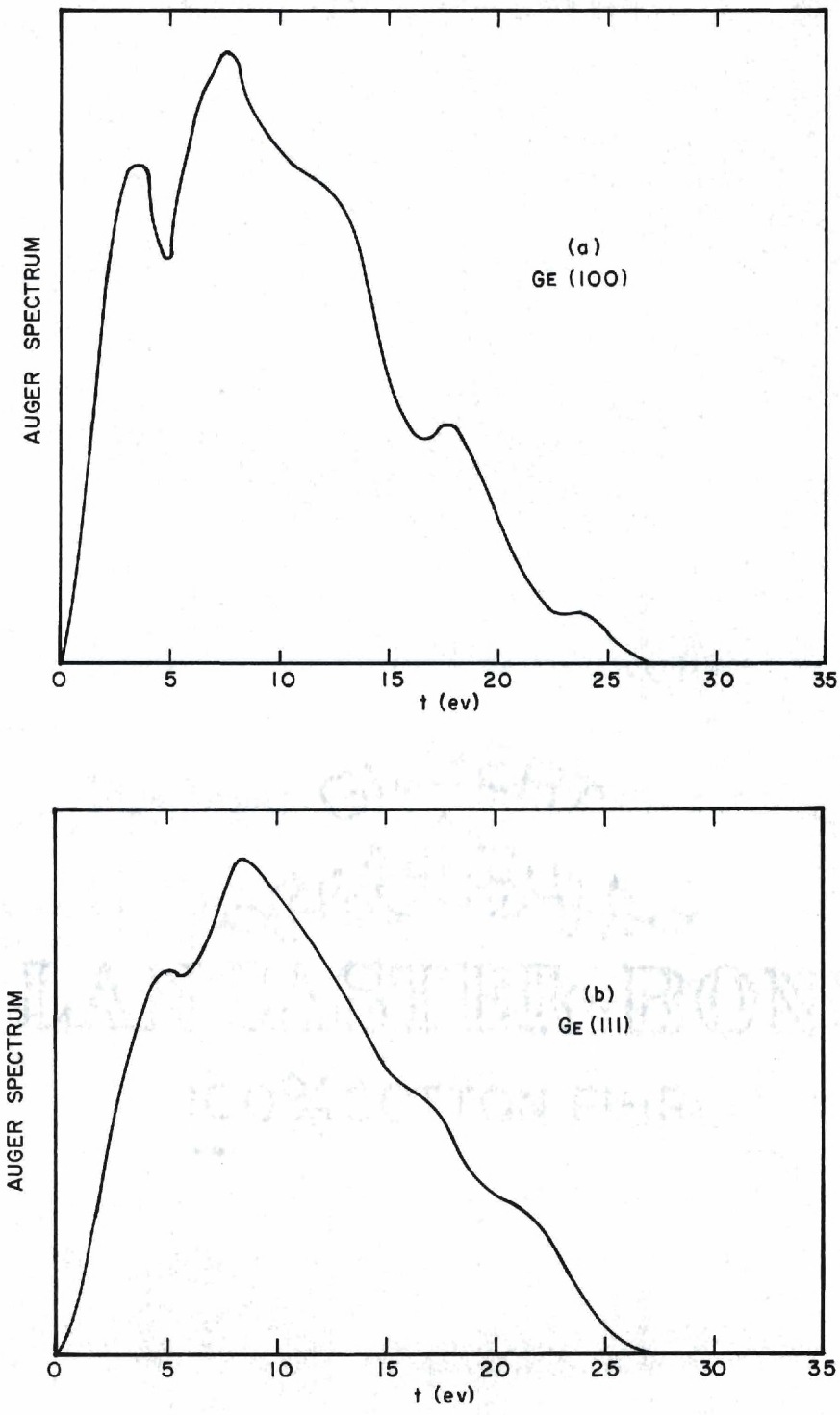

Figure 22. Auger Spectra for Germanium After Correcting for the Effects of Background and Inelastic Scattering Distortion (a) for (100) Surface (b) for (111) Surface.

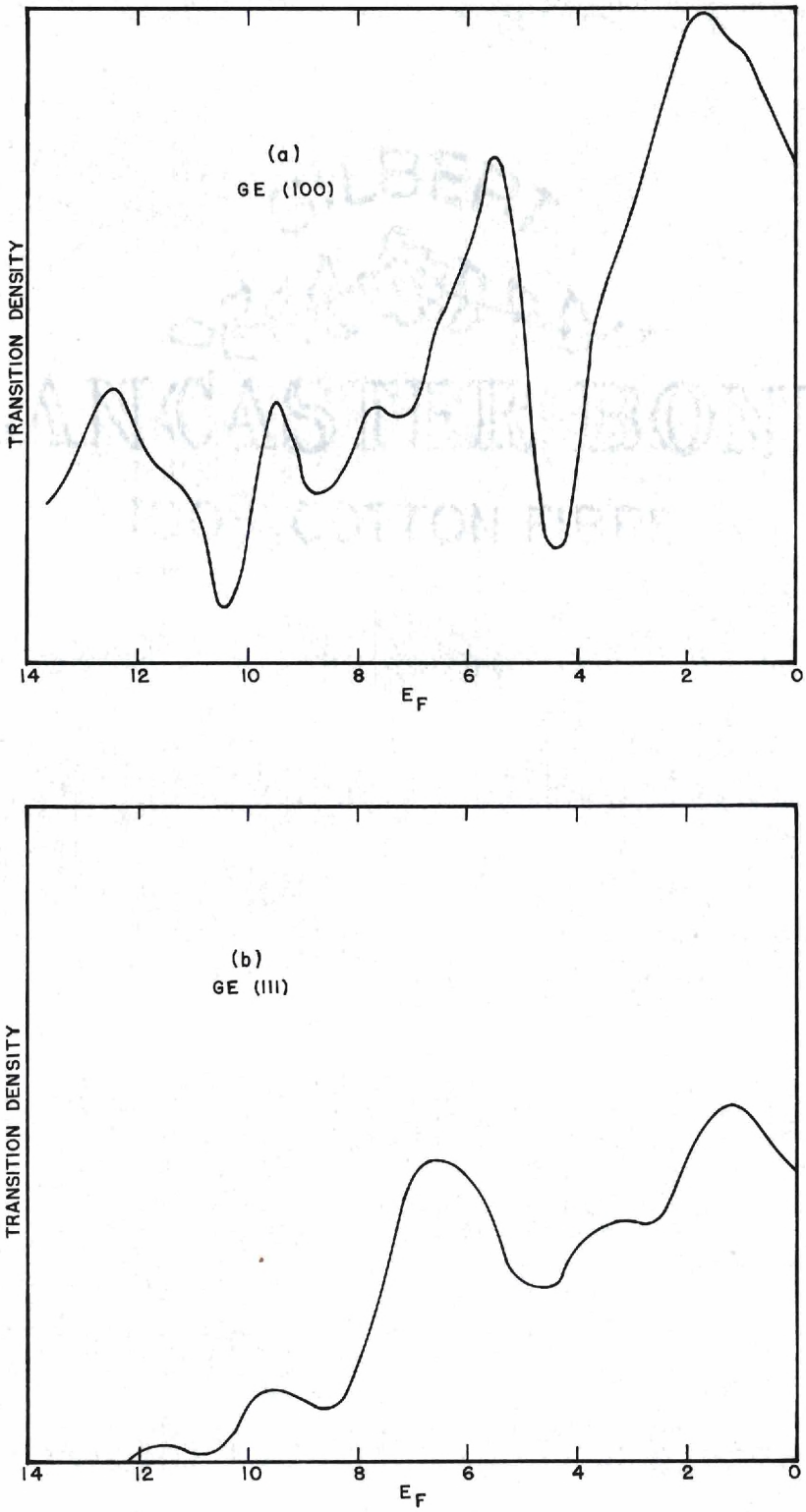

Figure 23. Transition Density of Germanium (a) (100) Surface (b) (111) Surface.

excited to the conduction band for it to conduct reasonably well. Furthermore, the wide spacing between the various planes justifies treating the system as a two dimensional entity at least as a first approximation (this is in fact the basis of Corbato's band calculation).

Preparation

The graphite single crystal is initially prepared by cleaving it in the air and immediately locating it in the vacuum system. Although a diffraction pattern is then attainable, the crystal is not atomically clean. This objective is achieved in the following way. Beginning with a background pressure of 5×10^{-10} torr, an O_2 treatment is administered in which oxygen is allowed to react at a pressure of 5×10^{-6} torr and an optical pyrometer temperature reading of 900°C for 30 minutes. Following this the crystal is allowed to cool slowly to room temperature and the sample chamber is permitted to return to the standard background pressure. This having been accomplished, the crystal is flashed to 1500°C for five seconds for the final step of cleaning. Figure 24 demonstrates the LEED patterns at various stages of the cleaning procedure. The reproducibility and cleanliness of the crystal surface is established in three ways. First of all, the LEED patterns must be sharp and clear. Secondly the energy distribution curves must be entirely reproducible. Finally, a residual gas analysis must reveal no gas desorption.

Use of the quadrupole residual gas analyzer interestingly revealed the tendency of graphite to adsorb CO, contrary to previously published results. During the oxygen treatment it is observed that the carbon monoxide background increased markedly implying that the oxygen was indeed reacting with the carbon. In Figure 25 the mass spectrum (actually m/e)

(a) Before cleaning the sample. Notice diffuse background.

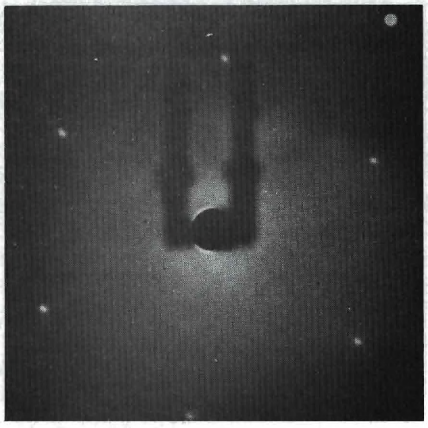

(b) After O_2 exposure @ $5X10^{-6}$ Torr for 30 minutes during which crystal heated to 900°C.

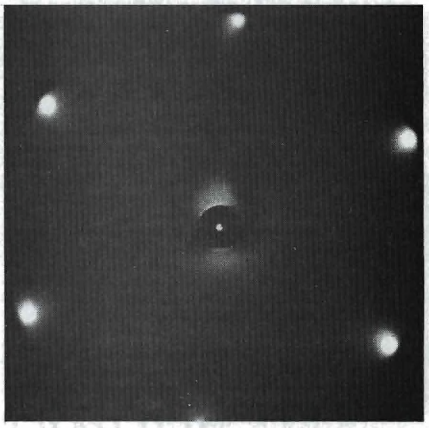

(c) After 5 second flash to 1500°C.

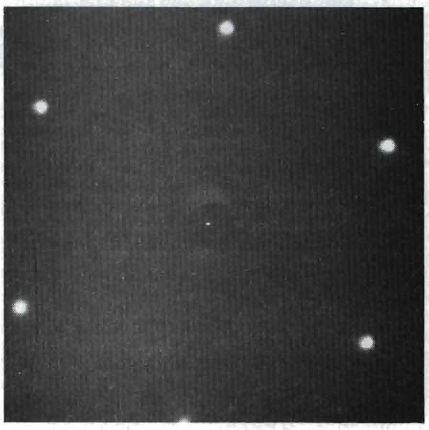

Figure 24. LEED Patterns for 70 Volt Primaries During Cleaning Procedure of Basal Plane of Graphite.

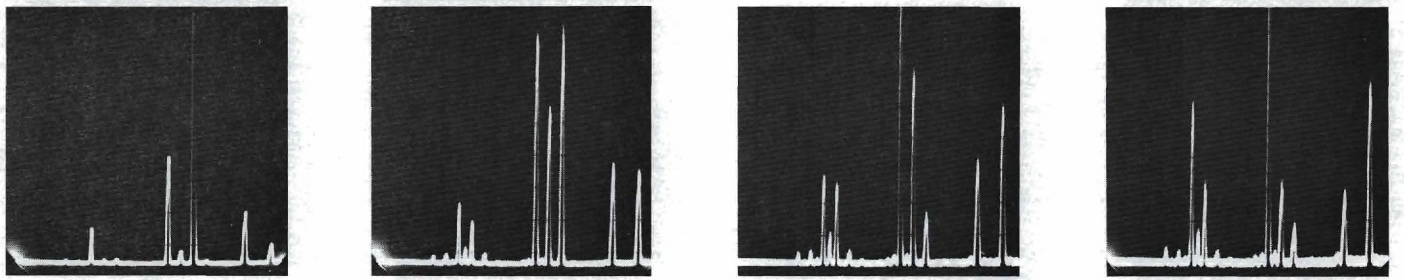

(a) Oxygen Treatment: (1) During O_2 exposure and heating. (100)

(2) At conclusion of O_2 treatment. (5)

(3) Short time after treatment. (2)

(4) Long time after treatment. (1)

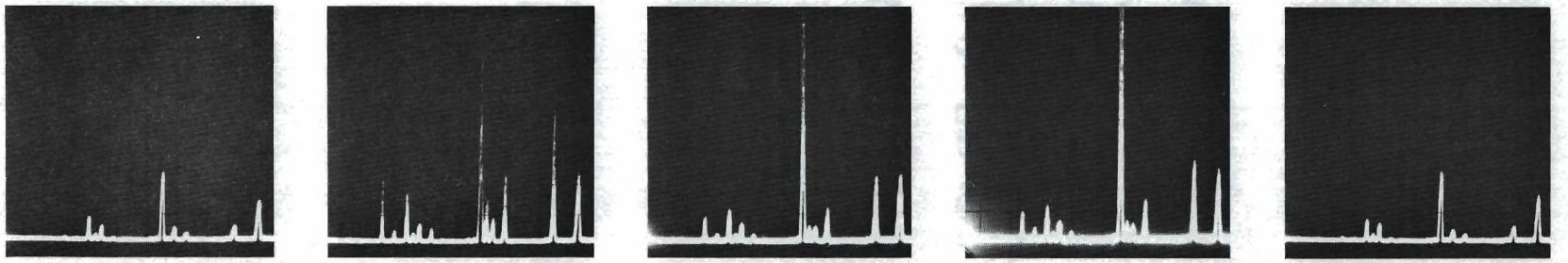

(b) Flash

Figure 25. Residual Gas Analyzer Mass Spectrum Traces During Cleaning Procedure of Graphite. Numbers in Parentheses Refer to Relative Scale Sensitivity.

is displayed at various times during the cleaning procedure. Notice, too, that during the flashing procedure a steady evolving of carbon monoxide is evident. This apparently means that carbon monoxide must have been physically adsorbed to the graphite surface. However, since there are no observable changes in the diffraction pattern, the adsorption must not be ordered.

Auger Spectrum and Transition Density

Because carbon has a low atomic number, graphite has only the K shell filled. Therefore, the only possible Auger transition is that which appears in the true secondary distribution at an energy of about 270 ev (Figure 26). This relatively high energy removes the Auger spectrum from the slow peak making corrections for background contributions of minor importance. Moreover, because of the two dimensional nature of the system the effects of distortion due to inelastic scattering are expected to be minimal. Nonetheless, some scheme to arrive at an expression for the true Auger distribution is needed. This is done in the case of graphite by correcting only for the effect of refraction across the surface potential, ignoring background and inelastic scattering distortion. Based on the earlier comments this should introduce only a small error. The resultant Auger spectrum is given in Figure 27 followed by the transition density solution next.[30]

Summary of Data Analysis Technique

In this section a step by step summary of how the analysis of characteristic Auger spectrum data proceeds is presented.

(1) The experimental data throughout the Auger region is digitalized (that is, each point is given an x and y coordinate).

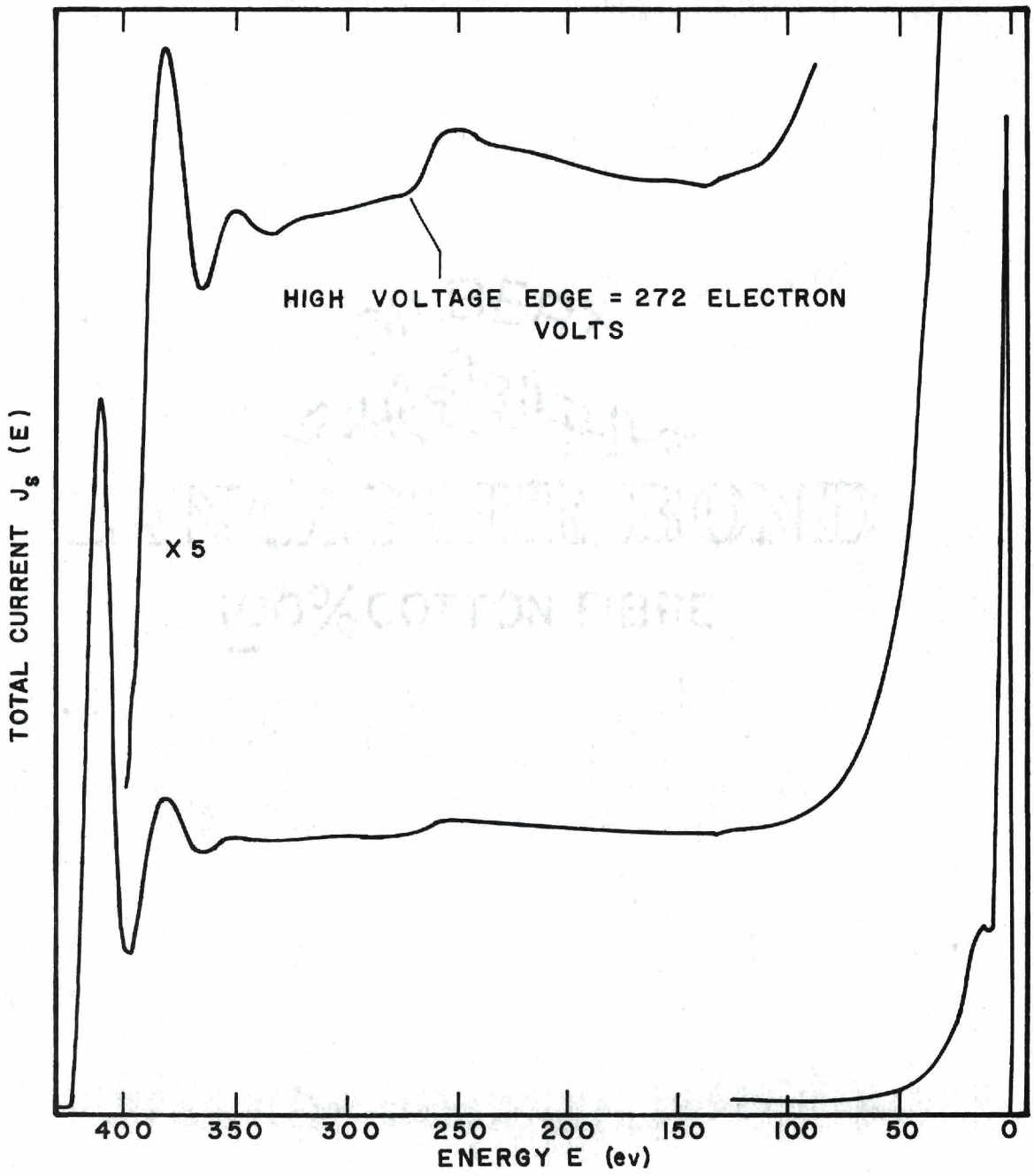

Figure 26. Emitted Electron Energy Distribution for 425 Electron Volt Primary Electrons on the Basal Plane of Graphite Showing the KVV Auger Peak.

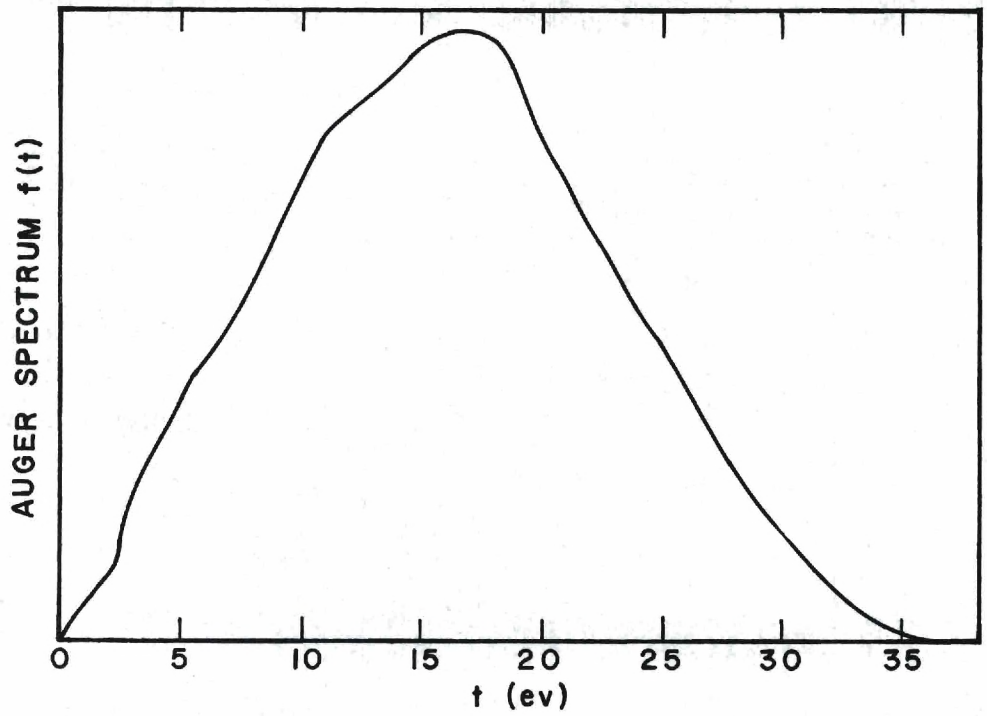

Figure 27. Corrected Auger Spectrum for the Basal Plane of Graphite.

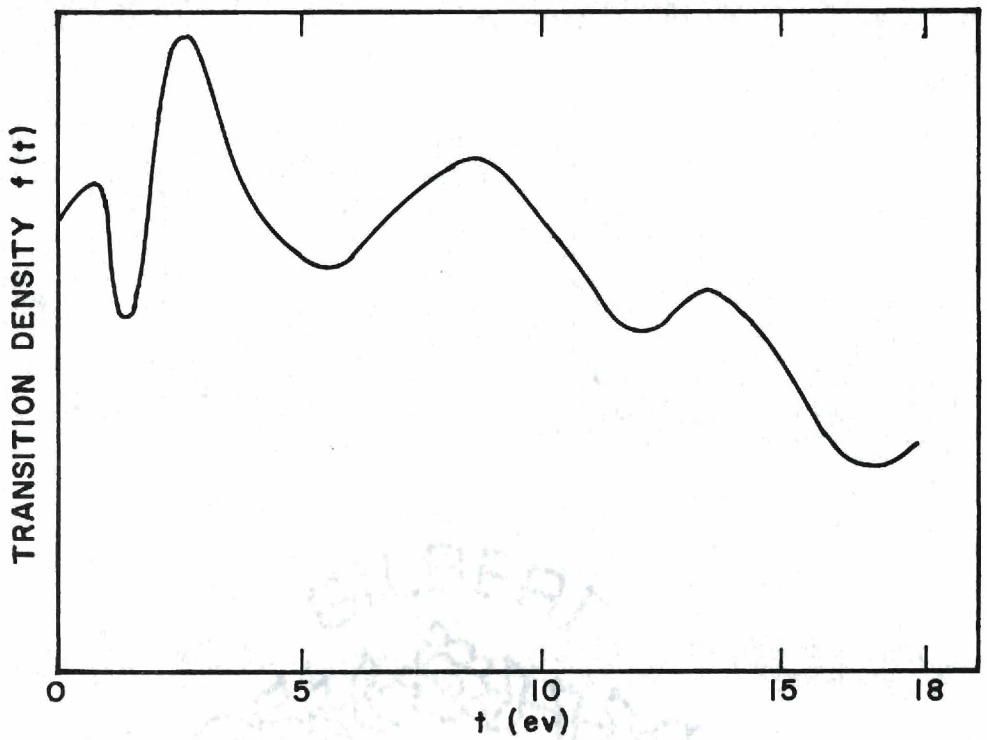

Figure 28. Transition Density of Graphite.

(2) A value for E_u and E_ℓ, the limits of the Auger distribution are selected. Alternatively, if E_ℓ is highly uncertain or unknown a value for the Auger amplitude K is estimated.

(3) The data is rescaled such that the y-coordinate at E_u is zero.

(4) Equation III-64 is evaluated for the cases i = 1, 2, 3 and 4 and adjusted so that the y-coordinate at E_u is zero. Values for fermi level E_F, the work function φ, the primary energy E_p, the mean free paths and any other required parameter are included at this point.

(5) The results of step (4) are subtracted from the digitalized experimental data after multiplication by $\varkappa = 1/K$ (K is the estimated Auger amplitude). At this point $\varkappa$ is just an initial estimate subject to refinement if E_ℓ is assumed known and K unknown.

(6) The result of (5) is corrected for refraction across the surface boundary to obtain $N_0^{(5 \text{ or } 6)}(E)$.

(7) This $N_0^{(5 \text{ or } 6)}(E)$ is then used to determine f(E), the "true" Auger spectrum. This is done either by

(a) Randomly adjusting f(E) in equation III-60a or equation III-62, whichever is applicable, starting at E_u and working toward E_ℓ so that each point predicted by the distribution matches the experimental data before going to the next point, or

(b) Inverting equation III-60a (which resulted in III-60b) or equation III-62, whichever is applicable, and putting the experimentally determined $N_0^{(5 \text{ or } 6)}(E)$ in the resulting equation.

In either case above, the analysis goes back to step (5) and is repeated for varying $\varkappa$ until $f(E_\ell) = 0$ as required. That is, neither

(a) nor (b) are said to give the "true" Auger distribution unless they predict $f(E_\ell) = 0$. This condition can always be met by adjusting $\varkappa$. Alternatively, if $\varkappa$ is fixed, E_ℓ is variable and is determined to be that point at which $f(E_\ell)$ is zero. Whether one chooses to vary K or E_ℓ depends on which can be estimated most accurately.

(8) Step (7) results in the "true" Auger spectrum which can be analyzed to determine the transition density. The distribution is generally first analyzed by the self consistent derivative expansion (equation II-42). For purely qualitative considerations it is often satisfactory to keep only the first term (α $f'(t/2)$). For more complete studies, at least three terms must be kept.

(9) A better estimate of the transition density can be made by employing the Unfold approximation (equation II-24). It is often necessary, however, to employ smoothing and/or truncation procedures in this analysis in the manner discussed earlier.

(10) Based on steps (9) and (10) a final estimated transition density solution is established by a knowledge of the possible errors in the two techniques.

(11) This new estimate is refined, if necessary, by inserting it into one of the Laplace transform methods and adjusting the solution, beginning at ζ_1, until agreement within estimated experimental limitations is achieved.

CHAPTER VI

DISCUSSION OF RESULTS

Although the transition densities for the various group IV elements studied are now known, it remains to consider in greater detail the significance and usefulness of such a quantity with particular reference to the materials studied. It is to be recalled that the transition density according to first-order time-dependent perturbation theory is proportional to a product of the density of occupied states and the square root of the spatially integrated square of the Auger matrix element including exchange. If the latter quantity is a rather monotonic function of the energy then it is useful to compare the results of the Auger electron spectroscopy with the theoretically obtained density of occupied states and band structure as well as with other spectrographic methods. In this chapter such comparisons are made not only to lend credibility to Auger electron spectroscopy as a valid technique but also to infer information about the electronic nature of the materials studied.

Comparison with Other Results

In Figure 29 the transition density obtained for silicon is shown on the same energy scale as two of the accepted energy band calculations. It is to be noted that the maxima in the transition density occur at energies very close to energies where the E versus k curves cross the Brillouin zone boundaries. This is the expected behavior. At the Brillouin zone boundaries, it is easy to see that $v = dE/dk \approx 0$ (v is the

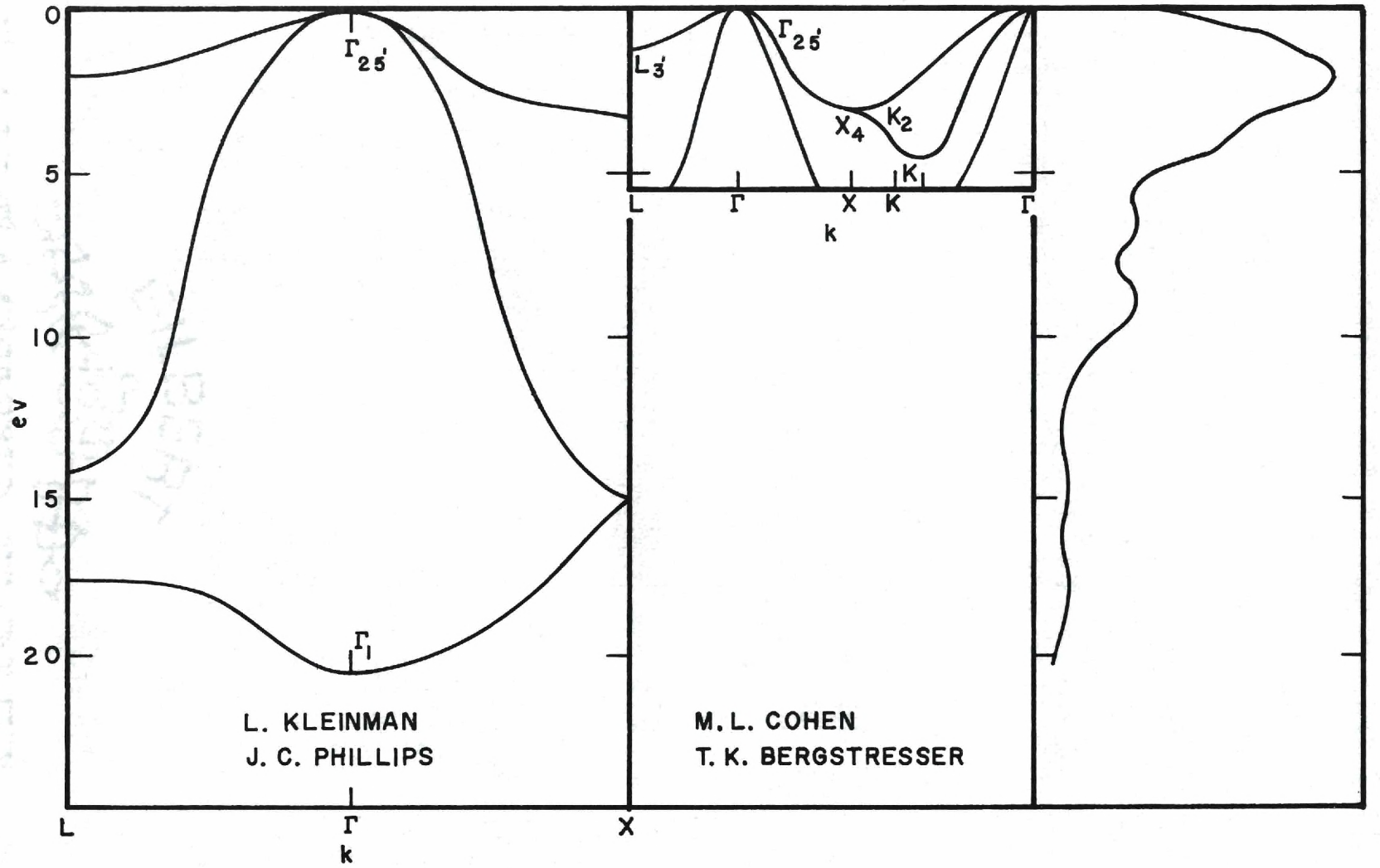

Figure 29. Transition Density of Silicon as Compared with Two Energy Band Calculations.

average velocity of a Bloch state). The expression for the density of states in the one electron model is given by

$$N(E) = \frac{V}{\hbar(2\pi)^3} \oint \frac{dS}{|v|}$$

where the integration is over a constant-energy surface in the Brillouin zone. This predicts that the density of states should be large when the energy surfaces cross points of small v. The state density for silicon has been calculated by Kane[61] and is compared with the transition density in Figure 30. Also included in the figure is the result of a soft x-ray study[62] of silicon. Since the transition density includes the density of states in a dominant manner the results shown are not surprising and give support to Kane's calculations. The difference in the results of the soft x-ray work may result from contaminated surface conditions (or x-ray absorption). However, the author of that work makes no report on the state of the surface.

The comparison between the energy band calculations and the transition density for germanium and graphite are given in the next two figures. Structure comparison can be made in a manner analogous to that described above. For the case of germanium the transition density results are also compared with the work of Hagstrum[67] who used ion neutralization spectroscopy. The method is similar to characteristic Auger electron spectroscopy except that the Auger mechanism is initiated by the neutralization of an inert gas ion (e.g. helium) accelerated to the vicinity of the surface. The transition density result for germanium is

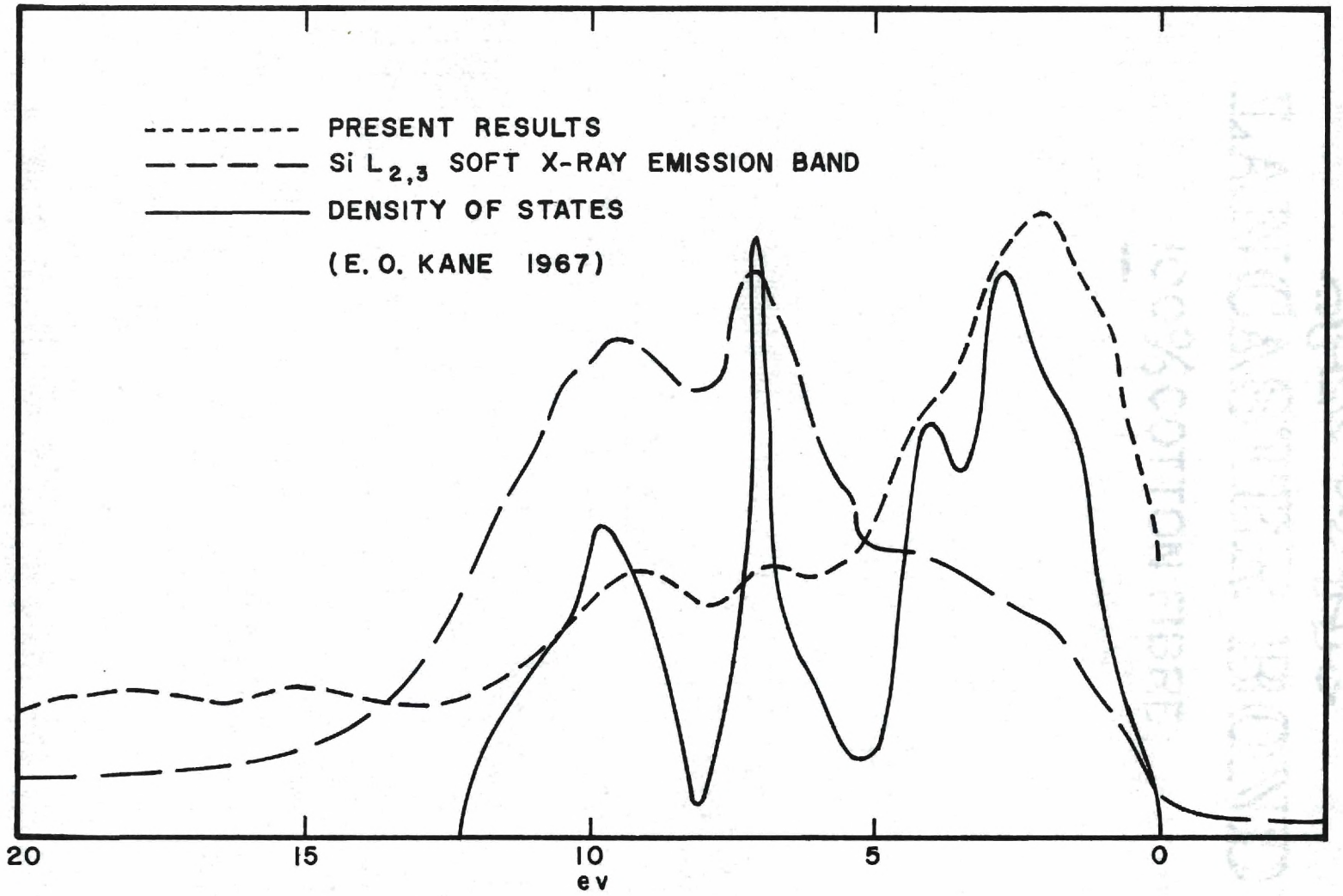

Figure 30. Comparison of the Silicon State Density as Calculated by Kane with the Present Results and the Results of Soft X-Ray Spectroscopy.

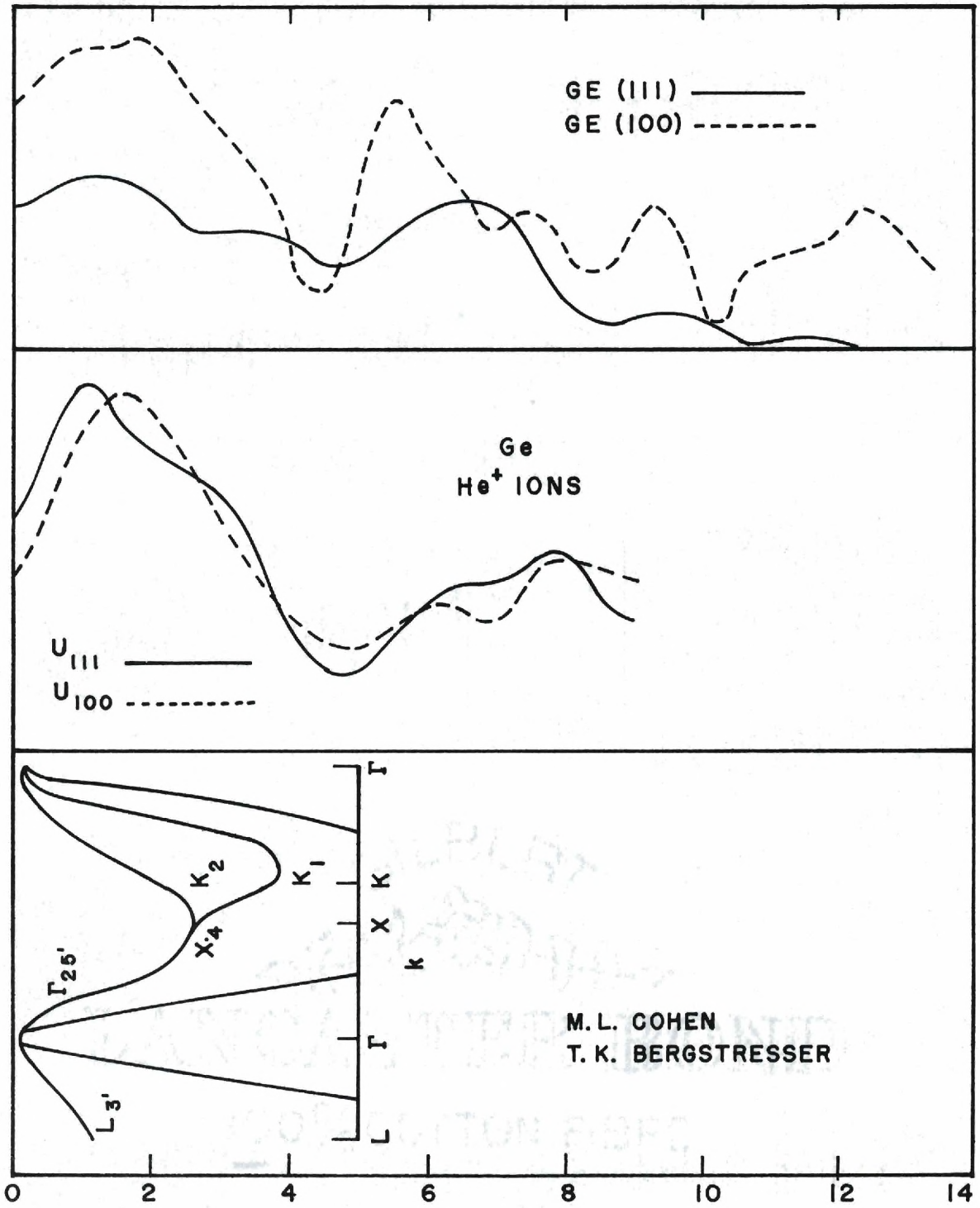

Figure 31. Transition Density of Germanium Compared with an Energy Band Calculation and the Results of Ion Neutralization Spectroscopy.

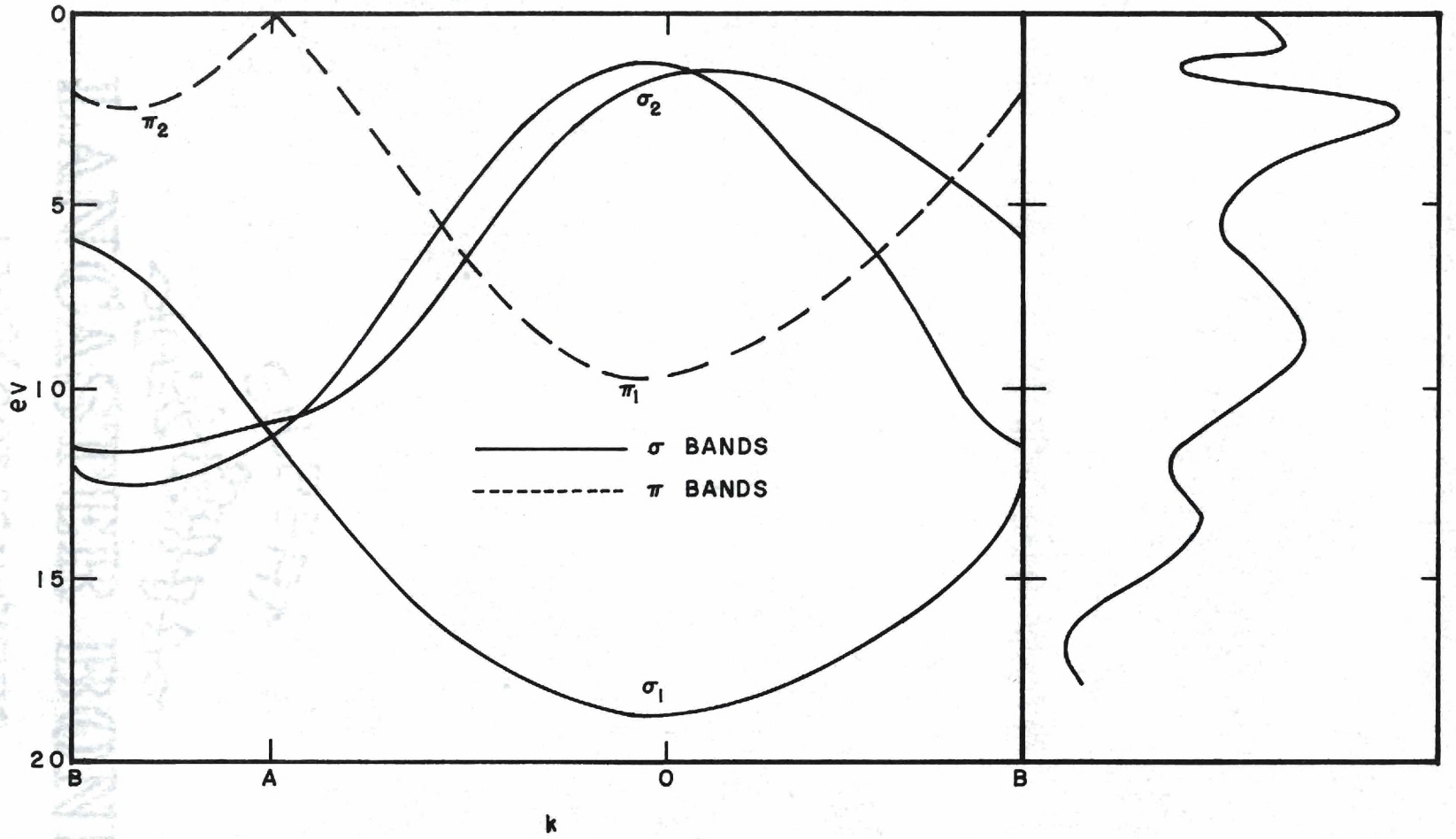

Figure 32. Comparison of the Graphite Transition Density with the Band Structure of Corbato.

seen to be similar in character to that of silicon. This is attributable to the very similar energy band structure of the two materials. The germanium results given here by the method of Auger electron spectroscopy are reasonable. The same is true for the graphite results. The comparison with the two dimensional band calculation of Corbato indicates that the transition density peaks where the σ and π states cross the Brillouin zone boundaries as expected by the arguments above. The germanium surfaces showed sensitivity of the Auger spectrum to surface adsorption as in the case of silicon. This was not investigated quantitatively however. Graphite did not demonstrate such a tendency. This, perhaps, can be explained by the fact that at room temperature graphite is reluctant to adsorb most atmospheric gases; the only adsorbed gas detected being carbon monoxide as mentioned earlier. However, this adsorption is apparently weak because (1) no diffraction pattern showing ordered adsorption was observed as one would expect if the bonding were strong, and (2) simply heating was generally sufficient to clean the surface. Moreover, the surface tended to stay clean for considerable lengths of time (on the order of one or two days). Consequently, it is not expected that such a weak adsorption would affect the electronic structure significantly.

It is by now evident that the predominant characteristic of the comparisons is the high correlation of the peak location and low correlation of the corresponding amplitudes. This unfortunately appears to be typical of the energy band work to date. And likewise with the technique offered here there is not an insignificant uncertainty in the amplitude information due to the several corrections which must be made. One must

therefore be cautious with respect to how much emphasis is placed on the absolute amplitudes given. However, relative amplitude comparisons such as those made between two different surface conditions on the same crystal are probably sound because the same sort of uncertainty enters into both results. Furthermore, the locations of the maxima and minima offer a good deal of information in themselves and shifts in these probably imply greater significance than amplitude modifications. Such shifts are observable without undo difficulty in the present technique.

Effects of Surface Modification

When oxygen is adsorbed on a silicon surface the transition density and likewise the Auger spectrum are modified. Similarly in germanium the (111) and (100) surfaces reveal different transition densities and Auger spectra. These are clearly seen in the results already presented. As a consequence of this sensitivity to surface modification characteristic Auger electron spectroscopy offers not only the ability to detect surface changes but also the possibility of interpreting the effects of these changes on the electronic structure of the system.

In the oxygen contaminated silicon system the primary alteration of the transition density is in the vicinity of the top of the valence band, the lower-lying states being relatively unaffected. This is reasonable since one might intuitively expect the less tightly bound states to be more easily perturbed. However the perturbing effect is manifested most probably on the so-called surface states as opposed to the bulk states. This is because the bulk states by their very nature are unaffected by the presence of a surface whereas the surface states are defined in terms of the boundary conditions that exist there. The sensi-

tivity of the Auger spectrum to the surface conditions seems to suggest that the surface states play an important role in the transition density. Apparently then the modification in the transition density witnessed in the oxygen contaminated silicon system is a demonstration of the presence of new and different surface states resulting from the new potential array at the surface. In addition the bonding character of the foreign species should influence the results but any quantitative statements about this aspect would have to be based on a careful study of adsorption and are beyond the scope of the present effort.

There is yet one problem remaining to be discussed which arises from the apparent contradiction between the observed results and the sensitivity to the surface. On the one hand the transition density has been shown to be nicely consistent with the energy band results based on a bulk state model (e.g., energy band calculations and density of states) whereas on the other hand a heavy dependence on the surface state structure has been demonstrated. This apparent inconsistency is not actually a problem and can be resolved by considering the character of the bulk and surface states of a clean system.

The energy band crystal problem can be conveniently divided into two parts:

(1) The "unperturbed" infinite crystal that has no surface (i.e., periodic boundary conditions).

(2) The effect on this unperturbed lattice when a surface at z = constant is introduced.

In the first case, all three dimensions are periodic and k_x, k_y, and k_z are all good quantum numbers. Any acceptable wave function must obey

the fundamental Bloch condition

$$\psi_n(\vec{k}, \vec{r} + R_\nu) = e^{i\vec{k} \cdot \vec{R}_\nu} \psi_n(\vec{k}, \vec{r})$$

where

$$\vec{R}_\nu = \nu_1\vec{a}_1 + \nu_2\vec{a}_2 + \nu_3\vec{a}_3$$

are the symmetry translations in three dimensions.

The second case (that of the perturbed lattice) where a surface has been introduced can be thought of as creating a reduction in the symmetry. Thus the quantum number k_z is no longer sharp since translations in the z direction no longer leave the crystal invariant. Acceptable wave functions for this "perturbed" crystal are characterized by

$$\psi_\lambda'(\vec{K}, \vec{r} + \vec{\rho}\nu) = e^{i\vec{K} \cdot \vec{\rho}_\nu} \psi_\lambda'(\vec{K}, \vec{r})$$

where

$\vec{\rho}_\nu$ = symmetry translation in the x-y plane

$\vec{K}$ = $k_x x + k_y y$ = good quantum numbers related to the two dimensional translational symmetry.

This reduction in symmetry in going from the "unperturbed" to

the "perturbed" crystal in general results in a mixing of states.[64] In this particular case, the reduction of symmetry in the z-direction will result in a mixing of Bloch states of different $\vec{k}_z$

$$\psi_\lambda'(\vec{K}, \vec{r}) = \sum_n \sum_{k_z} C_{\lambda n}(k_z)\ \psi_n(\vec{k}, \vec{r})$$

However, even though the z translational symmetry has been destroyed in the strict sense, there still remains a great deal of periodicity in this direction as long as the point in consideration is deep in the bulk of the crystal. One might therefore expect this to lead to a simplification of the mixing coefficients $C_{\lambda n}(\vec{k})$. Indeed these mixing coefficients fall into two broad categories:

A. All assume a value of zero except for those for which k is in the neighborhood of the surface value (i.e., k_z). In this vicinity there is a sharp distribution of non-zero terms with half width Δk_z.

B. Same as A except the distribution of non-zero values is wide.

A. Sharp Distribution

This case arises when E_n is not flat ($dE/dk \neq 0$) around $\vec{k} = \vec{K} + k_z^\lambda \hat{z}$. This means that since the energies vary strongly with k_z in this region there is qualitatively little mixing of Bloch states of different k_z and hence k_z remains relatively sharp. Placing the origin at the center of the crystal one gets

$$\psi_\lambda'(\vec{K}, \vec{r} + \vec{R}_\nu) = \sum_n \sum_{k_z} C_{\lambda n}(k_z)\, \psi_n(\vec{k}, \vec{r} + \vec{R}_\nu)$$

$$= \sum_n \sum_{k_z} e^{i\vec{k} \cdot \vec{R}_\nu} C_{\lambda n}(k_z) \psi_n(k,r)$$

If $\vec{r} \cdot \hat{z}$ and $\vec{R}_\nu \cdot \hat{z}$ are small in comparison to the distance to the surface then

$$\psi_\lambda'(\vec{K}, \vec{r} + \vec{R}_\nu) \approx e^{i\vec{k} \cdot \vec{R}_\nu} \psi_\lambda'(\vec{K}, \vec{r})$$

As the crystal gets larger and larger the $C_{\lambda n}(k_z)$ become sharper and sharper until finally in the limit of an infinite crystal the $\approx$ sign in the above equation becomes an = sign and k_z is again a good quantum number. However for a finite crystal the $\approx$ sign in the last equation will not hold for $\vec{R}_\nu \cdot \hat{z}$ large with respect to the crystal size for then waves of different k_z within the spike of the $C_{\lambda n}$ will have radically different phases and will be cancelling each other out. As has been demonstrated by Slater and Koster[65] the effect of the surface potential is to cut these states out of the surface region. Note also that taking the limit of letting the crystal surface go to infinity will have no effect on the cancellation at the surface since even though $\Delta k_z \to 0$ the value of $\vec{r}$ to the surface will tend to infinity and the surface cancellation will remain.

The wave functions for this case therefore look like Bloch waves within the bulk and damp out strongly to zero as the surface is

approached. For crystals of macroscopic dimensions Δk_z is so small for this case that k_z is approximately a good quantum number. For this reason crystal states which fall into this category are called the bulk states.

B. Flat Distributions

Qualitatively speaking this case arises when E_n is flat around $\vec{k} = \vec{K} + k_z^{\lambda}\hat{z}$. This means that since the energies are nearly degenerate about k_z there is a much stronger mixing of the associate Bloch states over a much wider range of k_z about k_z^{λ} than was the case in A. As one can easily imagine, the wider the peak in $|C_{\lambda n}(k_z)|$, the more localized the $\psi_{\lambda}'(\vec{K},\vec{r})$ are going to be. Indeed it is just these functions which give rise to the localized surface states. Taking the limit of moving the surface to infinity will have little effect on these states since they will follow the surface. Furthermore, deep within the bulk these states are essentially zero and thus obey the Bloch condition in a trivial manner. The way these $\psi_{\lambda}'(\vec{K},\vec{r})$ oscillate from layer to layer is determined roughly by the $\exp(ik_z^{\lambda}z)$. Thus a surface state arising from the $\Gamma(k = 0)$ point will decrease in a monotonic manner from outer to inner layers while that arising from an X point ($k = \frac{2\pi}{a}(0, 0, 1)$) will oscillate from layer to layer with an exponentially decaying envelope.

Notice that as a consequence of this analysis it is apparent that the surface states arise from only those Bloch states which correspond to points of high state density in the k_z direction. Most of these states will be approximately centered about the unperturbed energies although this is not exact since the effect of the surface potential will be to shift the energies of the surface states somewhat. This relation-

ship between the surface state picture and the identification of the Auger spectrum in terms of the points of high density of states of the unperturbed crystal is very direct. In fact the slight differences between the Auger spectrum analysis and the actual density of states spectrum might be used in a more quantitative analysis to give direct measurements of the surface potential and of the energy spectrum of these surface states. Obviously these surface states would be strongly affected by the presence of an adsorbate.

Also notice that this analysis has little or no bearing on the interpretation of the graphite results, for in graphite each layer acts to a large extent as an isolated two dimensional crystal. In fact in his analysis of the band structure of graphite Corbato did not directly consider Bloch waves moving in the z direction. To the extent that such an approximation is suitable (and in such an extreme case as graphite such an approximation is probably quite satisfactory for this particular analysis), the analysis of Corbato will have validity even for the surface layers. The effect of the surface potential will be relatively small when compared to the dominant free atom contributions and the relative positions of the two dimensional density of states will remain approximately unmoved. It is only when going to a more general case (such as silicon), where running Bloch waves in the z direction are important, that an analysis of the origin of the surface states in terms of the regions $\frac{dE}{dk_z}\Big|_{k_z^\lambda} = 0$ becomes a crucial factor.

CHAPTER VII

CONCLUSIONS AND RECOMMENDATIONS

The work presented herein has described the theoretical and experimental investigations into the energy spectrum of electrons ejected from selected semiconductor surfaces with energy less than one half the primary electron energy with particular reference to the characteristic Auger process. It was found that the details of the characteristic Auger spectrum could be interpreted in terms of the energy band information in the surface vicinity. The Auger spectrum was extracted from the experimental distribution by subtraction of the background and correction of inelastic scattering distortion by a theory of electron diffusion based on a statistical model. This theory predicted the true secondary spectrum reasonably well and indicated the fundamental importance of plasmon creation as a loss mechanism in semiconductors. The transition density ($\approx$ density of occupied states times square root of the spatially integrated square of the Auger matrix element) was established as a physical quantity of interest and was related to various energy band quantities. It was found that the transition density is sensitive to the conditions at the surface and indicated that modifications in the transition density due to adsorption, for example, could be interpreted in terms of surface states.

Characteristic Auger electron spectroscopy has some advantages over other electronic structure analysis techniques. First, as has already been established, it is sensitive to surface conditions. Second,

it is not energy limited as to the depth below the fermi surface which can be studied. Finally, it is readily experimentally realizable. Most LEED systems can be easily adapted to allow for the semi-quantitative investigation of Auger spectra. Moreover, if the instrumentation is equipped to take the derivative of the energy distribution, the first derivative of the Auger spectrum can be obtained. This has been shown to be the lead term in an expansion of the transition density and often looks very much like the true solution.[40] Consequently, a purely experimental approach to qualitative energy band information is possible. For adsorption studies this could prove to be extremely useful.

The work was restricted somewhat by experimental limitations. It would be highly desirable to include the following items in any future efforts along this line:

(1) better energy resolution

(2) the ability to select a small solid angle

(3) increased primary energies and flux.

Such modifications would not only yield more detailed information than is currently attainable but also permit the technique to be used satisfactorily on a much wider class of materials (particularly compounds, which have competing Auger processes).

From the theoretical standpoint, much effort is needed in the understanding of the influence of surface states on the transition density beyond the qualitative discussion of the last chapter. In particular, it would be of extreme value to know what quantitative inferences can be drawn from the transition density modifications as a result of chemisorption or physisorption. Is it simply surface potential modifi-

cation, virtual bound state creation, or a complicated alteration of the wave function and energy band character in the surface vicinity? The arguments given herein suggest the latter case but more definitive investigations are needed.

Finally, the applicability of the technique to the results of Auger neutralization studies needs exploration. In this situation the primary electron excites a low lying state in an adsorbed species as the initial step in the Auger mechanism. The energy of the resultant distribution is thus characteristic of the adsorbed atoms. If the adsorption is small enough and if the foreign atoms do not cluster, then the details of the resultant distribution are expected to be characteristic of the substrate. However, if these conditions are not met it is not at all clear what kind of spectrum one should expect. As of yet the necessary experimental data to resolve the situation is not available because of the low relative probability of these events. It is difficult therefore to make further comments but the importance of the phenomenon as a means of identifying and studying the effects of surface impurities is evident.

The results of this investigation can be briefly summarized in the following:

1. The concept of the transition density introduced in Chapter II as a result of a perturbation theory analysis of the Auger process is a physically meaningful quantity. Interpretations in terms of it have been shown to be generally consistent with existing knowledge.

2. The transition density contains terms associated with the density of occupied states and the energy band structure and is relatable

to these parameters most notably at points of high symmetry. Thus, for example, it is expected that for a "clean" system the transition density will peak at or close to the values assumed by the system energy eigenvalues at the Brillouin zone boundaries.

3. The transition density is sensitive to surface modifications and should be useful as a qualitative measure of the state of a solid surface and the effects rearrangements or impurities have on the electronic structure of the host system.

4. With increased instrument sensitivity the general technique should be extendable to analysis of spectra resulting from the Auger neutralization of ionized impurities. Such measurements should prove valuable not only as a means for identifying foreign species but also as a possible means for interpreting the nature of the bonding between the foreign and bulk species.

5. In comparison with other quantitative techniques of energy band analysis (such as photoemission spectroscopy) Auger electron spectroscopy offers a great deal in experimental simplicity with the additional advantage that second derivative measurements can often be directly interpreted in terms of transition density features.

6. The theory of electron diffusion presented in Chapter III as a means of correcting observed Auger spectra for background and inelastic scattering effects, although somewhat idealized by numerous approximations, offers a reasonably accurate quantitative means of analyzing experimental true secondary electron energy distributions in detail.

7. This theory of electron diffusion made clear the intrinsic importance of plasmon excitation as an energy loss mechanism for ex-

cited electrons. If the plasmon contribution is ignored the predicted half-width of the slow peak can be in error by as much as one hundred per cent with a similar error for the most probably energy.

8. The diffusion theory formalism is of a general nature and with minor modifications should be applicable to other problems concerned with the diffusion of excited crystal electrons.

In performing the work reported in this dissertation it was established that study of the inelastic mechanism of the true secondary electron energy distribution is of definite value in adding to the understanding of the electronic nature of solid matter. In particular the development of characteristic Auger electron spectroscopy as a tool in quantifying this understanding has verified this value and given impetus to the achievement of a greater comprehension of the behavior of crystal electrons in the vicinity of the surface. To this end some select comments have been offered above as possible avenues of departure for further study and are meant to suggest that this may be the beginning -- not the end -- of understanding solid surfaces.

APPENDICES

APPENDIX A

INTEGRATION OF EXCITATION FUNCTION OVER POLAR ANGLE

Consider the integral

$$S(E') = \frac{2\, m^3 e^4 k'}{\pi^2 \hbar^6 p} \sum_{\vec{t}} \int\int d^3\vec{k}\, d\Omega_{\vec{k}'} \frac{|I|^2}{(q^2+\lambda^2)^2} \delta(k'^2 + p'^2 - k^2 - p^2)$$

define the following quantities

$$\vec{C}_{\vec{t}} = \vec{p} + \vec{k} + 2\pi\vec{t}$$

$$\vec{\rho} = \tfrac{1}{2}\vec{C}_{\vec{t}} - \vec{k}'$$

$$K_1 = \vec{p} \cdot (\vec{k} + 2\pi\vec{t})$$

$$\rho_o^2 = \tfrac{1}{4}(p^2 - 2K_1 + k^2 - 4\pi^2 t^2 - 4\pi\vec{k} \cdot \vec{t})$$

Now

$$\rho^2 = \tfrac{1}{4} C_{\vec{t}}^2 + k'^2 - \vec{C}_t \cdot \vec{k}'$$

Thus the argument of the delta function above can be written

$$k'^2 + p'^2 - k^2 - p^2 = 2\,(\rho_o^2 - \rho^2)$$

If $\vec{C}_{\vec{t}}$ is chosen as the polar direction then

$$d\Omega_{\vec{k}'} = d(\cos(\hat{k}' \cdot \hat{C}_t))d\varphi$$

with

$$\cos(\hat{k}' \cdot \hat{C}_t) = \frac{\frac{1}{4}C_t^2 + k'^2 - \rho^2}{|k'|\ |C_t|}$$

Hence,

$$d(\cos(\hat{k}' \cdot \hat{C}_t)) = -\frac{2\rho}{|k'|\ |C_t|}\, d|\rho|$$

Consequently,

$$S(E') = \frac{m^3 e^4 k'}{\pi^3 \hbar^6 p} \sum_{\vec{t}} \int d^3k \int \frac{\rho\, d|\rho|}{|k'|\ |C^t|}\, d\varphi\, \frac{|I|^2}{(q^2+\lambda^2)^2}$$

$$\times \frac{1}{\rho_o}\left[\delta(|\rho| - \rho_o) + \delta(|\rho| + \rho_o)\right]$$

Recognizing that there is no contribution from the second delta function, this becomes

$$S(E') = \frac{m^3 e^4}{\pi^3 \hbar^6 p} \sum_{\vec{t}} \int_{\substack{\text{fermi} \\ \text{sphere}}} \frac{d^3\vec{k}}{|C_t|} \int_0^{2\pi} \frac{|I|^2}{(q^2+\lambda^2)^2} \, d\varphi \, .$$

APPENDIX B

INTEGRATION OF EXCITATION FUNCTION OVER AZIMUTHAL ANGLE

Consider the integral

$$S(E') = \frac{m^3 e^4}{\pi^3 \hbar^6 p} \int \frac{d^3\vec{k}}{|C_o|} \int^{2\pi} \frac{d\varphi}{(q)^4}$$

where q is the momentum transferred. Thus

$$\vec{q} = \vec{p} - \vec{p}'$$

and

$$q^2 = 2\rho_o^2(1 - \cos(\hat{\beta} \cdot \hat{\rho}))$$

where

$$\vec{\beta} = \tfrac{1}{2}(\vec{p} - \vec{k})$$

and ρ_o and $\vec{\rho}$ have the meaning given in Appendix A. If $\hat{\beta}$ makes an angle of γ with the polar axis defined by $\vec{C}_t$ and $\vec{\rho}$ makes an angle θ, then

$$\int_0^{2\pi} \frac{d\varphi}{q^4} = \int_0^{2\pi} \frac{d\varphi}{4\rho_o^4(1 - \cos\gamma\cos\theta - \sin\gamma\sin\theta\cos\varphi)^2}$$

$$= \frac{1}{4\rho_o^4}\,\frac{1}{\alpha_2^2}\int^{2\pi} \frac{d\varphi}{\left(\frac{\alpha_1}{\alpha_2} - \cos\varphi\right)^2}$$

with the definitions

$$\alpha_1 = 1 - \cos\gamma\cos\theta\ ,$$

$$\alpha_2 = \sin\gamma\sin\theta$$

Making the variable change $\cos\varphi = \frac{1 - Z^2}{1 + Z^2}$ one obtains

$$\int_0^{2\pi} \frac{d\varphi}{q^4} = \frac{1}{\rho_o^4}\int_0^{\infty} \frac{1 + Z^2 dZ}{(a + bZ^2)^2}$$

where

$$a = \alpha - \beta\ , \quad b = \alpha + \beta\ .$$

The integral is now easily done by parts. After re-inserting the defined quantities

$$\int_0^{2\pi} \frac{d\varphi}{q^4} = \frac{\pi(1 - \cos\gamma\cos\theta)}{2\rho_o{}^4(\cos\gamma - \cos\theta)^3} \quad .$$

Now

$$\cos\gamma = \frac{\vec{\beta} \cdot \vec{C}_o}{|\beta|\,|C_o|} = \frac{p^2 - k^2}{2\rho_o|C_o|}$$

$$\cos\theta = \frac{\vec{\rho}_o \cdot \vec{C}_o}{|\rho|\,|C_o|} = \frac{\frac{1}{2}C_o{}^2 - \vec{k}' \cdot \vec{C}_o}{\rho_o|C_o|} = \frac{p^2 + k^2 - 2k'^2}{2\rho_o|C_o|}$$

Hence

$$S(E') = \frac{m^3e^4}{\pi^3\hbar^6 p} \int \frac{d^3\vec{k}}{|C_o|} \frac{\pi}{2\rho_o{}^4} \frac{4\rho_o{}^2C_o{}^2 - (p^2 - k^2)(p^2 + k^2 - 2k'^2)}{(k'^2 - k^2)^3}$$

$$= \frac{m^3e^4}{\pi^2\hbar^6 p} \int d^3\vec{k} \frac{(\vec{p} + \vec{k})^2(\vec{p} - \vec{k})^2 - (p^2 - k^2)(p^2 + k^2 - 2k^2)}{(k'^2 - k^2)^3|\vec{p} - \vec{k}|^3}$$

$$= \frac{2m^3e^4}{\pi^2\hbar^6 p} \int d^3\vec{k} \frac{p^2(k^2 + k'^2) - 2(\vec{p} \cdot \vec{k})^2 + k^2(p^2 - k'^2)}{(k'^2 - k^2)^3|\vec{p} - \vec{k}|^3} \quad .$$

APPENDIX C

INTEGRATION OF EXCITATION FUNCTION OVER THE FERMI SPHERE OF INITIAL ELECTRON STATES

Consider the integral

$$S = \frac{2m^3e^4}{\pi^2\hbar^6 p} I \ , \quad \text{with}$$

$$I = \int_{\substack{\text{fermi}\\ \text{sphere}}} d^3\vec{k} \ \frac{p^2(q^2 + k^2) - 2(\vec{p}\cdot\vec{k})^2 - k^2(q^2 - k^2)}{(q^2 - k^2)^3 |\vec{p} - \vec{k}|^3}$$

$$= \int_0^{k_F} \int_0^{2\pi} \int_0^{\pi} \frac{p^2(q^2+k^2) - k^2(q^2-k^2) - 2p^2k^2\cos^2\theta}{(q^2-k^2)^3 \ (p^2+k^2-2pk\cos\theta)^{3/2}} k^2 \sin\theta \ d\theta d\varphi dk$$

$$= 2\pi \left\{ \int_0^{k_F} \frac{p^2(q^2+k^2) - k^2(q^2-k^2)}{(q^2-k^2)^3} k^2 \left[\underbrace{\int_0^{\pi} \frac{\sin\theta \ d\theta}{(p^2+k^2-2pk\cos\theta)^{3/2}}}_{I_a} \right] dk \right.$$

$$- \int_0^{k_F} \frac{2p^2k^4}{(q^2-k^2)^3} \Big[\underbrace{\int_0^{\pi} \frac{\cos^2\theta \sin\theta \, d\theta}{(p^2+k^2-2pk\cos\theta)^{3/2}}}_{I_b} \Big] dk \Big\} .$$

The integrals I_a and I_b are now considered. First I_a,

$$I_a = \int_0^{\pi} \frac{\sin\theta \, d\theta}{(p^2+k^2-2pk\cos\theta)^{3/2}} = \int_{-1}^{1} \frac{dx}{(a+bx)^{3/2}}$$

where $x = \cos\theta$, $a = p^2+k^2$ and $b = -2pk$

$$I_a = \frac{-2}{b(a+bx)^{1/2}} \Bigg/_{-1}^{1} = \frac{2}{p(p^2-k^2)} .$$

And for I_b, using the same substitutions,

$$I_b = \int_0^{\pi} \frac{\cos^2\theta \sin\theta \, d\theta}{(p^2+k^2-2pk\cos\theta)^{3/2}} = \int_{-1}^{1} \frac{X^2 dx}{(a+bx)^{3/2}}$$

$$= \frac{2}{b^3}\left[\frac{(a+bx)^{3/2}}{3} - 2a(a+bx)^{1/2} - \frac{a^2}{(a+bx)^{1/2}} \right]\Bigg/_{-1}^{1}$$

$$= \frac{2}{3b^3}\left[\frac{(b^2-4ab-8a^2)\ (a-b)^{1/2} - (b^2+4ab-8a^2)\ (a+b)^{1/2}}{(a+b)^{1/2}\ (a-b)^{1/2}} \right]$$

$$= \frac{2}{3p^3}\ \frac{p^2 + 2k^2}{p^2 - k^2}\ .$$

The integral I then becomes

$$I = 2\pi \left\{ \int_0^{k_F} \frac{p^2(q^2+k^2)k^2 - k^4(q^2-k^2)}{(q^2-k^2)^3}\ \frac{2}{p(p^2-k^2)}\ dk \right.$$

$$\left. - \int_0^{k_F} \frac{2p^2k^4}{(q^2-k^2)^3}\ \frac{2}{3p^3}\ \frac{p^2+2k^2}{p^2-k^2}\ dk \right\}$$

$$= \frac{4\pi}{p} \left\{ \int_0^{k_F} \frac{(p^2-k^2)q^2k^2 + k^4(p^2+k^2)}{(q^2-k^2)^3\ (p^2-k^2)}\ dk \right.$$

$$\left. - \int_0^{k_F} \frac{2k^4(p^2+2k^2)}{3(q^2-k^2)^3\ (p^2-k^2)}\ dk \right\}$$

$$= \frac{4\pi}{3p} \left\{ \int_0^{k_F} \frac{3q^2k^2(p^2-k^2) + 3k^4(p^2+k^2) - 2k^4(p^2+2k^2)}{(q^2-k^2)^3\ (p^2-k^2)}\ dk \right\}$$

$$= \frac{4\pi}{3p} \left\{ \int_0^{k_F} \frac{3q^2k^2 + k^4}{(q^2-k^2)^3}\ dk \right\}$$

$$= \frac{4\pi}{3p} \left\{ \frac{k^3}{(q^2-k^2)^2} \right\} \Bigg/_0^{k_F} = \frac{4\pi}{3p}\ \frac{k_F^3}{(q^2-k_F^2)^2}\ .$$

Consequently

$$S = \frac{2m^3e^4}{\pi^2\hbar^6p} \cdot \frac{4\pi}{3p} \cdot \frac{k_F^3}{(q^2-k_F^2)^2} = \frac{e^4(2m)^3k_F^3}{3\pi\hbar^6p^2\,(q^2-k_F^2)^2}$$

if

$$E_p = \frac{\hbar^2p^2}{2m} \quad \text{and} \quad E' = \frac{\hbar^2q^2}{2m}, \quad E_F = \frac{\hbar^2k_F^2}{2m}$$

Then

$$S = \frac{e^4k_F^3}{3\pi E_p(E' - E_F)^2} .$$

APPENDIX D

DETERMINATION OF THE GREEN'S FUNCTION FROM EQUATION III-11 FOR A SPECIFIC CHOICE OF SCATTERING FUNCTION

It is desired to solve equation III-11 for the Green's function in the case of a particular scattering function

$$F_\ell(E,E') = \frac{2}{E'} P_\ell\left(\sqrt{\frac{E}{E'}}\right) . \qquad \text{(III-30)}$$

The Green's function condition then takes on the form

$$G_\ell(E,E'') = \delta(E-E'') + 2\int_E^\infty G_\ell(E',E'')P_\ell\left(\sqrt{\frac{E}{E'}}\right)\frac{dE'}{E'} . \qquad \text{(D-1)}$$

The Mellin transform of the Green's function is defined

$$\Gamma_\ell(s,E') = \int_0^\infty E^{s-1}G_\ell(E,E')\,dE \qquad \text{(D-2)}$$

and that of the delta function

$$\Delta(s,E') = \int_0^\infty E^{s-1}\,\delta(E-E')dE = E'^{s-1}\,. \tag{D-3}$$

For later convenience we also define

$$\epsilon(E,E') = \begin{cases} 1 & ;\ E' \geq E \\ 0 & ;\ E' < E \end{cases} \tag{D-4}$$

Consider now the Mellin transform of the integral in expression (D-1),

$$\int_0^\infty E^{s-1} \int_E^\infty G_\ell(E'',E')P_\ell\left(\sqrt{\frac{E}{E''}}\right)\frac{dE''}{E''}\,dE$$

$$= \int_0^\infty \int_0^\infty E''^{s-1} G_\ell(E'',E')P_\ell\left(\sqrt{\frac{E}{E''}}\right)\left(\frac{E}{E''}\right)^s \frac{1}{E}\,\epsilon\left(\frac{E}{E''}\right)dE''\,dE$$

$$= \int_0^{\infty} E''^{s-1} G_\ell(E'',E') \left\{ \int_0^{E''} P_\ell \left(\sqrt{\frac{E}{E''}} \right) \left(\frac{E}{E''} \right)^s \frac{1}{E} \, dE \right\} dE''. \qquad \text{(D-5)}$$

The integral in brackets in (D-5) can be written with $x = \left(\frac{E}{E''}\right)^{\frac{1}{2}}$

$$2 \int_0^1 P_\ell(x) \, x^{2s-1} dx = 2 \, C_{2s-1,\ell} \, .$$

But this is independent of E'', thus (D-5) becomes

$$\text{Integral transformation} = 2\Gamma_\ell(s;E') \, C_{2s-1,\ell} \, . \qquad \text{(D-6)}$$

Using (D-2), (D-3) and (D-6), the Green's function condition (D-1) transforms to

$$\Gamma_\ell(s;E') = \Delta(s;E') + 4\Gamma_\ell(s;E')C_{2s-1,\ell} \, .$$

Hence

$$\Gamma_\ell(s;E') = \frac{\Delta(s;E')}{1 - 4C_{2s-1,\ell}} = \frac{E'^{s-1}}{1 - 4C_{2s-1,\ell}} \quad .$$

An expression for the Green's function now follows from the inverse Mellin transform

$$G_\ell(E,E') = \frac{1}{2\pi i} \frac{1}{E'} \int_{\Omega_\ell} \frac{1}{1-4C_{2s-1,\ell}} \left(\frac{E'}{E}\right)^s ds \quad .$$

The contour Ω_ℓ is parallel to the imaginary axis of the complex s-plane and to the right of all singularities in the integral. To carry out the integration it is convenient to replace $\frac{E'}{E}$ by e^μ ($\mu = \ell n(E'/E)$ and $\mu < 0$ when $E' < E$ and $\mu > 0$ when $E' > E$) . Consider the case $\mu < 0$: Take as an integration path an infinitely large semicircle closed in the right half plane. One obtains immediately

$$G_\ell(E,E') = 0 \quad ; \quad E > E'$$

For $\mu > 0$: Take the corresponding integration path closed in the left half-plane. The integration can be carried out using Cauchy residues.

Thus for

(1) $\underline{\ell = 0}$:

$$G_o(E,E') = \frac{1}{2\pi i} \frac{1}{E'} \int_{\Omega_o} \frac{s}{s-2} e^{\mu s} ds$$

$$= \frac{2}{E'} \left(\frac{E'}{E}\right)^2 ; E' > E .$$

Note, however, that in the case $E' = E$, the convergence factor $e^{\mu s} = 1$ and the integral diverges. This case can be treated in the following way.

$$\lim_{\epsilon \to 0} \int_{E'-\epsilon}^{E'+\epsilon} G_o(E,E')dE = \frac{1}{2\pi i} \frac{1}{E'} \int_{\Omega_o} \frac{s}{s-2} \left\{ \lim_{\epsilon \to o} \int_{E'-\epsilon}^{E'+\epsilon} \left(\frac{E'}{E}\right)^s dE \right\} ds$$

$$= \lim_{\epsilon \to o} \frac{1}{2\pi i} \int_{\Omega_o} \frac{s}{(s-2)(s-1)} \left[\left(\frac{E'}{E'-\epsilon}\right)^{s-1} - \left(\frac{E'}{E'+\epsilon}\right)^{s-1} \right] ds$$

$$= \lim_{\epsilon \to o} \frac{1}{2\pi i} \int_{\Omega_o} \frac{s}{(s-2)(s-1)} \left(\frac{E'}{E'-\epsilon} \right)^{s-1} ds = 1 .$$

But this implies that $G_o(E',E')$ has the properties of a delta distribution. Since G_o always appears under an integral, we write

$$G_o(E,E') = \begin{cases} \frac{2}{E'} \left(\frac{E'}{E} \right)^2 + \delta(E-E') & E \leq E' \\ 0 & E > E' \end{cases}$$

(2) $\underline{\ell = 2}$:

$$G_2(E,E') = \frac{1}{4\pi i} \frac{1}{E'} \int_{\Omega_2} \frac{(2s+2)}{(s^2-s+1)} e^{\mu s} ds$$

$$= \frac{1}{4\pi i} \frac{1}{E'} \left\{ 2\pi i \left[\frac{s(2s+2)e^{\mu s}}{s - \frac{1+i\sqrt{3}}{2}} \right]_{s=\frac{1-i\sqrt{3}}{2}} \right.$$

$$+ \frac{s(2s+2)e^{\mu s}}{s - \frac{1-i\sqrt{3}}{2}} \Bigg/ s = \frac{1+i\sqrt{3}}{2} \Bigg] \Bigg\}$$

$$= \frac{2}{\sqrt{E'E}} \cos\left(\frac{\sqrt{3}}{2} \ell n \frac{E'}{E}\right) \quad E' > E .$$

When $E = E'$

$$\lim_{\epsilon \to o} \int_{E'-\epsilon}^{E'+\epsilon} G_2(E,E')dE = \lim_{\epsilon \to o} \frac{1}{4\pi i} \int_{\Omega_2} \frac{s(2s+2)}{(s^2-s+1)(s-1)} \left(\frac{E'}{E'-\epsilon}\right)^{s-1} ds$$

$$= \lim_{\epsilon \to o} \left\{ 2 - \tfrac{1}{2} \left[\left(1 - i\sqrt{3}\right) \left(\frac{E'}{E'-\epsilon}\right)^{\frac{-1-i\sqrt{3}}{2}} + \left(1+i\sqrt{3}\right) \left(\frac{E'}{E'-\epsilon}\right)^{\frac{-1+i\sqrt{3}}{2}} \right] \right\}$$

$$= 1 .$$

Again the result implies a delta distribution. Hence

$$G_2(E,E') = \begin{cases} \dfrac{2}{\sqrt{EE'}} \cos\left(\dfrac{\sqrt{3}}{2} \ell n \dfrac{E'}{E}\right) + \delta(E-E') \; ; & E \leqq E' \\ 0 \; ; & E > E' \end{cases}$$

BIBLIOGRAPHY†

1. L. Austin and H. Starke, Ann. Physik 9 (1902).
2. E. Rudberg, Kgl. Svenska Velenskabssakad. Handl. 7 (1929).
3. E. Rudberg, Proc. Roy. Soc. (London) A127, 111 (1930).
4. E. Rudberg, Phys. Rev. 50, 138 (1936).
5. H. Fröhlich, Ann. Physik 13, 229 (1932).
6. A. E. Kadyschevitsch, J. of Phys. (U.S.S.R.) 2, 115 (1940).
7. A. E. Kadyschevitsch, J. of Phys. (U.S.S.R.) 4, 341 (1941).
8. D. A. Wooldridge, Phys. Rev. 56, 562 (1939).
9. E. M. Baroody, Phys. Rev. 78, 780 (1950).
10. H. Salow, Zeit Technical Physik 21, 8 (1940).
11. A. J. Dekker and A. van der Ziel, Phys. Rev. 86, 416 (1952).
12. J. F. Marshall, Phys. Rev. 88, 416 (1952).
13. A. van der Zeil, Phys. Rev. 92, 35 (1953).
14. E. M. Baroody, Phys. Rev. 89, 910 (1953).
15. E. M. Baroody, Phys. Rev. 101, 1679 (1956).
16. H. W. Streitwolf, Ann. Physik 3, 183 (1959).
17. P. A. Wolff, Phys. Rev. 95, 56 (1954).
18. R. E. Marshak, Revs. Modern Phys. 19, 185 (1947).
19. H. Stolz, Ann. Physik 3, 197 (1959).
20. A. I. Guba, Soviet Phys.-Solid State 4, 1197 (1962).
21. A. I. Grinchak, Soviet Phys.-Solid State 8, 1000 (1966).

---

† Abbreviations herein follow the form recommended by the American Institute of Physics.

22. J. J. Lander, Phys. Rev. 191, 1382 (1953).

23. H. D. Hagstrum, Phys. Rev. 89, 244 (1953).

24. H. D. Hagstrum, Phys. Rev. 91, 543 (1953).

25. H. D. Hagstrum, Phys. Rev. 96, 325 (1954).

26. H. D. Hagstrum, Phys. Rev. 96, 336 (1954).

27. H. D. Hagstrum, Phys. Rev. 150, 495 (1966).

28. E. J. Scheibner, L. H. Germer, and C. D. Hartman, Rev. Sci. Instr. 31, 112 (1960).

29. E. J. Scheibner, L. N. Tharp, Surface Science 8, 247 (1967).

30. G. F. Amelio and E. J. Scheibner, Surface Science 11, 242 (1968).

31. G. Wentzel, Z. Physik 43, 524 (1927).

32. R. A. Rubenstein, Ph.D. Thesis, University of Illinois, 1955.

33. W. N. Asaad and E. H. S. Burhop, Proc. Phys. Soc. 71, 369 (1958).

34. W. Melhorn, Z. Physik 208, 1 (1968).

35. Mott and Massey, The Theory of Atomic Collisions, Oxford, Clarendon Press, 1965.

36. M. A. Listengarten, Izv. Ann. U.S.S.R., Ser. fiz. 25, 792 (1961). (Trans. Bulletin 25, 803).

37. E. Merzbacher, Quantum Mechanics, John Wiley and Sons, Inc., New York, 1961.

38. R. V. Churchill, Operational Mathematics, 2nd ed. McGraw Hill Book Company, Inc., New York, 1958, p. 37.

39. H. D. Hagstrum, private communication.

40. G. F. Amelio, Surface Science, to be published.

41. H. Seiler, Z. Angew. Physik 22, 249 (1967).

42. John Weymouth, Phys. Rev. 84, 766 (1951).

43. J. J. Quinn, Phys. Rev. 126, 1453 (1962).

44. D. Pains, UFN 62, 399 (1957).

45. L. N. Tharp, Ph.D. Thesis, Georgia Institute of Technology, June, 1968.

46. P. W. Palmberg and T. N. Rhodin, J. Appl. Phys. 39, 2425 (1968).

47. J. T. Grissom, D. R. Koehler and B. G. Gibbs, Nuclear Instruments and Methods 45, 190 (1966).

48. H. D. Hagstrum and G. E. Becker, Phys. Rev. 159, 572 (1967).

49. J. A. Simpson, Rev. Sci. Instr. 32, 1283 (1961).

50. J. A. Simpson, Rev. Sci. Instr. 35, 1698 (1964).

51. C. E. Kuyatt and J. A. Simpson, Rev. Sci. Instr. 38, 103 (1967).

52. L. Gregor, P. Balk and F. J. Campagna, IBM Journal 9, 327 (1965).

53. G. A. Baraff, Phys. Rev. 135, A528 (1964).

54. E. O. Kane, Phys. Rev. 159, 624 (1967).

55. J. A. Dillon, Jr. and H. E. Farnsworth, J. Appl. Phys. 29, 1195 (1958).

56. W. J. Tegart, The Electrolytic and Chemical Polishing of Metals in Research and Industry, London, Pergamon Press, 1956.

57. A. Reisman and R. Rohr, J. Electrochem. Soc. 111, 1425 (1964).

58. J. A. Bearden and A. F. Burr, Revs. Modern Phys. 39, 125 (1967).

59. Graphite single crystals obtained from D. E. Soule of Union Carbide.

60. F. J. Corbato, in: Proc. Third Carbon Conference (Pergamon Press, New York, 1957).

61. E. O. Kane, Phys. Rev. 146, 558 (1966).

62. T. Sagawa, Private communication.

63. H. D. Hagstrum and Y. Takeishi, Bell Telephone Laboratories, internal publication (1967).

64. E. E. Lafon, private communication.

65. J. C. Slater and G. F. Koster, Phys. Rev. 95, 1167 (1954).

OTHER REFERENCES

1. Burhop, E. H. S., The Auger Effect and Other Radiationless Transitions, Cambridge University Press, Great Britain, 1952.

2. Bruining, H., Secondary Electron Emission, Pergamon Press, 1954.

3. Dekker, A. J. in Solid State Physics, Vol. 6, p. 251, Academic Press, Inc., New York, 1958.

4. Hachenberg, V. O. and W. Brauer, Advances in Electronics and Electron Physics, Vol. XI, p. 413, Academic Press, Inc., New York, 1959.

5. Hachenberg, V. O. and W. Brauer, Fortschs. Phys. 1, 439 (1954).

VITA

Gilbert Frank Amelio was born March 1, 1943 in New York City. When he was four his parents relocated in Miami, Florida where he attended public schools. He graduated magna cum laude from Miami Senior High School in June 1961 and entered the Georgia Institute of Technology the following fall. He married the former Miriam LaDora Rupert in April, 1963 and received B.S. and M.S. degrees in Physics in June, 1965 and June, 1967 respectively.

While at the Georgia Institute of Technology he participated in a number of extra-curricular activities including serving as his class officer for four consecutive years, serving on the President's Advisory Board and student representative to the Faculty Student Activities Committee. In addition he was a member of the Ramblin' Wreck Club and Pi Kappa Alpha Social Fraternity. He was selected to be a member of such honor societies as Phi Eta Sigma, Sigma Pi Sigma, Tau Beta Pi, Phi Kappa Phi, Omicron Delta Kappa, and Koseme.

While an undergraduate he taught sophomore physics laboratories as well as worked for a small Atlanta based technical firm, Technical Information Systems and Service, Inc. By the time the company was acquired by Brown Engineering in March, 1965 he was serving as technical advisor to the president and directly responsible for two large contracts with NASA and Lockheed. He continued to work with the Brown Engineering directed company (Information Services, Inc.) until returning to graduate school in the fall of 1965. While in graduate school

he taught a sophomore physics course and established a consulting relationship with a number of Atlanta businesses. In March, 1966 he joined the Low Energy Electron Diffraction group of the Physical Sciences Division at Georgia Tech as a graduate research assistant. While there he engaged in research on the inelastic scattering of low energy electrons from which several publications followed.